The Identification and Characterisation of a Ribokinase and a Putative D-Ribose Permease in *Arabidopsis thaliana*

Von der Naturwissenschaftlichen Fakultät der
Gottfried Wilhelm Leibniz Universität Hannover

Zur Erlangung des Grades
Doktorin der Naturwissenschaften (Dr. rer. nat)

genehmigte Dissertation
von
Rebekka Schröder, M. Sc.

2019

Referent: Prof. Dr. Claus-Peter Witte

Korreferent: Prof. Dr. Thomas Brüser

Tag der Promotion: 01.10.2019

Abstract

Plants are stationary organisms that rely on the efficient uptake and remobilization of nutrients for growth and reproduction. One of the most abundant nutrients is nitrogen (N), of which the majority is located in proteins, however. N can also be found in nucleotides as part of the purine and pyrimidine nucleobases and can furthermore be recycled by the nucleotide catabolism pathway. During the degradation of ribo-nucleosides, derived from RNA, the enzyme nucleoside hydrolase 1 (NSH1) hydrolyses the N-glycosidic bond between the nucleobase and the D-ribose residue. The N from the nucleobase is then recycled to ammonia in a multi-step process via uric acid and allantoin. The process of D-ribose recycling is unknown up to now. Plant lines of mutant genes involved in this purine nucleotide catabolism, like the guanosine deaminase (GSDA), show a necrotic phenotype under prolonged dark stress conditions, suggesting that carbon starvation, due to the lack of recycled D-ribose, could lead to this drastic phenotype. The enzyme responsible for the recycling of D-ribose is ribokinase (RBSK). It phosphorylates D-ribose to D-ribose 5-phosphate, which can be used afterwards in the non-oxidative pentose phosphate pathway, the nucleotide *de novo* synthesis or the nucleotide salvage reactions.

In this study, the RBSK from *Arabidopsis thaliana* is described (*At*RBSK) as the first plant RBSK. The homologous enzyme from *Saccharomyces cerevisiae* was included into the analysis, because of contradicting results regarding the identification of yeast RBSK in a former study (Xu *et al.,* 2013). The proteins were transiently produced in *Nicotiana benthamiana* with a C-terminal StrepII tag for protein purification and detection. For the evaluation of the kinetic constants, a HPLC kinase assay was developed and established. In the *in vivo* analysis, metabolites from double mutant lines of the purine and pyrimidine nucleotide metabolic pathways and the *RBSK* mutant line were extracted to clarify the contribution of nucleotide metabolism to the D-ribose pool in plants. A comprehensive dark stress experiment coupled with metabolite analysis by mass spectrometry, showed an impact of prolonged dark stress on nucleotide metabolism and the D-ribose pool in plants. Furthermore, it could be excluded that the lack of D-ribose is causing the *gsda* dark stress phenotype.

In the second part of this work, candidate genes for a plastidic D-ribose transporter were found by comparative expression data analysis in legumes, linking cytosolic D-ribose, released by the nucleotide metabolism, with the plastidic D-ribose phosphorylation by RBSK. A promising candidate gene was found in *pGLCT* which is transcriptionally up-regulated in a situation of high D-ribose turnover, as found in nodules of ureide exporting legumes. Furthermore, metabolite analysis in *A. thaliana* and transient overexpression in *S. cerevisiae* were used for the investigation of the role of pGLCT in D-ribose translocation.

By investigating the plant RBSK from *A. thaliana* together with the homologous enzyme

from *S. cerevisiae* and furthermore with pGLCT as the plastidic D-ribose transporter, the metabolic process of D-ribose recycling during purine nucleotide degradation was revealed.

Keywords: ribokinase, ribose transporter, nucleotide metabolism

Zusammenfassung

Pflanzen sind stationäre Organismen und somit auf eine effiziente Nährstoffaufnahme und -recycling angewiesen. Einer der wichtigsten Makronährstoffe ist Stickstoff (N), welcher hauptsächlich in Proteinen gebunden ist. Aber auch in den Nukleobasen der Nuklein-säuren (DNA und RNA) ist N gebunden und kann durch den Abbau der Nukleotide wiederverwertet werden. Während des Abbaus von Ribonukleotiden aus der RNA hy-drolysiert das Enzym Nukleosidhydrolase 1 (NSH1) die Bindung zwischen der Purin-bzw. Pyrimidinbase und der D-Ribose. Der in der Nukleobase gebundene N wird in einem mehrstufigen Prozess über Harnsäure und Allantoat zu Ammonium umgesetzt, wohingegen die Schritte der D-Ribose Wiederverwendung bislang unbekannt sind. In dem Modellorganismus *Arabidopsis thaliana* zeigt eine Mutante in der Guanosinedeam-inase (*GSDA*), die ein Defizit im Purinnukleosidabbau besitzt, einen starken Phänotyp während eines lang anhaltenden Dunkelstresses. Als eine mögliche Ursache für diesen Phänotypen wurde ein Kohlenstoffmangel in Betracht gezogen, da D-Ribose hier nicht aus den Purinnukleotiden frei gesetzt werden kann. An der Wiedergewinnung von D-Ribose ist eine Ribokinase (RBSK), welche die Pentose aus dem Nukleotidabbau zu D-Ribose-5-phosphat phosphoryliert, beteiligt. So wird der Zuckerrest zurück in den nicht oxidativen Pentosephosphatweg, die Neusynthese von Nukleotiden oder Wiederverwertung von Nuk-leobasen geschleust.

In dieser Arbeit wurde die Ribokinase aus *A. thaliana* (*At*RBSK) untersucht. Ein homolo-ges Gen aus *Saccharomyces cerevisiae* (*Sc*RBSK) wurde in die Analyse mit einbezogen, da es in der Literatur widersprüchliche Aussagen bezüglich der Identität von *Sc*RBSK vor-liegen (Xu *et al.,* 2013). Zur Ermittlung der kinetischen Konstanten wurde ein geeignetes Testverfahren entwickelt. *In vivo* wurden *A. thaliana* Mutantenlinien verwendet, um eine umfassende Metabolitanalyse des Nucleotidmetabolismus durch Massenspektrome-trie zu ermöglichen. In einer umfassenden Metabolitanalyse zeigte verlängerter Dunkel-stress einen Einfluss auf den Nukleotidmetabolismus und die D-Ribose in Pflanzen.

Weiterhin wurden in dieser Arbeit Kandidatengene für einen potentiellen D-Ribose Trans-porter in der Chloroplastenmembran gesucht. Dieser verbindet die Freisetzung der D-Ribose durch den Nukleotidabbau im Cytosol mit der Phosphorylierung durch die RBSK im Chloroplasten. Die Auswertung einer, in unserem Labor durchgeführten, vergle-ichenden Expressionsanalyse in verschiedenen Leguminosen ergab mögliche Kandidaten-gene für den gesuchten Transporter. Das erfolgversprechendste Gen kodiert für einen beschriebenen Glukosetransporter (*pGLCT*), welcher transkriptionell hochreguliert ist in den Knöllchen von Ureide transportierenden Leguminosen während erhöhter D-Ribose Produktion. Massenspektrometrischer Analysen in *A. thaliana* linien und transiente Über-expression von pGLCT in Hefe wurden verwendet um die Rolle von pGLCT im D-Ribose Transport zu untersuchen.

Die Untersuchung der ersten pflanzlichen RBSK, die Bestätigung der Funktion der RBSK aus *S. cerevisiae* und die Beschreibung des ersten plastidären Ribosetransporters (pGLCT) tragen zu der Aufklärung des D-Ribosemetabolismus bei. PGLCT könnte somit als Verknüpfung zwischen Nukleotidabbau und Pentosephosphatweg dienen.

Schlagwörter: Ribokinase, Ribosetransporter, Nukleotidmetabolismus

Table of Contents

List of Figures

List of Tables

Abbreviations

Abbrivation	Meaning
A. thaliana	*Arabidopsis thaliana*
ADP	adenosine diphosphate
APS	ammonium persulfate
ATP	adenosine triphosphate
bp	base pairs
°C	degree centigrade
cAMP	cyclic adenosine monophosphate
cds	coding sequence
cDNA	complementary desoxyribonucleic acid
CLSM	confocal laser scanning microscopy
Col-0	Columbia-0
ddH$_2$0	double distilled water
DMSO	dimethyl sulfoxide
DNA	desoxyribonucleic acid
dNTPs	desoxyribonucleoside triphosphate
DTT	dithiothreitol
dw	dry weight
E. coli	*Escherichia coli*
EDTA	ethylendiamintetraacetic acid
fw	fresh weight
g	gram
GSDA	guanosine deaminase
h	hour
HGPRT	hypoxanthine guanine phosphoribosyl transferase
IMP	inosine monophosphate
kDa	kilodalton
l	liter
LB	*Lysogeny Broth*
LC-MS	liquid chromatography - mass spectrometry
μg	microgram
μl	microliter
μM	micromolar
mg	milligram
min	minute
ml	milliliter
mM	millimolar

M	molar
N	nitrogen
NAD	nicotinamide adenine dinucleotide
nm	nanometer
nM	nanomolar
NSH1	nucleoside hydrolase 1
N. bethamiana	*Nicotiana benthamiana*
PAGE	polyacrylamide gel eletrophoresis
PCR	polymerase chain reaction
PfkB	phosphofructokinase B
pGLCT	plastidic glucose transporter
PRPP	5-phosphoribosyl 1-pyrophosphate
PPPW	pentose phosphate pathway
RBSK	ribokinase
*At*RBSK	ribokinase *Arabidopsis thaliana*
*Sc*RBSK	ribokinase *Saccharomyces cerevisiae*
RNA	ribonucleic acid
RPI	ribulose 5-phosphate isomerase
rpm	rotations per minute
s	second
S. cerevisiae	*Saccharomyces cerevisiae*
SD	standard deviation
SDS	sodium dodecyl sulfate
TAE	tris acetate EDTA
T-DNA	transfer DNA
TEMED	N,N,N,N'- tetramethyl ethlydiamin
TRIS	2-amino-2hydroxymethyl-propane-1,3-diol
UMP	uridine monophosphate
V	volt
w/v	weight per volume
XDH1	xanthine dehydrogenase 1
YFP	yellow flourescent protein

1 Introduction

In the year 2018, nearly 20 years after the Arabidopsis Genome Initiative (2000) has made the full genome sequence of the model plant *Arabidopsis thaliana* (*A. thaliana*) available, many gene functions are still unknown. Phylogenetic analyses, protein structure prediction, RNA sequencing analysis and many more techniques has given new insights into the function of unknown genes.

Yet, the functions of many of the 25,000 genes of *A. thaliana* still have to be discovered. This lack of knowledge leads to missing links in many metabolic pathways. This thesis contributes to closing the gap of knowledge between the nucleotide metabolism and the recycling of the D-ribose 5-phosphate into the non-oxidative pentose phosphate pathway. Not only is the enzyme of a putative ribokinase the focus of this work, but also the putative transport protein localised in the chloroplastidic membrane involved in translocating D-ribose from the cytosol to the chloroplast.

1.1 Nucleotides are a Key Component for Plant Metabolism

For the growth and proliferation plants use carbon-dioxide, water, minerals (macro and micro minerals), and sunlight. By this complex biochemical process, carbon compounds like sugars are produced not only as an energy source, but as carbon storage compounds (starch) as well. All metabolites have to be recycled efficiently to support optimal growth to the plant. The building blocks of DNA (Deoxyribonucleic acid) and RNA (Ribonucleic acid) can be recycled as well. In stressful situations like minimal fertilised soil or prolonged darkness, the recycling of all metabolites is the key to the plant survival (Smith and Stitt, 2007).

When plants proliferate, new macromolecules like DNA and RNA are synthesised in the dividing tissue, which nucleotides are the building blocks of (Figure 1). Nucleotides are precursor components of other important metabolites like NAD (nicotinamide adenine dinucleotide), FAD (flavin adenine dinucleotide) and S-adenosylmethionine (Zrenner *et al.,* 2006). The nucleotide ATP (adenosine triphosphate) is involved in the transfer of phosphate, photosynthesis, photorespiration, multiple enzymatic processes, and is the main energy carrier.
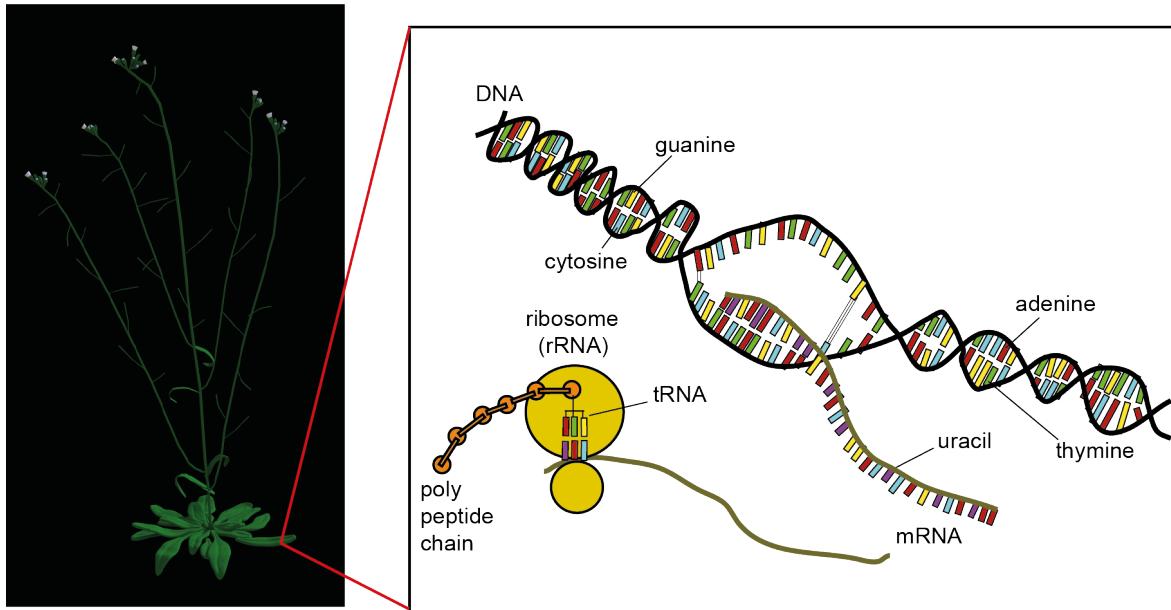
Figure 1: Overview of the transcriptional and translational process from DNA and RNA into protein.

UDP (uridine diphosphate), a pyrimidine nucleoside diphosphate molecule, contributes to the metabolism of sucrose. UDP is as well precursor for cellulose and cell wall polysaccharide synthesis, lipid synthesis and part of diverse defence mechanisms (Zrenner *et al.*, 2006; 2009). Nucleotides are furthermore part of the bacterial signal transduction cascade in form of cAMP (cyclic adenosine monophosphate) or cGMP (cyclic guanosine monophosphate) (Berg 2013; Voet 2011)
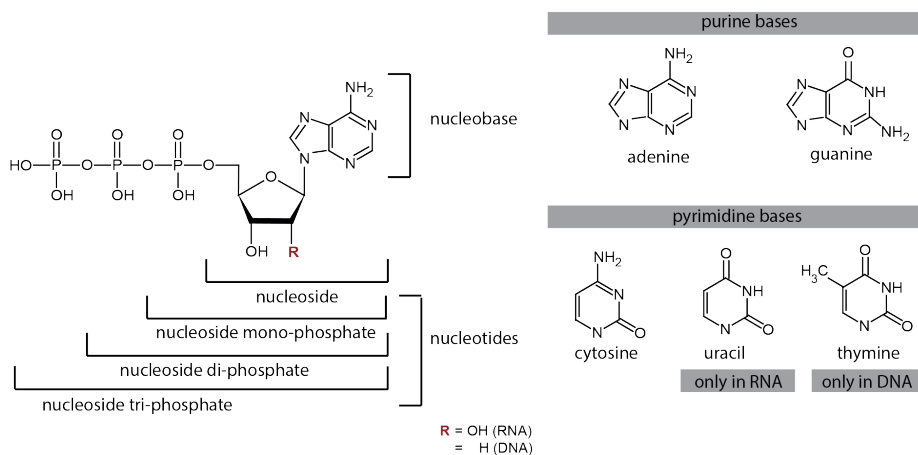
Figure 2: Overview over the general structure of purine and pyrimidine nucleotides. Nucleotides include nucleotide mono-, nucleotide di- and nucleotide tri-phosphates whereas nucleosides only consist of the ribose residue and the nucleobase. Shown are the differences of deoxyribonucleic acid (DNA) nucleotides and ribonucleic acid (RNA) nucleotides in red. The nucleobase thymine can only be found in DNA whereas uracil is unique for RNA nucleotides.

DNA or RNA nucleotides consist of a nucleobase, one to three phosphate residues and a pentose sugar residue (Figure 2). This pentose sugar is - in the case of RNA a D-ribose and in the case of DNA a D-deoxyribose residue, distinguishable by the hydroxyl group at the second C atom (red). The nucleobase can either be adenine and guanine in case of purine nucleotides or cytosine and thymine in the case of pyrimidine nucleotides. Thymine however is only present in DNA whereas uracil substitutes for thymine in RNA. A nucleoside includes only the sugar (D-ribose) and a purine or pyrimidine nucleobase, respectively.

The nucleotide metabolism can be differentiated into three different phases: the *de novo* synthesis of new nucleotides, the nucleotide degradation and the salvage pathway of nucleobases back to nucleosides or nucleotides, respectively (Zrenner *et al.,* 2009).

1.2 Nucleotide *De Novo* Synthesis

Nucleotide *de novo* synthesis is defined as the synthesis of nucleotides from the basic building blocks. An obligatory substance for *de novo* synthesis, of not only purine but also pyrimidine nucleotides, is 5-phosphoribosyl 1-pyrophosphate (PRPP). PRPP is produced by the PRPP synthase, using D-ribose 5-phosphate and ATP. In human medicine, nucleotide *de novo* synthesis and especially the PRPP synthase reaction is a common target for cancer treatment (Parry *et al.,* 1996; Yin *et al.,* 2018).

The biosynthesis of pyrimidine nucleotides follows six enzymatic steps using carbamoyl phosphate, PRPP and aspartate to form UMP. This pathway is also known as the orotic acid pathway due to an intermediate product (Zrenner *et al.,* 2006; Nara *et al.,* 2000).

The purine *de novo* synthesis uses amino acids like glycine, glutamine and aspartate together with PRPP, 10-formyl tetrahydrofolate and carbon dioxide (CO_2) to form inosine monophosphate (IMP) in nine steps (Traut *et al.,* 1996; Zrenner *et al.,* 2006). IMP is the basis for the further synthesis of AMP, but can also be converted to xanthosine monophosphate (XMP) and guanosine monophosphate (GMP).

1.3 Nucleotide Degradation

The degradation of purine nucleotides can be subdivided into two different parts. The degradation of monophosphate-nucleosides in multiple steps to the nucleobase xanthine and the further degradation of xanthine for the recycling of nitrogen by allantoate. The formation of purines and purine nucleotide degradation starts from IMP (inosine monophosphate) (Van der Graaf *et al.,* 2004).
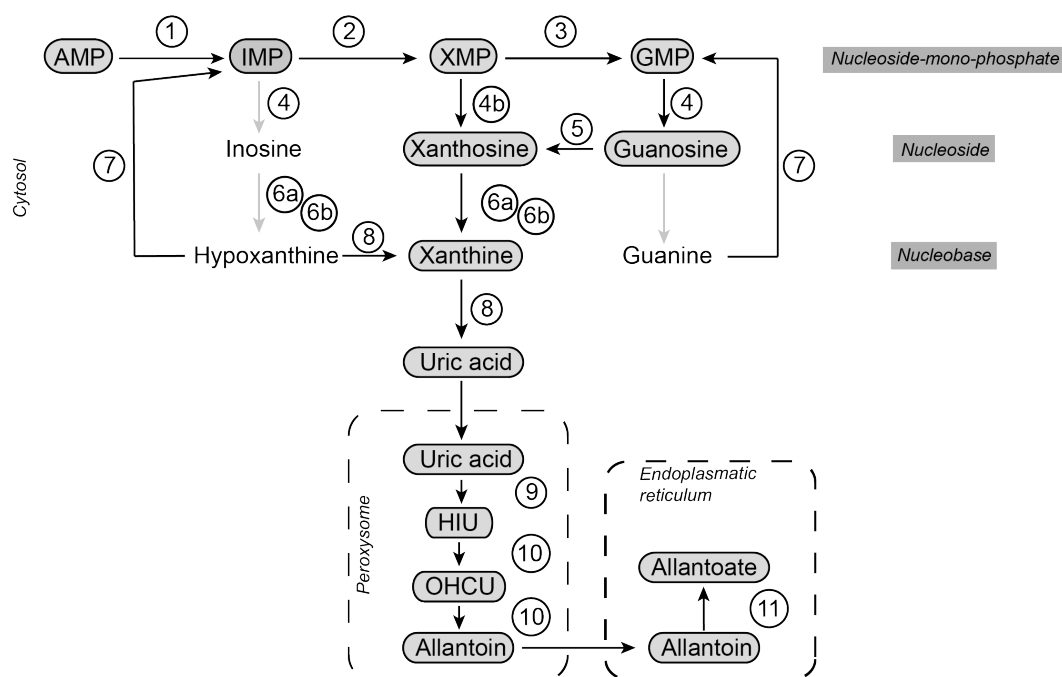
Figure 3: Purine nucleotide metabolism in *A. thaliana*. AMP: Adenosine monophosphate; IMP: Inosine monophosphate; XMP: Xanthosine monophosphate; GMP: Guanosine monophosphate; HIU: 5-hydroxyisourate; OHCU: 2-oxo-4-hydroxy-4-carboxy-5-ureido-imidazoline. Enzyme 1: Adenosine monophosphate deaminase; 2: Inosine monophosphat dehydrogenase; 3: Guanosine monophosphate synthetase; 4: 5' Nucleotidase; 4b: XMP phosphatase; 5: Guanosine deaminase; 6: Nucleoside hydrolase 1; 6b: Nucleoside hydrolase 2; 7: Hypoxanthine guanine phosphoribosyltransferase; 8: Xanthine dehydrogenase; 9: Uric acid oxidase; 10: Allantoin synthase; 11: Allantoinase. Grey arrows indicate reactions not preferred route in *A. thaliana*. (Zrenner *et al.,* 2009; Werner and Witte 2011; Baccolini and Witte 2019)

IMP is oxidised to XMP (xanthosine monophosphate) and further to GMP (guanosine monophosphate) by IMP dehydrogenase and XMP deaminase (Figure 3). The step from the nucleotide to nucleoside level is catalysed by a yet unknown 5'nucleotidase, resulting in a nucleoside and a free phosphate residue. The gene encoding for an IMP phosphatase is still unknown in plants, according to Zrenner *et al.* (2006). XMP and GMP can be dephosphorylated to their corresponding nucleosides xanthosine and guanosine by a 5' nucleotidase. However, a dephosphorylation of XMP has up to now only been observed in nodules of ureide exporting legumes (Shelp and Atkins, 1983), and the study of Dahncke *et al.*(2013) suggests degradation uniquely through GMP to guanosine. In this pathway, the GSDA reaction is the only source of xanthosine in *A. thaliana* by the deamination of guanosine. A recent study suggests that the degradation of IMP via inosine and hypoxanthine has a low contribution to the xanthine pool. Confirming that the major route

of purine nucleotide degradation is going from IMP to XMP, GMP and further through guanosine and xanthosine to xanthine. A secondary route directly from XMP to xanthosine and further to xanthine is possible by a putative XMP phosphatase (Baccolini and Witte 2019).

Furthermore, the deamination of guanosine to xanthosine is the gateway to nucleobase degradation, from which point on xanthosine is only degraded and cannot be salvaged (Ashihara 2012; Dahncke *et al.*, 2013). Hydrolysis of the nucleobase xanthine from the sugar residue (D-ribose) is mediated by a nucleoside hydrolase complex of two enzymes, NSH1 (nucleoside hydrolase 1) and NSH2 (nucleoside hydrolase 2). As a secondary substrate, inosine can be hydrolysed to hypoxanthine and D-ribose by this complex. However, metabolite analysis with mutant lines of *NSH1* and *NSH2* show a low impact of the reactions through inosine to the xanthine pool (Baccolini and Witte 2019). The enzyme xanthine dehydrogenase (XDH) is not only using xanthosine as a substrate, producing xanthine, but is facilitating the following reaction from xanthine to uric acid as well (Figure 3 number 8; Brychkova *et al.*, 2008). Afterwards uric acid is converted to HIU (5-hydroxyisourate) by the uric acid oxidase in the peroxisome and furthermore to OHCU (2-oxo-4-hydroxy-4-carboxy-5-ureido-imidazoline) and allantoin by allantoin synthase (Hauck *et al.*, 2014). After the transport into the endoplasmatic reticulum (ER), allantoin is then converted to allantoate by the allantoinase (Werner and Witte 2011).

Intermediate products of the purine nucleotide degradation have secondary functions besides being broken down. Uric acid, produced by XDH, is potentially acting as a ROS (reactive oxygen species) scavenger to protect cells from oxidative stress during a powdery mildew infection (Ma *et al.*, 2016). Furthermore, allantoin and allantoate are used as N transport compounds in ureide exporting legumes. An accumulation of these ureides (especially allantoate) can occur as a response to environmental stresses like drought stress in *Phaseolus vulgaris* (Alamillo *et al.*, 2010).
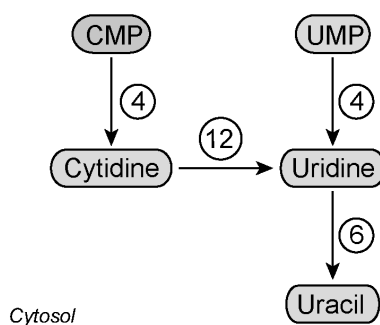
Figure 4: Pyrimidine nucleotide metabolism in *A. thaliana.* CMP: Cytidine monophosphate; UMP: Uridine monophosphate. Enzyme 4: 5' Nucleotidase; 6: Nucleoside hydrolase 1 (NSH1); 12: Cytidine deaminase; (Zrenner *et al.*, 2009; Chen *et al.*, 2016)

The first step of pyrimidine nucleotide breakdown (CMP or UMP) is mediated by still

unknown 5'nulceotidases, resulting in the phosphate residue and the pyrimidine nucleoside cytidine or uridine, respectively (Figure 4). Cytidine is deaminated to uridine by cytidine deaminase (CDA) and in the following step the N-glycosidic bond between the nucleoside and D-ribose residue is hydrolysed by NSH1 (Chen *et al.,* 2016). Hydrolysis from cytidine to cytosine only occurs in *CDA* mutant lines, due to the accumulation of cytidine. Neither plants nor animals posses a cytosine deaminase. Therefore, only the route for nucleoside degradation to uracil by the deamination of cytidine to uridine is shown (Zrenner *et al.,* 2006).
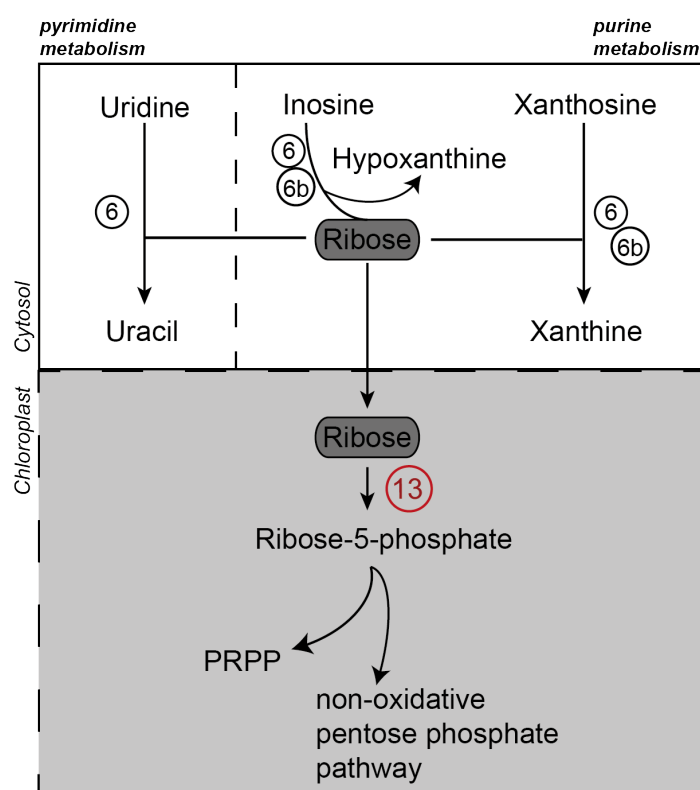
Figure 5: Purine and pyrimidine nucleoside metabolism lead to the hydrolysis of D-ribose from the nucleobase (either purine or pyrimidine) by NSH1 (6) or NSH1 and NSH2 (6 and 6b). The D-ribose is transported into the chloroplast and phosphorylated by a kinase (13) to D-ribose 5-phosphate.

D-Ribose is an aldopentose and an integral component of the sugar backbone of ribonucleosides and nucleotides, for example in adenosine triphosphate (ATP), which is used as a energy currency and in nicotinamide adenine dinucleotide phosphate (NADP) which is part of the electron transport or redox-reactions.

For the use of D-ribose, the sugar has to be activated by phosphorylation (Anderson and Cooper, 1969; Lopilato *et al.,* 1984) This reaction is catalysed by a ribokinase (RBSK) producing a phosphate sugar (D-ribose 5-phosphate) (Figure 5). Once the D-ribose is phosphorylated, it is trapped inside the chloroplast and can be used as a substrate for PRPP (5-phosphoribosyl 1-pyrophosphate) production. PRPP is an important precursor for the

nucleotide *de novo* synthesis and salvage reactions. Therefore, carbohydrate metabolism has a direct influence on the synthesis of new purine nucleotides (Boer *et al.,* 1995).

The D-ribose 5-phosphate can be directed into the non-oxidative pentose phosphate pathway (non-ox. PPP) where it can be used in the transketolase reaction together with xylulose 5-phosphate to produce seduheptulose 7-phosphate and glyceraldehyde 3-phosphate, the latter one being an intermediate of the glycolysis and gluconeogenesis reaction by the Calvin-Benson cycle (Stincone *et al.,* 2014). In the following transaldolase reaction of seduheptulose 7-phosphate with glyceraldehyde 3-phosphate, the C4 sugar erythrose 4-phosphate together with fructose 6-phosphate are produced with erythrose 4-phosphate being an important precursor for histidine synthesis which is involved in vitamin B6 production (Zhao *et al.,* 1995; Stincone *et al.,* 2014). The RBSK reaction however, is not the only source of D-ribose 5-phosphate in the non-ox.PPPW. The ribulose 5-phosphate isomerase reaction (RPI) converts ribulose 5-phosphate to D-ribose 5-phosphate. Mutations in *RPI* led to severe neurological damage in a single known human patient with psychomotoric retardation, epilepsy, neurological regression and impaired vision and speech whereas two mutant alleles led to a non-functional and a partially functional RPI protein. A full *RPI* mutation however seems to be lethal, underlining the importance of a functional non-ox. PPP (Huck *et al.,* 2004). In *A. thaliana*, a mutation of the *RPI2* gene leads to impaired chloroplast function with decreased photosynthetic activity and therefore decreased starch accumulation (Xiong *et al.,* 2009).

1.4 Nucleotide Salvage Pathway

The catabolism of nucleotides to nucleobases is a multi-step pathway involving phosphatase and hydrolysis reactions. But intermediates of the this pathway can be salvaged back to nucleotides as well. The advantage of not only synthesising nucleotides by the *de novo* pathway, but instead recycling nucleosides and nucleobases back to nucleotides, appear to have lower energy costs in form of ATP (Zrenner et al., 2006).

Nucleobases can be ribophosphorylated by phosphoribosyl transferases under the consumption of PRPP to the nucleotide mono-phosphate level. One such enzyme is the hypoxanthine guanine phosphoribosyltransferase (HGPRT; enzyme 7 in Figure 3), which ribophosphorylates either guanine or hypoxanthine to GMP or IMP, respectively. Data from a seedling culture experiment in *A. thaliana* suggests that only AMP and GMP are salvaged from adenine or guanine and are afterwards used in RNA synthesis (Yin *et al.,* 2014). For the pyrimidine salvage, an uridine phosphoribosyltrasnferase (UPRT1) in *A. thaliana* is reported to ribophosphorylate uracil to UMP under PRPP consumption (Islam *et al.,* 2007). The salvage of nucleosides to nucleotides is performed by nucleoside kinases phosphorylating the C5-atom of the D-ribose residue under consumption of ATP. For the pyrimidine salvage up to five uridine kinases genes (*UKL*) are reported in *A. thaliana*. Two

of them are located inside of the chloroplast (Chen and Thelen, 2011). For the salvage of purine nucleosides an adenosine kinase activity is reported in *A. thaliana* and potato (*Solanum tuberosum*), furthermore an inosine guanosine kinase activity in S. tuberosum was reported as well (Katahira and Ashihara 2006). There is no report of a functional xanthosine kinase in *A. thaliana*, suggesting that there is no xanthosine salvage to XMP in *A. thaliana* seedlings (Yin *et al.,* 2014).

The ability to salvage nucleobases to nucleosides is vital for all organisms. A mutation of the HGPRT in *H. sapiens* leads to the Lesh-Nyhan-Syndrome by accumulation of uric acid in the body. This accumulation leads to neurological dysfunction with impaired intelligence and behavioural disorders up to self mutilation (Sculley *et al.,* 1992), leaving the mostly male patients impaired for a life-time. In *A. thaliana* the mutation of an adenine phosphoribosyl transferase leads to sterile pollen in the male plant organs (Moffat *et al.,* 1988). For *HGPRT A. thaliana* mutants such a phenotype is not reported.

1.5 Ribokinase is a Part of the PfkB Sugar Kinase Family

During the catabolism of nucleosides, the nucleoside hydrolases, like NSH1 and NSH2 in *A. thaliana*, cleave the N-glycosidic bond between the nucleobase and the D-ribose working as a D-ribose source (Jung *et al,.* 2011; Kopecná *et al,.* 2013; Baccolini and Witte, 2019). To activate this pentose, it has to be phosphorylated for further use and thus can be trapped inside the cell (Park *et al.,* 2008; Quiroga-Roger *et al.,* 2015). Kinases mediating this activation reaction are part of the group of phosphotransferases using ATP to transfer a phosphate group onto an acceptor.

Carbohydrate kinases are grouped together in the sugar kinase super family within three subfamiles: the PfkB kinases, the hexokinase, and the galactokinase family (Bork *et al.,* 1993; Park *et al.,* 2008). Characteristic motifs for the PfkB family are a glycine rich area at the N-terminus for the sugar binding, a C-terminal motif involved in ATP (adenosine triphosphate) binding (IPR002173), and a characteristic NXXE motif (IPR011611) (Guixé *et al.,* 2009). The asparagine and glutaminic acid in this motif are used for phosphate activation prior to the transfer of the phosphate group to the carbohydrate (Sigrell *et al.,* 1999; Maj *et al.,* 2002; Park *et al.,* 2008).

Part of the PfkB family is not only the eponymous phosphofructokinase family but as well the adenosine kinase, ribokinase, ketohexokinase, and fructokinase family (Park *et al.,* 2008). For this phylogeny of the PfkB family analysis by Park *et al.,* (2008), protein sequences of RBSKs and adenosine kinases (AK) from *Homo sapiens* (*H.sapiens*) and *Escherichia coli* (*E. coli*), but not from plants were used. In *Zea mays* however, a myoinositol kinase was described as an additional member of the PfkB family (Shi *et al.,* 2005) and this shows that not all of the clades of this sugar kinase family are functionally described yet. By using the sequences of plant enzymes from monocotyl and dicotyl plants like *A. thaliana*,

Phaseolus vulgaris (*P.vulgaris*), *Solanum lycopersicum* (*S.lycopersicum*), *Sorghum bicolor* (*S.bicolor*), and *Oryza sativa* (*O.sativa*) it was shown that the PfkB family is containing additional enzymes with a so far unknown function (Schroeder *et al.*, 2018). This indicates that the PfkB sugar kinase family and the specific sub-branches are not fully understood yet.
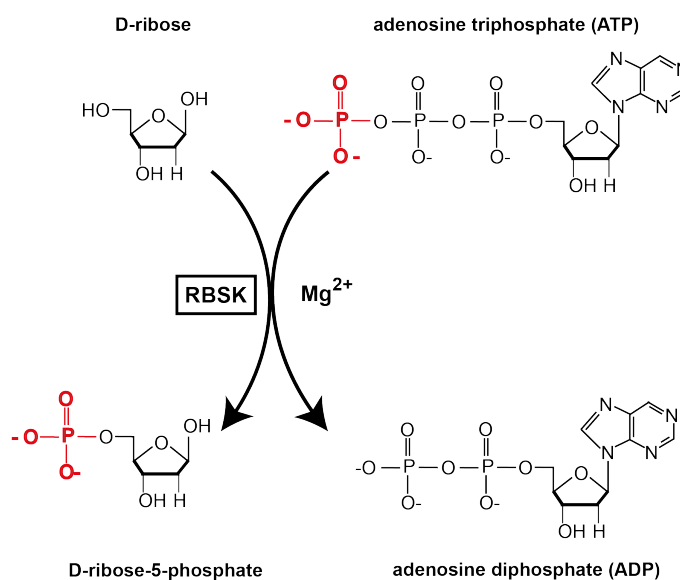
Figure 6: The ribokinase (RBSK) is a phosphotransferase using the γ-phosphate (red) from adenosine triphosphate (ATP) and transfers it on to the alcohol group at the fith carbon atom of D-ribose. In result D-ribose 5 phosphate and adenosine diphosphate (ADP) are produced. For this reaction magnesium (Mg^{2+}) is used as a cofactor.

The D-ribose hydrolysed from the nucleobase during nucleotide degradation is activated by phosphorylation by RBSK (E.C: 2.7.1.15). The RBSK is transferring the γ-phosphate residue from ATP to the hydroxyl group at the 5-C atom of the D-ribose creating D-ribose-5-phosphate and ADP (adenosine diphosphate) (Figure 6). In solution RBSK exists as a dimer (Sigrell *et al.*, 1997) and the first crystal structure of the *Escherichia coli* (*E. coli*) RBSK was published in 1998 by Sigrell *et al.*.

Besides for the RBSK enzyme in *E. coli*, the function of prokaryotic RBSKs was confirmed in *Corynebacterium glutamicum* (Brinkrolf *et al.*, 2008), *Mycobacterium smegmatis* and *Mycobacterium tuberculosis* (Yang *et al.*, 2011), *Staphylococcus aureus* (Li *et al.*, 2012) and lately in *Vibrio cholerae* (Paul *et al.*, 2015). Eukaryotic RBSK function is shown in *Bos taurus* (Agranoff *et al.*, 1956) and *H.sapiens* (Park *et al.*, 2007), and *Leishmania major* (Ogbunude *et al.*, 2007). *In planta*, a RBSK was published by Riggs *et al.* (2016) shortly prior to our study (Schroeder *et al.*, 2018) and a closely related adenosine kinase was described by Moffat *et al.*, (2000) in *A. thaliana*.

The crystal structure analysis from the *E. coli* RBSK revealed an α/β/α barrel structure

with a lid-like structure covering the active site the reaction (Figure 7) (Sigrell *et al.*, 1998). Prior to the reaction, the enzyme is in an open apo configuration. After D-ribose binds to the active centre the lid closes and the affinity towards ATP is increased and the phosphate donor binds at the active site (Sigrell *et al.*, 1997; Sigrell *et al.*, 1998; Sigrell *et al.*, 1999).
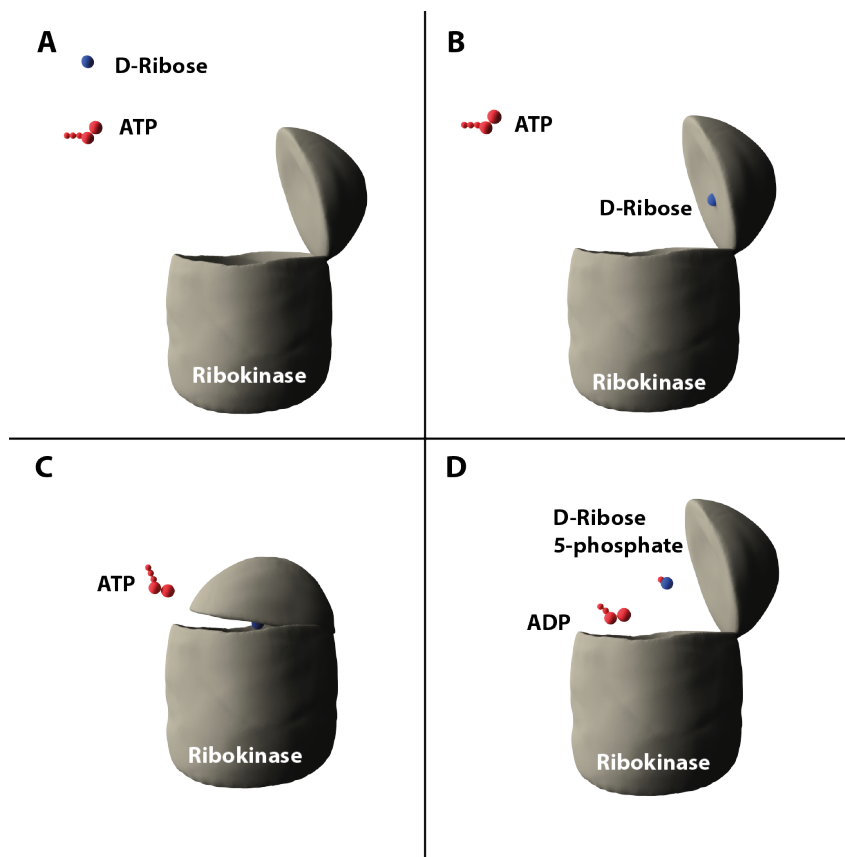
Figure 7: Scheme of the RBSK reaction with D-ribose and ATP. The RBSK protein is showing a barrel type structure with an lid type structure in the apo-conformation prior to the binding of D-ribose (A). D-ribose binds to the lid structure (B) followed by an conformation change which increases the affinity towards ATP (C). After the transfer of the phosphate residues is completed the lid structure opens, releasing the reaction products ADP and D-ribose 5-phosphate (D).

Furthermore, monovalent and divalent cations are necessary for the RBSK reaction. Magnesium (Mg^{2+}) ions are used as a metal chelator in transfer of the γ-phosphate from ATP to D-ribose (Andersson *et al.*, 2002; Chuvikovski *et al.*, 2006). Potassium (K^+) ions stabilise the three dimensional protein structure and a lack of this ions leads to a reduced enzyme activity (Li *et al.*, 2012). Further studies show an influence of inorganic phosphate on the enzymatic activity of the *E. coli* RBSK and the adenosine kinase (Maj *et al.*, 2001). Recently, the crystal structure of the *A.thaliana* RBSK was reported by Kang *et al.* (2019).

1.6 The Link Between Nucleotide Degradation and D-Ribose Recycling

The hydrolysis reaction of purine and pyrimidine nucleosides by NSH1, or the NSH1/NSH2 complex, is localised in the cytosol (Jung *et al.,* 2011). Proteomic data suggests that the RBSK reaction is localised in the chloroplast, which was confirmed independently by Riggs et al. (2016) and Schroeder et al. (2018). Therefore, it is necessary for D-ribose to change the subcellular compartment through the double lipid layer of the chloroplastic membrane (Figure 8).
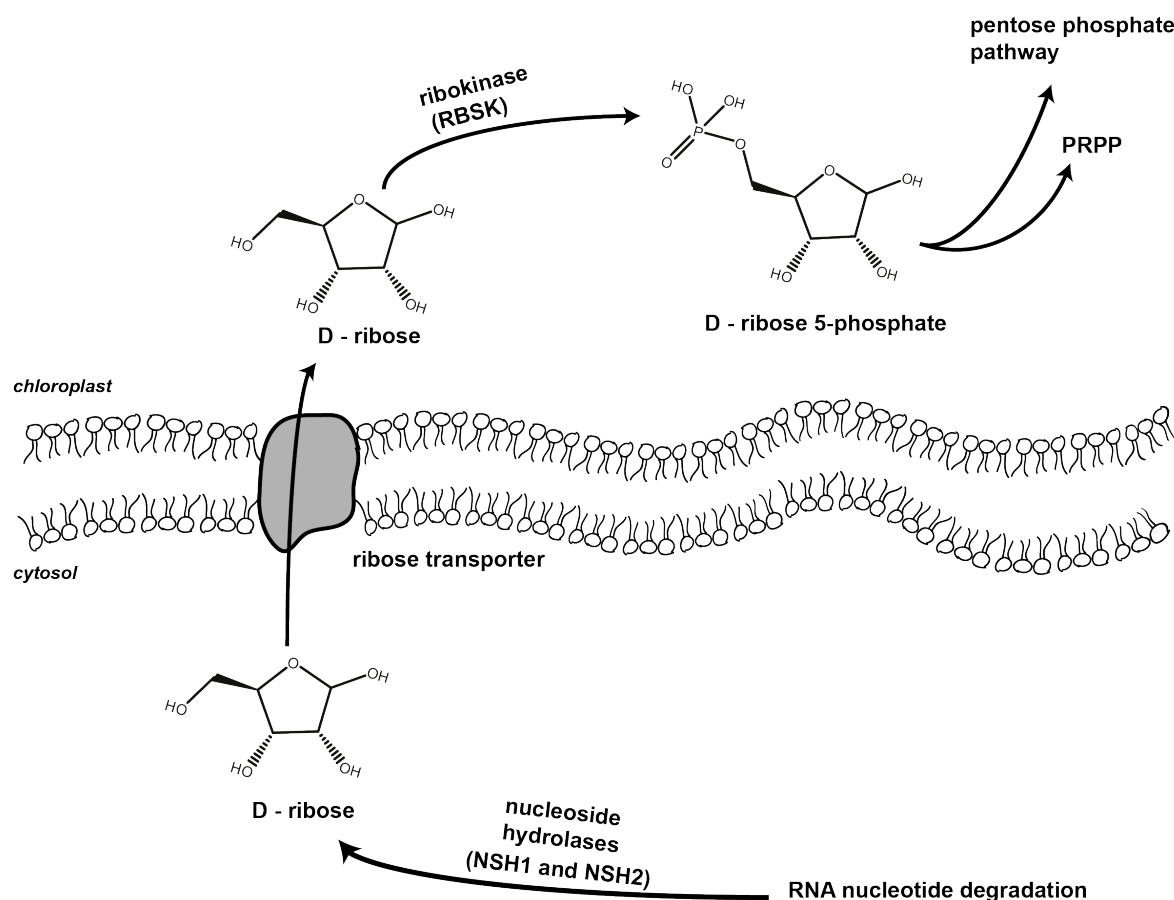
Figure 8: Ribonucleotide hydrolysis is localised in the cytosol leading to a nucleobase (not shown) and a D-ribose residue, which is shuttled into the chloroplast by an unknown transport protein and afterwards phosphorylised by the ribokinase (RBSK) to produce ribose-5-phosphate. PRPP: phosphoribosyl pyrophosphate

Until now, there is no report of a D-ribose transporter located at the inner plastidic membrane in plants. In general, the transport across a double lipid layer can be distinguished into non-mediated transport (diffusion) along the concentration gradient and mediated transport by channels or transport proteins (Figure 9). The transport proteins are grouped into passive and active transporters, with the active transporters using an

energy source like ATP.
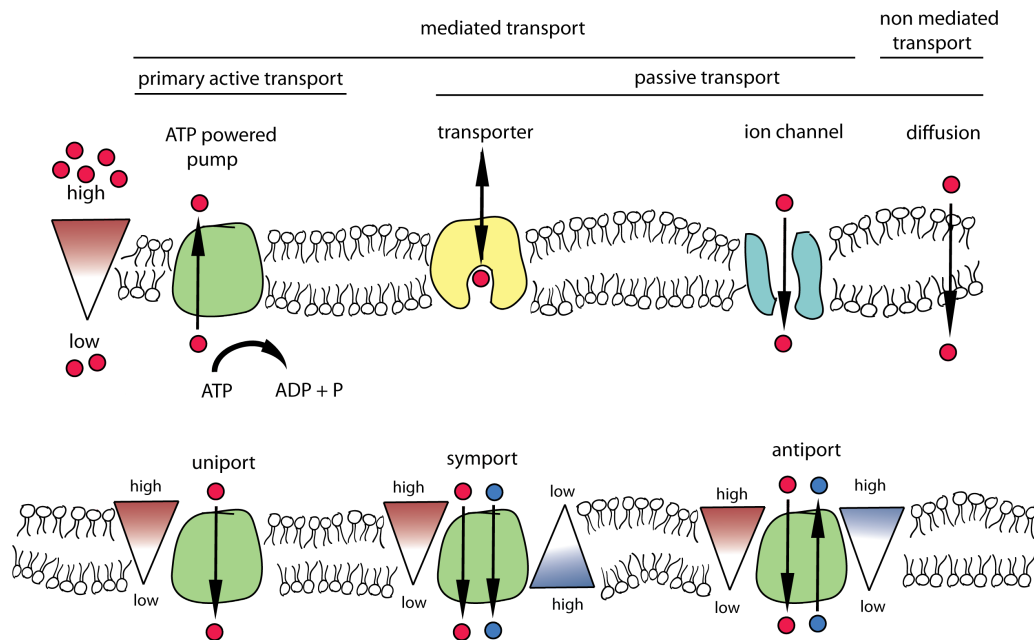
Figure 9: General overview over transmembrane transport of molecules and type of proteins facilitating the mediated transport of molecules. Transport activity is distinguished into non mediated transport (diffusion) and mediated transport facilitated by transport proteins (ATP powered pump, transporter, ion channels) and into active transport under consumption of ATP and passive transport along a concentration gradient. Furthermore the compound can be transported uniquely (uniport), in symport or in exchange with a second compound (antiport). (Voet,2011; Campbell,2009)

The transport of molecules can be performed one molecule at a time (uniport), together with second compound (symport) or in exchange for second compound (antiport) (Voet *et al.,* 2011).

The transporter of all known organisms are grouped into a large number of super families including the ATP-binding cassette (ABC) transporter family and the major facilitator super family (MFS) containing the characteristic MFS domain (IPR020846). For the MFS family, more than 23 subfamilies are described (Pao *et al.,* 1998). The glucose transporter 1 (GLUT1) from *H. sapiens* is a protein facilitating the transport of glucose into the erythrocytes (Mueckler *et al.,* 1985; Yan *et al.,* 2015). An altered expression of this uniporter has a significant medical impact. On one hand, a decreased activity of GLUT1 leads to developmental deficiencies in the patient. On the other hand, an elevated *GLUT1* expression can be an indicator of cancer development (Amann *et al.,* 2009; Deng *et al.,* 2014).

A D-ribose transport function however is shown only for a few transporters. In *E. coli,*

the D-ribose ABC transporter is described and three genes within the *rbsDACBK* operon code for this transporter (Lopilato et al., 1984). The *rbsB* codes for a soluble receptor, *rbsC* for the transmembrane protein, and *rbsA* codes for an ATPase, making this transporter part of the primary active transport system. RbsD is reported to be a mutarotase converting the D-ribose pyranose and furanose form and *rbsK* is coding for the actual *E. coli* ribokinase (Park *et al., 1999*). In *Leishmania mexicana*, (*L. mexicana*) is the glucose transporter *Lm*GT2 is described as possessing a high affinity towards D-ribose (Naula *et al., 2010*). LmGT2 is a member of the GLUT family and was reported to be the first D-ribose transporter described in eukaryotes.

In plants, two different families of sugar transporter are known. The family of disaccharide transporter (DST) is primarily facilitating the sucrose transport across the plant. Sucrose, a disaccharide consisting of fructose and glucose, is the major transport sugar *in planta* and the SUC/SUT sucrose transporter are part of the DST family (Williams *et al., 2000*). The monosaccharide transport family (MST) includes genes, encoding for sugar transporters like the GLUT (glucose) transporter, hexose transporters (HEX) and MST-like transporters. Homologs of the plant MST family proteins are described as well in bacteria (Büttner *et al., 2007*; Büttner *et al., 2010*; Williams *et al., 2000*).

The *A. thaliana* polyol transporter 5 (AtPLT5), a member of the polyol transporter subfamily (PLT) within the MST-like family, is localised at the plasma membrane. This H^+-symporter is described as a broad spectrum transporter using cyclic polyol myoinositol, other hexoses and pentoses. Additionally AtPLT5 is transporting D-ribose from the apoplast into the cytosol and therefore is the first described D-ribose transporter *in planta* (Klepek *et al., 2005*; Büttner *et al., 2007*).

The latest discovered sugar transporter family is the SWEET family (Sugars Will Eventually be Exported Transporter) in 2010 (Chen *et al.*). In *A. thaliana* 20 genes are coding for glucose, fructose or sucrose transporter in this family, expressed in almost all tissues. SWEET-like genes were as well discovered in *Caenorhabditis elegans* and *H. sapiens* (Chen *et al., 2010*). In this family, no D-ribose transporter is reported up to now.

In summary, the D-ribose transport in plants is not well understood up to now. Due to the complexity of sugar transport in plants and the over-all low sequence similarity of the reported D-ribose transporter, isolating promising candidate genes for a plastidic D-ribose transporter is challenging.

1.7 Ureid and Amid Export in Legumes

Nucleotides, nucleosides and nucleobases are not only part of macromolecules like DNA or RNA. They are as well part of the secondary methabolism. Xanthosine and xanthine are the origin for several purine alkaloids, for example caffeine in *Coffee arabica*, theobromine in *Theobroma cacao* and theophylline in *Camellia sinensis* (Ashihara *et al., 2008*). In

tropical legumes however, the degradation of purine nucleotides is source of the nitrogen transport compounds allantoin and allantoate.

Nitrogen is an essential macro nutrient necessary for growth and proliferation of plants. 1 - 5% of the total dry matter of plants is N (Marschner 2012). Since plants cannot access the atmospheric nitrogen on their own, some plants undergo a symbiotic relationship with nitrogen fixing bacteria. Economically, the most important one is the symbiosis of legumes with bacteria of the genus *Rhizobium*. In a similar case the N-fixing *Frankia*, a member of the actinomycete family, undergoes a symbiotic relationship with non-legume plants of the orders *Rosales* or *Fagales* (Santi et al., 2013). In this way, plants can access the rich source of atmospheric dinitrogen gas (N_2) in exchange for carbon compounds of the photosynthesis. Rhizobia infect the plant root tissue through micro fractions and the young root hairs forming a new plant organ, the nodules. These nodules are the location where the atmospheric nitrogen is fixed by the incorporated bacterioids (Frank 1889; Hellriegel and Willfahrt, 1889).
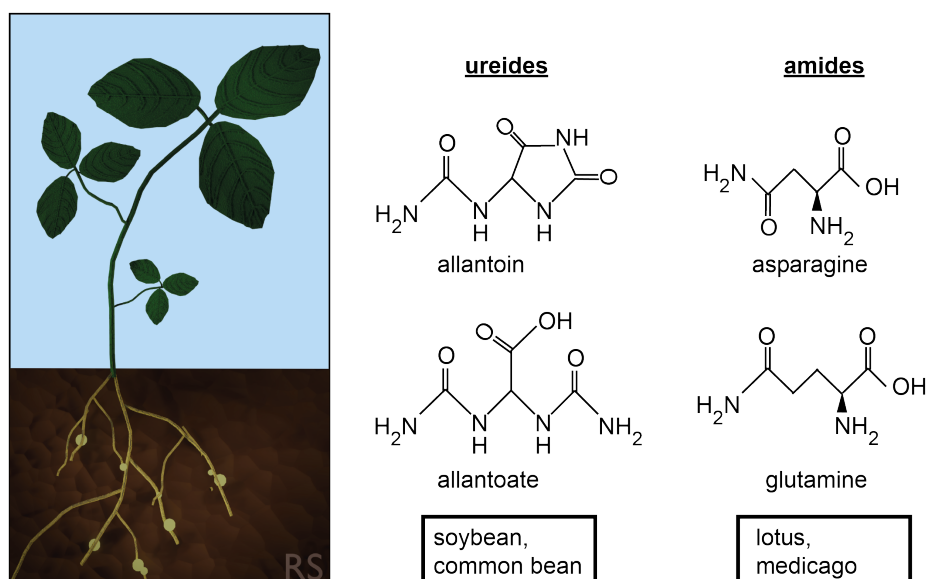
Figure 10: Overview of transported compounds in legumes in symbiosis with *Rhyzobac-teria*. As an example a soybean plant (*Glycine max*) is shown on the left belonging to the ureide exporting plants, exporting allantoin and allantoate from the nodules, similar to the common bean (*Phasaeolus vulgaris*). In contrast to the ureide exporting plants the legumes lotus (*Lotus japonicus*) and medicago (*Medicago truncatula*) export asparagine and glutamine which belong to the group of amides.

The legumes soybean *Glycine max* (*G. max*) and the common bean *Phasaeolus vulgaris* (*P. vulgaris*) are using ureides (allantoin and allantoate) as nitrogen transport compounds in contrast to amide exporting legumes like *Lotus japonicus* and *Medicago truncatula* (Figure 10). The transport compound in amide exporting legumes are the amino acids

glutamine and asparagine (Lodwig *et al.,* 2003).

Ureides are derived from purine nucleotide metabolism and produced by the ureide synthesis pathway from xanthosine, to xanthine, further to uric acid and in several steps to allantoin and allantoate (Figure 3) (Zrenner *et al.,* 2009; Werner and Witte 2011).

These transport compounds are important to shuttle nitrogen from the point of fixation, the nodules, into the sink tissues like pods or young leaves trough the xylem.

1.8 Aim of This Study

The biochemistry of plant purine or pyrimidine nucleotide catabolism, is fairly understood up to now. During nucleotide catabolism, D-ribose is released from nucleoside hydrolysis by NSH1 and NSH2, but the metabolic fate of this metabolite has not been elucidated so far.

The research presented here focuses on the *in vitro* and *in vivo* characterisation of a ribokinase (RBSK) from *A. thaliana* and a homologue from *S.cerevisiae*, which was claimed not to represent a RBSK in a previous study. To elucidate the contribution of nucleotide catabolism to the D-ribose pool *in vivo*, a comprehensive metabolite analysis was conducted. Single and double mutants lines of *rbsk* with other genes involved in nucleotide catabolism were used. Another goal was to elucidate whether carbon starvation, potentially aggravated due to insufficient D-ribose recycling from purine nucleotide catabolism, contributes to the strong dark stress phenotype of a *guanosine deaminase* mutant. In general, the question whether nucleotide catabolism and in particular D-ribose recycling is playing a role in dark-stress survival was addressed.

D-Ribose released in the cytosol by nucleotide catabolism must be transported into the plastids for phosphorylation by RBSK. An additional aim of this work was the characterisation of the plastidic glucose permease pGLCT, which - according to RNAseq analyses conducted in our laboratory - might also represent a plastidic D-ribose transporter. Recombinant pGLCT was expressed in *S. cerevisiae* in an attempt to demonstrate transport activity in growth assays. Metabolite analyses employing *pGLCT* variants, as well as mutants of a closely related *pGLCT-LIKE* gene, were conducted aiming to detect alterations in D-ribose accumulation under various conditions. The idea was that compromised transport capacity for D-ribose over the chloroplast inner membrane should result in an increased D-ribose concentration in the cell, because D-ribose released in the cytosol cannot be brought into contact with RBSK residing in the plastids.

1.9 Work Performed Prior to This Study

The author of this study started the work on the RBSK from *A. thaliana* and *S. cerevisiae* as a Master thesis program in 2014 (Schroeder 2014). Therefore the genes At1g17160 (*AtRBSK*) and YCR36W (*ScRBSK*) were cloned in vectors with C-terminal tags for

transient expression in *Agrobacterium thumefaciens*. The initial protein purification was established but not optimized and a preliminary enzyme essay was conducted but no conclusive data to the kinetic constants was reached. A subcellular localization study by confocal laser scan microscopy analysis (CLSM) of *At*RBSK was conducted successfully. Confirming that the *At*RBSK is localised in the chloroplast.

2 Material and Methods

2.1 Material

2.1.1 Antibiotics

Table 2: Antibiotics used for bacterial selection in this study

Antibiotica	Concentration [mg ml^{-1}]
Ampicillin	100
Carbenicillin	75
Gentamycin	15
Kanamycin	50
Rifampicin in dimethyl sulfoxide (DMSO)	100

2.1.2 Microorganisms

Table 3: Microorganisms used in this study including informations about strains and the selektion marker

Organism	Strain	Selection marker
Escherichia coli	K-12 DH10α (*Invitrogen*)	-
Escherichia coli	BL21(DE3) (*Novagen*)	-
Agrobacterium tumefaciens	GV3101 (pMP90RK) (Koncz and Schell 1986)	Rif^R, Gent^R, Kan^R
Agrobacterium tumefaciens (19K)	C58C1::pCH322 (Voinnet *et al.* 2003)	Rif^R, Tet^R
Saccharomyces cerevisiae	BY4743 (*transomic*) (his3Δ1/his3Δ1, leu2Δ0/leu2Δ0, lys2Δ0/LYS2, MET15/met15Δ0, ura3Δ0)	-

2.1.3 Bacteria Growth Media

Table 4: Bacterial growth media used for the growth of *Escherichia coli* (*E. coli*), Agrobacterium tumefaciens (*A. tumefaciens*) and Saccharomyces cerevisiae (*S. cerevisiae*).

Name	Content
LB media (1 l) (Bertani 1951)	10 g Difco bactro tryptone 5 g yeast extract 10 g sodium cloride pH 7.5 adjusted with HCl
YEB media (1 l) (Vervliet *et al.,* 1975)	5,0 g meat extract (dry) 1 g yeast extract 5 g proteose peptone number 3 5 g sucrose 2 ml MgSO$_4$ (1 M) pH 7.5 adjusted with HCl
YPD media (1 l) (Ausubel *et al.,* 1989)	20 g yeast extract 20 g proteose peptone Number 3 20 g glucose
SD media (1 l) (Cold spring harbor protocol, 2015)	1.6 g yeast droput media (-leucine) 6.7 g yeast media without amino acids

2.1.4 Bacterial Vectors for Protein Production

The expression vectors used in this study are collected in the following Table: 5.

Table 5: Vector backbones used for cloning in this study.

No.:	Vector	Description	Usage
-	pJET1.2/blunt (Fermentas)	ep(pMB1), Amp^R, eco47IR, PlacUV5, T7 promotor	blunt end vector for cloning of PCR products
V36	pXCS-YFP (Feys *et al.*, 2006)	Ori ColE1, ori RK2, pA35S, p35S, *Basta*, eYFP	binary vector for C-terminal YFP tagging and protein production in plants by a 35S promotor
V69	pXCScpmv-HA-Strep (Myrach *et al.*, 2017),	ori ColE1, ori RK2, Amp^R/Car^R, Basta, pA35S, 35S promotor, 5'UTR and 3'UTR of CPMV, HA-StrepII,	binary vector for C-terminal tagging with a HA-StrepII tag and (transient) protein production in plants, 35S promotor, viral enchancers (CMPV)
19k	p35A::p19 (Voinnet *et al.*,2003)	p35S, p19, Kan^R	binary vector for overexpression of the *silencing inhibitor p19*
V107	p415Cyc1 (ATCC®, Mumberg *et al.,* 1995)	Cyc1 Promotor, ori ColE1, Amp^R, LEU2	binary vector for protein production in *S. cerevisiae.*
V2	pET30-CTH	ori ColE1, ori RK2, Kan^R, His	*E. coli* expression vector for protein production with a C-terminal His tag

2.1.5 Contructs for the Ribokinase Study

The constructs for the study of a putative RBSKs from *A. thaliana* and *S. cerevisiae* were generated by ligation of the coding sequence (cds) into the expression vectors listed in Table 6.

Table 6: Constructs gnerated for the study of the ribokinases from *A. thaliana* and *S. cerevisiae*. Vector No.[1]: see Table 5 for vector names and descriptions.

Name	Sequence	Vector No.:[1]	Cloning	Usage
X184	At1g17160.1 cds	V69	*ClaI, XmaI*	cloning ribokinase of *A. thaliana* for C-terminal StrepII tagging and transient overexpression in *N. benthamiana*
X185	At1g17160.1 cds	V36	*ClaI, XmaI*	C-terminal tagging of *A. thaliana* ribokinase with eYFP for overexpression in *N. benthamiana* for subcellular localisation studies by confocal laser microscopy
X188	YCR036W	V69	*EcoRI, XmaI*	C-terminal tagging of ribokinase from *S. cerevisiae* for transient overexpression in *N. benthamiana*
H73	At1g17160.1 cds	V2	*NdeI, SmaI*	overexpression of *A. thaliana* ribokinase in *E. coli* for antibody production. Cloned without tag.
H131	YCR036W	V107	*XbaI, BamHI*	Overexpression of ribokinase *S. cerevisiae* in *S. cerevisiae* ribokinase mutant as complementation line

2.1.6 Constructs for Ribose Transporter Study

The constructs for the study of two putative ribose transporter in *A. thaliana* were generated by ligation into the expression vectors listed in Table 5. The resulting constructs are listed in Table 7.

Table 7: Constructs for the study on the putative ribose transporter At5g16150 (*pGLCT*) and At1g05030 (*pGLCT-LIKE*) from *A. thaliana*. Vector No.[1]: see Table 5 for vector names and descriptions.

Name	Sequence	Vector No.:[1]	Cloning	Usage
H390	At5g16150 cds	V69	*ClaI*, *XmaI*	C-terminal tagging of the pGLCT permease and transient protein production in *N. benthamiana*
H391	At5g16150 cds	V36	*ClaI*, *XmaI*	C-terminal tagging of pGLCT permease with eYFP for production in *N. benthamiana* for subcellular localisation studies by confocal laser microscopy
H392	At5g16150 cds	V69	*ClaI*, *XmaI*	Overexpression of *pGLCT* permease without tag.
H438	At1g05030 cds	V69	*ClaI*, *XmaI*	pGLCT-LIKE transporter C-terminally tagged for further analysis.
H439	At1g05030 cds	V36	*ClaI*, *XmaI*	pGLCT-LIKE transporter C-terminally tagged for confocal laser microscopy analysis.
H470	At5g16150 cds	V107	*XbaI*, *PstI*	*pGLCT-StrepII* tagged cloned without signal peptide for transient overxpression in *S. cerevisiae*
H610	At5g16150 cds	V107	*XbaI*, *PstI*	*pGLCT-YFP* tagged cloned full length for overexpression in *S. cerevisiae*
H611	At5g16150 cds	V107	*XbaI*, *PstI*	*pGLCT* without Tag cloned full length for overexpression in *S. cerevisiae*

2.1.7 Primer for the Genotyping of *A. thaliana* Plant Lines

In Table 8 the primers used for genotyping *A. thaliana* lines are listed.

Table 8: Primers used for genotyping *A. thaliana* plant line SALK005371C. No. (number of the primer). The sequence are listed in 5' - 3' orientation.

No.:	Name	5'- Sequence -3'	Description
N440	*RBSK* forward	TCCCGGGGATACTAAAT TTAAGGAGCTTCAAAA	Gene specific foward primer for genotyping the *RBSK* mutant
N443	*RBSK* reverse	GATACGCCTATACCAAA TGAGCTATTG	Gene specific reverse primer for genotyping the *RBSK* mutant
N61	T-DNA left border	TGGTTCACGTAGTGGG CCATC	Primer specific to the left border of the T-DNA

2.1.8 Primer for the Genotyping of *S. cerevisiae* Lines

Table 9: Primers used for genotyping the *S. cerevisiae* lines for the ribokinase study. The primers were recommended by the supplier Transomics (www.transomics.com). No. (number of the primer). The sequence are listed in 5' - 3' orientation.

No.:	Name	5'- Sequence -3'	Description
P28	A primer	TGATTCCTAGGGA TAAGTGTCTTTG	confirmation of yeast wild type genotype
P29	B primer	CAGCGTTAGGTAAT CTATCCGTAAA	confirmation of yeast wild type genotype
P30	kanB primer	CTGCAGCGAG GAGCCGTAAT	confirmation of yeast mutant genotype
P31	D primer	AACGTTACTGCTAT TTCTATGACCG	confirmation of yeast mutant genotype

2.1.9 Primers for Cloning *pGLCT* and *pGLCT-LIKE* into *A. tumefaciens* and *S. cerevisiae* Expression Vectors

Table 10: Primers used for cloning of *pGLCT* into *A. tumefaciens* and *S. cerevisiae* expression vectors with different c-terminal tags. The sequences are listed in 5' - 3' orientation

No.:	Name	5'- Sequence -3'	Description
P1012	pGLCT-fw	TTATCGATAAAA TGCAGTCGT- CAACG	Introducing a *ClaI* site for cloning into V36 and V69.
P1013	pGLCT-rev	TTCCCGGGAGC TCCAGATGTAAG	Introducing a *XmaI* site for cloning into V36 and V69 with expression of an C-terminal tag.
P1014	pGLCT-rev with Stop	TTCCCGGGTCAA GCTCCAGATG- TAAG	Introducing a *XmaI* site for cloning into V36 and V69 including a stop codon for expression without a tag.
P1406	pGLCT-YFPfw	TTTCTAGAAAA ATGCAGTCGT- CAAC	Cloning into V107 for over-expression in yeast introducing a *XbaI* site.
P1407	pGLCT-YFPrev	TTCTGCAGTTAC TTGTACAGCTCGT	Cloning into V107 for over-expression in yeast introducing a *PstI* site with a C-terminal YFP tag
P1408	pGLCT-rev	TTCTGCAGTTAAG CTCCAGATGTAAG	Cloning into V107 for over-expression in yeast introducing a *PstI* site without any tag.
P1136	pGLCT-LIKE-fw	TTATCGATAAAAT GTGGGTGAC- GAAT	Introducing a *XmaI* site for cloning into V36 and V69 with expression of an c-terminal tag.
P1137	pGLCT-LIKE-rev	TTCCCGGGACT CAGGTCGTCTCT	Introducing a *XmaI* site for cloning into V36 and V69 with expression of an c-terminal tag.

2.1.10 Primer for Genotyping *pGLCT* and *pGLCT*-*LIKE* Mutant Lines

The primers used for amplification by PCR and cloning into transient expression vectors are listed in Table 11.

Table 11: Primers used for the genotyping of the T-DNA mutant lines of the putative ribose transporter At5g16150 (*pGLCT*) and *pGLCT-LIKE* (At1g05030) from *A. thaliana*. The sequences are listed in 5' - 3' orientation.

No.:	Name	5'- Sequence -3'	Description
P733	At5g16150-RP	ATTTCGTGATGTTG CGTCTTC	Gene specific forward primer for genotyping the *pGLCT* mutant 1 (Ko166)
P734	At5g16150-LP	TCTGCACACTCTGA GCTGTTG	Gene specific reverse primer for genotyping the *pGLCT* mutant 1 (Ko166)
P735	At5g16150-RP	TTCGGGATGCAAAT ATCTCTG	Gene specific forward primer for genotyping the *pGLCT* mutant 2 (Ko163)
P736	At5g16150-LP	GATAGCTGGATTAC CCCTTGC	Gene specific reverse primer for genotyping the *pGLCT* mutant 2 (Ko163)
P1199	At1g05030rev	TTGGAAAAGCCGA TAACCATCC	Gene specific reverse primer for genotyping the *pGLCT-LIKE* mutant (Ko172)
P1200	At1g05030fw	TTTCTGCAAAGTGC CTCAAATGGA	Gene specific forward primer for genotyping the *pGLCT-LIKE* mutant (Ko172)

2.1.11 Primer for Semi-Quantitative RT-PCR

For evaluation of the residual transcript level in the mutant *RBSK* line Ko127 primers were designed for amplification of the cDNA fragments upstream and flanking the t-DNA insertion between exon 2 and exon 3 (Table 12).

Table 12: Primers used for semi-quantitative reverse transcriptase PCR for evaluation of the *RBSK* transcript in *A. thaliana* mutant plant lines. The sequences are listed in 5' - 3' orientation.

No.:	Name	5'- Sequence -3'	Description
P374	At1g17160-E1 fw	GGTTCACTTGG ACTACGTGAGAT	Primer for RT-PCR binds in Exon 1 before the t-DNA insertion.
P375	At1g17160-E2 rev	AATCCAATAGCTCA TTTGGTATAGG	Primer for RT-PCR binds in Exon 2 before the t-DNA insertion.
P376	At1g17160-E2 fw	GGAATGGATACGC CTATACC	Primer for RT-PCR binds in Exon 2 overlapping the t-DNA insertion
P377	At1g17160-E3 rev	CATAGCGACTGCAA ATGCTG	Primer for RT-PCR binds in Exon 3 overlapping the t-DNA insertion

For evaluation of the residual transcript level in the mutant *pGLCT-LIKE* line Ko172 primers were designed for amplification of the cDNA fragments flanking the t-DNA insertion in exon 1 (Table 13).

Table 13: Primers used for semi-quantitative reverse transcriptase PCR for evaluation of the *pGLCT-LIKE* transcript in *A. thaliana* mutant plant lines. The sequences are listed in 5' - 3' orientation.

No.:	Name	5'- Sequence -3'	Description
P1199	Glct-like_RTrev	TTGGAAAAGCCGA TAACCATCC	Primer for RT-PCR binds in Exon 2 after the T-DNA insertion.
P1465	Glct-like_RTfw	CTCTCCGATCA TGTGGGTG	Forward primer for RT-PCR binds 10 bp upstream start ATG.

2.1.12 *A. thaliana* T-DNA Mutant Lines

The following *A. thaliana* T-DNA mutant lines were obtained from the SALK collection (Alonso *et al.*,2003) or the GABI-Kat collection (Kleinboelting *et al.*, 2012), respectively. The mutant lines used in this study are presented in the Table 14.

Table 14: *A. thaliana* T-DNA mutant lines. Ko. stands for the 'knock out' number

Ko.:	Name	Ecotype	Line	Mutagen	Reference
25	*xdh1-2*	Col-0	GK049D04	T-DNA	(Hauck *et al.*, 2014) ; (Ma *et al.*,2016)
28	*gsda2*	Col-0	GK432D08	T-DNA	(Dahncke *et al.*, 2013)
29	*hgprt-2*	Col-0	GK015E03	T-DNA	(Schroeder *et al.*,2018)
34	*nsh1-1*	Col-0	SALK083120C	T-DNA	(Jung *et al.*,2011)
83	*cda-2*	Col-0	GK64H07	T-DNA	(Chen *et al.*, 2016)
127	*rbsk*	Col-0	SALK005371C	T-DNA	(Riggs *et al.*,2016)
163	*pglct-2*	Col-0	SALK078684C	T-DNA	(Cho *et al.*,2011)
166	*pglct-1*	Col-0	SALK051876	T-DNA	(Cho *et al.*,2011)
172	*pglct-like*	Col-0	SALK050278	T-DNA	-

2.1.13 *A. thaliana* Stable Expression Lines

For the development of complementation lines, *A. thaliana* mutant lines were transformed with *A. tumefaciens* carrying constructs of interest for stable overexpression (Table 15). The procedure of *A. thaliana* transformation and selection is described in Chapter 2.2.26.

Table 15: Transgenic *A. thaliana* lines transformed with *A. tumefaciens* expression vectors.

No.:	Name	Background	Promotor	Gene	Tag	Resistence
X184	RBSK	*rbsk*	35S	RBSK	StrepII	*Basta*
H391	pGLCT-YFP	*pglct-2*	35S	*pGLCT*	eYFP	*Basta*
H392	pGLCT	*pglct-2*	35S	*pGLCT*	no tag	*Basta*

2.1.14 *A. thaliana* Double Mutant Lines

For this study *A. thaliana* double mutants were produced by manual pollination of the mutant mother plant with the male pollen of the mutant father plant. In Table 16 the double mutants used in this study are described with listing of the parental plants.

Table 16: Crosses of *A. thaliana* single mutants for production of homozygous double mutants.

No.:	Name	pollen donor	pollen recipient
C50	*xdh1 nsh1*	Ko25	Ko34
C68	*hgprt gsda2*	Ko29	Ko28
C168	*rbsk gsda2*	Ko127	Ko28
C169	*rbsk nsh1*	Ko127	Ko34
C170	*rbsk cda*	Ko127	Ko83

2.1.15 Software and Databases

Table 17: Software and databases used in this study for data collection and analysis.

Software name	Web address	Purpose
BLAST	https://blast.ncbi.nlm.nih.gov/Blast.cgi	sequence analysis
Blender	https://www.blender.org/	3D graphical design
Boxshade	https://embnet.vital-it.ch/software/BOX_form.html	visualisation of multiple sequence alignments
BRENDA	https://www.brenda-enzymes.org/	enzyme database
ClustalO	https://www.ebi.ac.uk/Tools/msa/clustalo/	multiple sequence alignments
eFP browser	http://bar.utoronto.ca/efp2/Arabidopsis/Arabidopsis_eFPBrowser2.html	gene expression analysis
GraphPad Prism 4	-	statistical analysis
Image J	https://imagej.nih.gov/ij/	photo analysis
ImagingWinGigE V2.47+	https://www.walz.com/index.html	darks stress analysis
Phytozome	https://phytozome.jgi.doe.gov/pz/portal.html	sequence analysis
TAIR	https://www.arabidopsis.org/	molecular and genetic database for *A. thaliana*
T-DNA express	http://signal.salk.edu/cgi-bin/tdnaexpress	T-DNA mutant line gene map database for *A. thaliana*

2.2 Methods

2.2.1 Genomic DNA Extraction From *A. thaliana* Leaf Material

For extraction of genomic DNA the extraction method by Edwards *et al.* (1991) was used. One leaf from an *A. thaliana* plant was cut and placed in a reaction tube together with five to seven 1 mm metallic beats and 200 µl DNA extraction buffer (Table 18) was added. The samples were ground by a retchmill (*Ratch*, MM400) for 1 minute at a frequency of 28 s^{-1}. Followed by adding 10 µl 10% SDS (sodium dodecyl sulfate) the solution was mixed by inverting the tube three to four times. After a centrifugation step at 17,000g

for 3 minutes 100 µl of the supernatant were transferred to a new reaction tube and 75 µl of isopropanol were added. The solutions were mixed by inverting the tube three to four times followed by a centrifugation step at $17,000\,g$ for 10 minutes. Afterwards the supernatant was discarded completely and the pellet was washed with 100 µl 70% ethanol followed by another centrifugation step at the same speed for 3 minutes. Subsequently the supernatant was discarded and the pellet was dried at room temperature until all residual Ethanol was evaporated. 100 µl ddH$_2$0 were added to dissolve the pellet.

Table 18: Buffer for DNA Extraction from *A. thaliana*

Name	Content
DNA extraction buffer	200 mM Tris(hydroxymethyl)aminomethane-HCl (Tris-HCl)(pH7.5)
	200 mM NaCl
	25 mM ethylendiamintetraacetate (EDTA)

2.2.2 RNA Extraction and cDNA Sythesis

50 mg of harvested leaf material were ground and 1 ml of *TRIsure* (Bioline) was added and the samples were vortexed. Followed by an incubation at room temperature for 10 minutes. The samples were centrifuged at $12000\,g$ for 10 minutes at 4°C and the supernatant was transferred to an new reaction tube followed by the addition of 200 µl chloroform. The samples were well mixed and incubated at RT for 3 minutes followed by a centrifugation for 15 minutes at $12000\,g$ (4°C). The upper liquid phase containing the RNA was transferred into a new reaction tube and mixed with 500 µl 2-propanol for RNA precipitation and incubated at RT for 10 minutes. After a centrifugation the supernatant was discarded and the pellet was washed with 1 ml 70% Ethanol. Following another centrifugation for 5 minutes at $7500\,g$ (4°C), the pellet was air dried and re-solubilized in 50 µl RNAse-free water.

To 20 µl RNA 2 µl of DNase were added and the mixture was incubated at 60°C for 30 minutes. The activity of the DNase was terminated by addition of 2 µl EDTA (50 mM) and incubation for 10 minutes at 65°C. 8 µl H$_2$O and 2 µl DNA-lading buffer were added to 1 µl RNA followed by an separation on a 1% agarose gel by electrophoresis. For the reverse transcriptase reaction the sample containing 1 µl oligodT primer (37,5 µM), 7 µl H$_2$O and 6 µl of the RNA (total 1 µg) was incubated for 5 minutes at 70°C and afterwards placed on ice. 11 µl of the reverse transcriptase master mix with 5 µl 5x buffer, 1,25 µl dNTPS (2,5 mM), 1 µl reverse transcriptase and 3,75 µl H$_2$O were added to the RNA and incubated for 1 h at 42°C. After the reaction was finished the sample was stored at -20°C.

2.2.3 Polymerase Chain Reaction

The polymerase chain reaction (PCR) is a technique to amplify specific DNA fragments from a mixed template sample by specific oligonucleotides, called primers. As template plant genomic DNA, cDNA or plasmid DNA be used. The primer binds during the 'Primer annealing' phase to the specific nucleotide sequence they were designed for. A default PCR program is shown in Table 19.

Table 19: Default PCR programm. Individual steps can vary for different polymerases and size of the amplificated DNA fragment

No.:	Step	Temperature	Duration
1	First denaturation	95°C	10 minutes
2	Denaturation	95°C	10 - 30 seconds
3	Primer Annealing	55 -65°C	10 - 30 seconds
4	Elongation	72°C	30 - 90 seconds
5	Termination	72°C	10 minutes
	Step 2 - 4 were repeated 25-40 time		

For amplification a Taq polymerase purified in our own lab was used in case of plant genotyping and a Phusion Taq polymerase (New England Biolabs) was used for gene amplification, if the PCR product was supposed to be used for cloning. The sample preparation is listed in Table 20.

Table 20: Chemicals used for one PCR reaction. The PCR buffer was chosen according to the polymerase protocol.

Chemical	Volume
Thermo Pol buffer (10x)	2 µl
(*New England Biolabs*)	
Primer (4 mM)	2.5 µl
dNTPs (10 mM)	1.6 µl
DNA	0.5 - 1 µl
ddH$_2$0	up to 20 µl

After the PCR reaction, 20 µl of the sample were mixed with 3 µl DNA loading buffer (10x) (Table 21). The gels were prepared by melting 1% agarose (w/v) in TAE Buffer (1x) and adding *Midori Green (Nippon Europe Genetics)* according to the supplier's recommendation.

Table 21: Loading and running buffers for 1% agarose gels for electrophoretic separation of DNA bands

Name	Content
DNA loading buffer (*Orange G*)	15 ml glycerol
	100 mg Orange-G (AppliChem GmbH)
	filled up to 50 ml with ddH$_2$O
TAE buffer (10x)	20 mM Tris-HCl
	10 mM acetic acid

2.2.4 Cloning

For cloning methods like PCR, gel electrophoresis, digestion with restriction enzymes and ligation were used. The DNA was separated on a 1% agarose gel and the bands of interest where extracted from the gel. The DNA was purified by a *high pure PCR Cleanup Makro Kit* (Roche) and the digestion was performed with restriction enzymes from New England Biolabs according to the supplier's recommendations. The target vectors where dephosphorylated by shrimp phosphatase prior to the ligation by T4 ligase (both *New England Biolabs*). For isolation of plasmid DNA from *E. coli* were performed with the *GenJet* plasmid miniprep kit (*Fermentas*).

2.2.5 Sequencing

Sequencing of the nucleic acids used for cloning was carried out by *GATC Biotech* or *SEQ-Lab*. 1 µg DNA was mixed with 3 µl of 10 mM primer and filled up to 15 µl total volume with ddH$_2$0. The tubes were send to the companies and the evaluation of the sequencing result was performed with *Vector NTI* (*Invitrogen*).

2.2.6 Preparation of Chemo Competent DH10α *Escherichia coli* Cells

Escherichia coli DH10α cells were grown for 24 h on a *LB* plate without antibiotic selection at 37°C. A colony was picked and used for inoculation of 250 ml liquid *SOB* media in a 1 l flask (Table 22). The flask was incubated over night at 19°C and 200 rpm in a shaker. The cells were grown up to an optical density (OD$_{600}$) of 0.5 (24 - 36 h) and afterwards placed on ice for 15 minutes. The cells were harvested by centrifugation at 3,000g for 10 minutes at 4°C.

The pellet was re-suspended by 80 ml of cold TB buffer (4°C) and incubated on ice for 10 minutes followed by another centrifugation step. The supernatant was discarded and

Table 22: Solutions used for the preparation of chemo competent *E. coli* cells

Solution	Content
SOB solution	0.5% yeast extract
	2% tryptone
	10 mM NaCl
	2.5 mM KCl
	10 mM MgCl$_2$
	10 mM MgSO$_4$
TB buffer	10 mM piperazine-N,N'-bis(2-ethansulfonic acid) (PIPES)
	15mM CaCl$_2$
	250 mM KCl
	adjust pH to 6.7
	55 mM MnCl$_2$
	sterile filtered through 45 µm filter and stored at 4°C

the cell pellet was resuspended in 20 ml cold TB buffer (4°C) and 1.4 ml dimethyl sulfoxide (DMSO). The DMSO was stored at -20°C overnight before usage. Afterwards the cells were separated into 50 µl aliquots and frozen by cooling in liquid nitrogen. The aliquots were stored at -80°C for further use.

2.2.7 Transformation of Chemo Competent *E. coli*

For transformation of chemo competent DH10α (*E. coli*) cells with a plasmid, 50 µl aliquots were thawed on ice. 3 µl of plasmid prep were added to the cells, mixed and incubated on ice for 10 minutes. The heat shock was performed by incubating the cells for 40 seconds at 42°C followed by a 2 minutes resting phase on ice. Afterwards 900 µl of *LB* media were added to the cells. For recovery, the *E. coli cells* were shaken for 1 h at 37°C and 200 rpm. The cells were centrifuged at 17,000g for 30 seconds. The supernatant was discarded and the pellet was resuspended and plated on plates with*LB* media, containing the antibiotic suitable selection.

2.2.8 Transformation of Electro Competent *Agrobacterium tumefaciens* Cells

Aliquots with 50 µl of electro competent *Agrobacterium tumefaciens* (*A. tumefaciens*) cells, thawed on ice and 0.5 µl of plasmid DNA was added to the cells (50 ng). The mixture was incubated on ice for 10 minutes and transferred to a electroporation cuvette with 5 mm gap, the *BioRad* electroporation system was used for transformation with the pre set *ArgT* program. 900 µl of *YEB* media were quickly added followed by an incubation for 1 h at 28°C in the shaker at 180 rpm. On *YEB* plates with 50 µg ml^{-1} Kanamycin,

100 µg ml $^{-1}$ Rifampicin, 15 µg ml $^{-1}$ Gentamicin and 75 µg ml $^{-1}$ Carbenicillin (*YEB* complete plates) 5 - 10 µl of the cells were plated and incubated for 2 - 4 days at 28°C. Afterwards single colonies were transferred to new *YEB* complete plates and grown for 2 days under similar conditions.

2.2.9 Preparation of an *A. tumefaciens* Glycerol Stock

The glycerol stocks of *A. tumefaciens* were prepared for long time storage of the transformed cells. For a liquid over night culture 12 ml of *YEB* were inoculated with 2 - 3 loops of bacterial cells from plates and incubated at 28°C and 180 rpm on a shaker over night. 1 ml of the liquid overnight culture was transferred in to a 2 ml screw lid tube and afterwards centrifuged at $3,000g$ for 3 minutes. The supernatant was discarded and the pellet was resuspended in 500 µl of bacterial culture and 500 µl of 50% glycerol solution were added to the bacterial solution. After vortexing the cells were cooled down in liquid nitrogen followed by the storage of the glycerol stocks at -80°C.

2.2.10 Growing Conditions of *A. tumefaciens* Cells

For the growth of *A. tumefaciens*, *YEB* plates with 2% agar (Thermo Fisher) were used including antibiotics (Chapter 2.2.8). The cells were streaked on the plates from a glycerol stock and incubated at 28°C for 2 - 3 days. Liquid over night cultures were prepared as in Chapter 2.2.9 described.
The growing conditions of the coinfiltrated *A. tumefaciens* strain p19 (Voinett *et al.*, 2003) differs in antibiotic resistance and were grown on *YEB* plates with 100 µg ml $^{-1}$ Rifampicin and 15 µg ml $^{-1}$ Gentamicin for 1 day at 28°C.

2.2.11 Transformation of *S. cerevisiae* Cells

From a *Saccharomyces cerevisiae* (*S. cerevisiae*) overnight culture cells were taken for inoculation of a 50 ml *YPD* media culture to an OD_{600} of 0.3. The 50 ml culture was incubated at 30°C until the OD_{600} reached 0.6 - 0.9. Afterwards the culture was transferred into a falcon tube and centrifuged at $3,000g$ for five minutes at room temperature.
The supernatant was discarded and the cell pellet was resuspended in 1 ml Mix 1 (Table 23) and incubated for 10 minutes at room temperature. During this step the herring sperm DNA (Sigma) was heated for five minutes at 95°C followed by cooling down the reaction tube on ice. 1 µg of plasmid DNA were mixed with 10 µl of boiled herrings sperm DNA and mixed with 700 µl of Mix 2. This solution was mixed by vortexing prior to addition of 100 µl of the *S. cerevisiae* cells and followed by another vortexing step. This transformation reaction was incubated at 30°C for 15 -30 minutes when 30 µl of DMSO were added to the reaction tube and vortexed again followed by an incubation at 42°C for another 15 - 30 minutes. Afterwards, the cells were centrifuged for 1 - 3 minutes at $5,000g$,

Table 23: Components used for preparation of the buffers necessary for *S. cerevisiae* transformation

Name	Content
Mix 1	0.1 M Li acetate
	1.0 M sorbitol
	0.5x TE buffer pH 7.5
	up to 10 ml with ddH$_2$O
	sterile filtration after preparation
Mix 2	0,1 M Li acetate
	60% PEG 3350
	1 x TE buffer pH 7.5
	ddH$_2$O up to 3 ml

the supernatant was discarded and the cell pellet was resuspended in 200 µl ddH$_2$O. The the cells were plated on *SD* selection media and incubated for three days at 30°C (50 µl).

2.2.12 Growing Conditions of *Saccharomyces cerevisiae* Cells

The strains of (*S. cerevisiae*) including the *rbsk* (YCR036W) and the parental lines where obtained from Transomics (www.transomics.com). The yeast cells were grown on *YPD* full media plates containing 2% of agar for 2 days at 30°C. The *rbsk* complementation strains was grown on special selection media (SD) lacking the amino acid leucine as selection marker for the introduced plasmid. The growth conditions on the plates were identical regardless of the media used.

2.2.13 Extraction of Genomic DNA from *S. cerevisiae*

The genomic DNA extraction from *S. cerevisiae* cells was performed by a protocol published by Harju *et al.* (2004). The composition of the *Harju* buffer can be found in Table 24. Alternatively to the usage of liquid overnight cultures the cells can be taken directly from the *YPD* media plates.

Table 24: buffers and solution for DNA extraction from *S. cerevisiae*

Name	Content
Harju buffer	2% Triton X-100
	1% SDS
	100 mM NaCl
	Tris-HCL (pH 8.0)
	1 mM EDTA

200 µl of Harju buffer were added to the pellet and the reaction tube was closed firmly. Alternating, the tube was frozen in liquid nitrogen for 2 minutes and boiled (85 - 95°C)in a water bath for 2 minutes, three times. In between the freezing and boiling procedure the cells were vortexed for 30 seconds. 200 µl chloroform were added followed by vortexing for 2 minutes. The cells were centrifuged for 3 minutes at room temperature ($20,000g$) and the upper aqueous phase was transferred into a new reaction tube with 400 µl ice cold ethanol (100%) and mixed by inversion of the tube. The samples were incubated for 5 minutes at room temperature followed by a cetrifugation at $20,000g$ for 5 minutes (room temperature). The supernatant was discarded and the pellet was washed with 500 µl 70% ethanol, followed by a centrifugation step. The supernatant was removed and the pellet was air dried at room temperature and afterwards resuspended in 25 to 50 µl ddH$_2$O and stored at -20°C. The extraction was followed by an RNaseA treatment to clean the preparation from residual RNA.

2.2.14 Transient Protein Production in *Nicotiana benthamiana*

For the agrobacteria mediated protein production in *Nicotiana benthamiana* (*N.bethamiana*), *A. tumefaciens* cells were grown as described in Chapter 2.2.10. After overnight incubation of the liquid culture, the cells were pelleted at $4,000g$ for 15 minutes. The supernatant was discarded and the pellet was resuspended in infiltration buffer (Table 25). The OD of the bacterial cultures were measured. Prior to infiltration of the *N. benthamiana* leaves, the *A. thumefaciens* cells with the construct of interest were mixed with *A. thumefaciens* cells carrying a plasmid with the cds of the tomato bushy stunt virus protein (p19) for prevention of post transcriptional gene silencing in *N. banthamiana* (Vionnet *et al.*, 2003). For the coexpression, an OD$_{600}$ of 0.5 for the *A. thumefaciens* with the construct of interest and an OD$_{600}$ of 0.25 for the *P19 A. tumefaciens* strain was adjusted. After mixing of the two *A. tumefaciens* strains the bacterial mixture rested at room temperature for 2 h prior to the infiltration of young *N.bethamiana* leaves by a syringe. After 3 to 5 days, the infiltrated leaves were harvested for further analysis.

Table 25: Buffer components used for infiltration of *N. benthamiana* plants.

Name	Content
Infiltration buffer	10 mM MES pH 5.,6 (2-(N-morpholino)ethanesulfonic acid)
	10 mM $MgCl_2$
	150 µM Acetosyringone

2.2.15 Protein Extraction and Affinity Purification from *N.bethamiana* Leaves

3-5 days after the infiltration with the *A. tumefaciens* strains, 0.75 g leaf material was harvested and ground with 1.5 ml of protein extraction buffer (Table 26) with a mortar and a pestle. The liquid was transferred into a 2 ml reaction tube and centrifuged at $20,000\,g$ for 15 minutes. This and the following centrifugation steps were performed at 4°C.

Table 26: Buffer components used for affinity protein purification by a StrepII tag.

Name	Content
Protein Extraction buffer	100 mM HEPES pH 8.0
	5 mM EDTA
	0.1 mg ml^{-1} Avidin
	15 mM DTT
	100 mM NaCl
	0.5% Triton X-100
Protein washing buffer	100 mM HEPES pH 8.0
	100 mM NaCl
	0.5 mM EDTA
	0.005% Triton X-100
	2 mM DTT
Protein elution buffer	100 mM HEPES pH 8.0
	0.5 mM EDTA
	100 mM NaCl
	0.005% Triton X-100
	2.5 mM Biotin
	2 mM DTT

After the centrifugation, the supernatant was transferred into a new reaction tube and mixed with 40 µl of *StrepTactin Macroprep* (50% suspension, IBA) and incubated for 10 minutes on a rotating wheel, for the StrepII tag to bind to the *StrepTactin* beads. The samples were centrifuged at $700g$ for 30 seconds and the supernatant was discarded. The pellet was resuspended in 500 µl washing buffer followed by another centrifugation. This washing procedure was repeated four times. The elution was performed in a two step procedure. After the fifth washing step the supernatant was discarded and 75 µl of elution buffer were added to the pellet. The samples were shaken at room temperature on a thermo block at 800 rpm for 5 minutes, followed by a 30 second centrifugation step at $700g$ and 4°C. This elution step was repeated and both elution fractions were combined in one reaction tube and cooled down in liquid nitrogen. The protein preparations were stored at -80°C.

2.2.16 Total Protein Extraction from *S. cerevisiae* Cells

The extraction of total protein was performed using a protocol from Zhang *et al.* (2011). For this 1.5 ml of *S. cerevisiae* cells with an OD_{600} of 1.0 were taken from a liquid over night culture and strongly centrifuged. The supernatant was discarded and the pellet was incubated for five minutes with 2 M LiAc (litium acetate) on ice followed by another centrifugation step. The supernatant was discarded again and the pellet was incubated in 0.4 M NaOH for 5 minutes on ice followed by a centrifugation step. Afterwards the cells were resuspended in 100 µl 1x SDS loading buffer and incubated at 95°C for five minutes followed again by a centrifugation step. The supernatant was transferred into a new reaction tube and 10 µl of the sample were loaded on a SDS polyacylamide gel. The protein sample was stored at -80°C if necessary.

2.2.17 SDS Polyacrylamide Gel Electrophoresis

For preparation of SDS polyacrylamide gels the chemicals for the resolving gel (Table 27) were mixed to reach a final acrylamide/ bis-acrylamide concentration of 10% and pipetted into the Biorad casting system resulting gels of 7.5 mm thickness. The solution was overlaid with water saturated N-butanol for guaranteeing an even surface between the stacking and the resolving gel. After 20 minutes of polymerisation the stacking gel mixture was prepared and poured into the casting system after the N-butanol was removed.
The samples were mixed with 5x SDS running buffer and incubated at 95°C for 10 minutes to denature the proteins. 10 µl of the samples were pipetted into the gel pockets and 5 µl of Protein pre-stained marker (*Thermo Scientific*) was included on each gel. The samples were separated at 80 V until they reach the resolving gel followed by an increase up to 120 V until the running front reaches the bottom end of the gel.

Table 27: Composition of the buffers used for preparation and perfomance of a SDS-polyacrylamide gel electrophoresis.

Name	Content
resolving gel (10%)	375 mM Tris-HCL (pH 8.8)
	10% acrylamide : Bis-acrylamide (37.5 : 1)
	0.1% (w/v) SDS
	0.075% (w/v) ammonium persulfate (APS)
	0.05% (w/v) tetramethylethylenediamine (TEMED)
SDS loading buffer (5x)	300 mM Tris-HCl pH6,8
	600 mM dithiotreitol (DTT)
	10% SDS
	50% glycerol
	0.2% bromphenol blue
SDS running buffer (10x)	250 mM Tris
	1.92 M glycine
	1% SDS
stacking gel buffer (4%)	125 mM Tris-HCl (pH 6.7)
	4% acrylamide : Bis-acrylamide (37.5 : 1)
	0.1% (w/v) SDS
	0.075% (w/v) APS
	0.05% (w/v) TEMED

2.2.18 Immunoblot

For an immunoblot analysis the proteins were separated by SDS polyacrylamide gel electrophoresis (Chapter 2.2.17) followed by a transfer of the proteins to a nitrocellulose membrane (*Roth*) by the semi dry procedure with 1x blotting buffer (Table 28). The transfer was performed according to supplier's recommendations (*BioRad*).

Table 28: Buffer solutions used for the semi dry immunoblot procedure

Name	Content
blotting buffer (1x)	80 ml blotting buffer (10x)
	200 ml methanol
	up to 1 l
blotting buffer (10x)	480 mM Tris-HCl
	390 mM glycine
	4.3 mM SDS

2.2.19 Immunoblot Detection

After the protein was transferred onto the nitrocellulose membrane 10 ml of blocking solution (Table 29) were added and the membrane was incubated over night at 4°C with moderate shaking. Afterwards the membrane was washed three times with 25 ml TBS-T before adding the first antibody in 10 ml TBS-T to the membrane (Table 30).

Table 29: Components used for alkaline phosphatase western blot detection

Name	content
AP buffer	100 mM Tris (pH 9.5)
	100 mM NaCl
	5 mM $MgCl_2$
BCIP	(50 ng ml^{-1}) 5-bromo-4-chloro-3-indolyl phosphate (BCIP) in dimethylformamide (DMF)
blocking solution	1 mg milk powder
	in 20 ml TBS-T
NBT	(50 ng ml^{-1}) nitro blue tetrazolium chloride (NBT) in 70% DMF
TBS buffer (10x)	1 M Tris-HCL (pH 7.5)
	5 M NaCl
	fill up to 1 l
TBS-T	100 ml TBS buffer (10x)
	1 : 1,000 Tween 20
	fill up to 1 l

After 1 h of incubation with the primary antibody, the membrane was washed again three times with 25 ml TBS-T for 10 minutes, followed by the incubation with the secondary

antibody in 10 ml TBS-T for 1 h. The membrane was again washed thoroughly for three times with TBS-T and afterwards 10 ml of the alkaline phosphatase detection solution was added containing 10 ml of AP buffer (Table 29) and 66 µl of NBT and 66 µl of BCIP.

Table 30: Antibodies used in this study

Antigen	organism	working concentration
YFP	mouse	1 : 5,000
StrepII	mouse	1 : 10,000
RK*At*	rabbit	1 : 500
mouse IgG - AP	goat	1 : 30,000

In case of the Strep-tag detection alternatively a one step detection with *StrepTactin* conjugated to an alkaline phosphatase was sometimes used. For this, after the first three times of washing the membrane with TBS-T for 10 minutes, 2,5 µl of the StrepTactin-AP-conjugate were added in 10 ml of TBS-T to the membrane and incubated for 1 h. This was followed by three washing steps with 25 ml of TBS-T for 10 minutes. The detection was performed similar as described before for the two step detection method.

2.2.20 ADP Assay for Kinase Activity Analysis by HPLC

This assay was established for the enzyme activity analysis of the ribokinase (RBSK) enzymes from *A. thaliana* and *S. cerevisiae*. Ribokinases are phosphotransferases using ATP to phosphoprylate ribose to D-ribose 5-phosphate releasing ADP. With HPLC (high performance liquid chromatography) the conversion of ATP to ADP was quantified. An Agilent 1200 SL system equipped with a diode array detector (254 nm and 360 nm reference) was used running an ion pairing reverse-phase chromatography column (Polaris 5 C18-A 150 x 4.6 mm, Agilent).

Table 31: HPLC method for the quantification of ATP and ADP. As organic phase B acetonitrile was used. For the entire method 1 ml min^{-1} flow was used.

Minute	% B
0	5
1	5
6	95
6.1	100
7	100
7.1	5
Stop at 9 minutes	

As mobile phase A 10 mM ammonium acetate with 10 mM TBA (tetra-butyl ammonia hydroxide) at pH 7.0 was used while for the organic phase 100% acetonitrile was used. The flow rate was set to 1 ml min^{-1} and the breakpoints of the method are shown in Table 31.

Table 32: Composition of the enzyme reaction sample for RBSK activity analysis. The concentration of the substrate D-ribose varied according to the assay parameter.

Volume	Chemical
10 µl	5x kinase buffer
10 µl	0.5 mM KCl
10 µl	0.5 mM ATP
10 µl	substrate (D-ribose)
10 µl	purified enzyme
50 µl	total volume

The enzyme reaction was started by addition of the purified enzyme to the premixed reaction mix (Table 32). The reaction was incubated at 30°C for different time periods depending on the assay conditions. The reaction was stopped by adding 100 µl methanol to precipitate the enzyme, followed by a strong centrifugation at 20,000g for 10 - 15 minutes. The supernatant was transferred carefully into a new reaction tube. The methanol was evaporated during in a speedvac for about 1 h. Afterwards the pellet was resuspended in 50 µl of mobile phase A and placed on a shaker for 10 - 15 minutes for resolubilisation of the pellet. The supernatant was subsequently transferred into a HPLC vial with a conic bottom tube and placed into the pre-cooled (4°C) HPLC sampler.

Table 33: Composition of the kinase reaction buffer

Name	Content
Kinase reaction buffer	200 mM Tris pH 7.5
(5x)	10 mM $MgCl_2$

2.2.21 Methabolite Analysis by LC-MS

For the metabolite analysis of plant extracts an Agilent HPLC 1200 system coupled to an Agilent 6460 triple quadrupole mass spectrometer (MS) was used. For analysis of the peaks detected by the MS the *Qualitative Analysis* tool was used (Agilent Technologies). The D-ribose was separated on a Hypercarb column (50 x 4.6 mm, particle size 5 μm) from Thermo Scientific. The other compounds were separated on a Polaris 5 C18A column (50 x 4.6 mm, particle size 5 μm) from Agilent Technologies. The organic solutions and water in LC-MS quality were obtained from AppliChem GmbH. The details for the LC-MS methods are provided in Table 34 and Table 35.

Table 34: LC-MS source parameters used for the different columns in this study.

	Hypercarb column	Polaris 5 C18A column
ion source	AJS ESI	AJS ESI
gas temperature	150°C	250°C
gas flow	11 l min^{-1}	12 l min^{-1}
nebulizer	40 psi	35 psi
sheat gas heater	300°C	400°C
sheat gas flow	11 l min^{-1}	12 l min^{-1}
capillary	2000 V	3,500 V

Table 35: Details of the metabolites detected by LC-MS. product ion[e]: product ions are experimentally identified and available in the METLIN database (metlin.scripps.edu).

metabolite	formula	mono-isotopic mass	precursor ion	fragmentor (V)	product ion[e]	collision energy (V)	retension time (min)
D-ribose	$C_5H_{10}O_5$	150.1	149.0	80	89 [e]	5	1.13
					59.1 [e]	13	
5-^{13}C-ribose	*$C_5H_{10}O_5$	151.1	150.1	80	89.9 [e]	5	1.13
					59.2 [e]	13	
guanosine	$C_{10}H_{13}N_5O_5$	283.1	284.1	90	152 [e]	10	3.21
					135 [e]	45	
^{15}N$_5$-guanosine	$C_{10}H_{13}$*N_5O_5	288.1	289.1	90	157 [e]	10	3.21
					139 [e]	45	
xantosine	$C_{10}H_{12}N_4O_6$	284.1	285.1	60	153 [e]	5	1.05
					135.9 [e]	35	
uridine	$C_{10}H_{12}N_2O_6$	244.1	245.2	85	113 [e]	14	1.68
					133 [e]	14	
^{15}N$_2$-uridine	$C_{10}H_{12}$*N_2O_6	246.1	247.2	85	115 [e]	14	1.68
					112	10	
cytidine	$C_9H_{13}N_3O_5$	243.1	244.2	150	112 [e]	10	1.14
					133	10	
^{13}C$_5$-cytidine	*$C_9H_{13}N_3O_5$	248.1	249.2	150	133	10	1.14
					112 [e]	18	
guanine	$C_5H_5N_5O$	151.0	152.1	118	135 [e]	18	1.59
					110 [e]	22	
xanthine	$C_5H_4N_4O_2$	152.0	153.1	100	136 [e]	15	1.29
					55.2 [e]	33	

2.2.22 Sample Preparation for D-Ribose Measurement by LC-MS

Sample preparation for metabolite analysis was usually performed using fresh plant material or from freeze dried samples in case of dark stressed plant material. Plants treated for several days with absence of light were harvested into falcon tubes by the end of the experiment. The samples were placed into a freeze drying machine (*Alpha 1-2 LDplus*, Christ) and dried for 24 h. From the freeze dried samples 10 - 20 mg were used for extraction. From fresh material, 50 - 100 mg were weight into new reaction tubes.

All of the following steps were performed under constant cooling. To the samples 500 µl LC-MS extraction buffer (Table 36), including the labelled internal standards (ISTD),

were pipetted and mixed by vigorously vortexing the samples. After a centrifugation (4°C) at 20,000g for 10 minutes, 300 µl of the supernatant were taken into a new reaction tube and the samples were placed into a speedvac for 1 hour. The pellets were re-suspended in 5% acetonitrile, and vortexed again to resolubilise residual metabolites sticking to the reaction tube wall. Followed by a strong centrifugation at 60,000g for 10 minutes (4°C) to dispose of potential precipitates in the sample. 120 µl of the samples were transferred into a 8 mm LC-MS vials with flat glass inlet and were placed into the LC-MS machine. The quantification of D-ribose during the ribokinase project was conducted in the single ion monitoring mode whereas for the ribose transporter project the dynamic multiple reaction monitoring (MRM) mode was used.

Table 36: Buffers used for extraction of metabolites from *A. thaliana* and *S. cerevisiae* for later analysis by LC-MS.

Name	Content
LC-MS extraction buffer	2 : 2 : 1 (v/v/v) methanol : acetronitrile : LC-MS grade water
LC-MS resuspension buffer	LC-MS grade water
	5% acetonitrile

In case of the measurement of other metabolites by LC-MS the extraction was performed as mentioned above. In Table 35 the labelled compounds used as internal standard (ISTD) are shown. The ISTDs were included into the LC-MS extraction buffer. For the compounds xanthosine, xanthine and guanine only external standards were available.

2.2.23 Extraction of Metabolites from *S. cerevisiae* Cell Culture Samples

S. cerevisiae cultures (25 ml) were inoculated from an over night culture to an OD$_{600}$ of 0.4 and grown at 30°C up to an OD$_{600}$ of 1.0. After a centrifugation step at 20,000g for 10 minutes (4°C), the cells were washed with ddH$_2$O followed by another centrifugation step at similar conditions. The pellet was solubilized in 500 µl ddH$_2$O and pressed trough a 18-gauge needle into steel grinding container, pre-cooled with liquid nitrogen and containing a 1 cm steel bead. The samples were ground three times at 26 Hz for 2:30 minutes with a swing mill (Ratch, MM400) with intermediate cooling steps in between the grinding steps. Afterwards the samples were aliquoted for later metabolite extraction (Chapter 2.2.22).

2.2.24 Growth Conditions for *A. thaliana* Plants

The growing conditions of *A. thaliana* were 16 h of light (100 µE) and 8 h of dark period at 22°C or 18°C, respectively, at 70% humidity and under full nutrient supply (Table 37). if the growing conditions were altered, these conditions are indicated in the respective experiment.

Table 37: *A. thaliana* plant soil composition

Soil name	Composition
Stecklingsmedium for *A. thaliana* (Klasmann-Deilmann GmbH)	75% high moor peat 25% perlite with full nutrient supply pH 5.5
White peat soil for dark stress experiments	100% white peat soil with full nutrient supply

2.2.25 Composition of the Modified *Murashige and Skoog* Media

For the cultivation of *A. thaliana* plants on *MS*-Agar plates the original Murashige & Skoog media (*Murashige and Skoog* 1962) was optimized according to the needs of *A. thaliana* plants. In the following Table 38 the concentrations of macro- and micro nutrient solutions as well as of the iron sulphate solution are listed. For the experiment 0,5 times concentrated *MS* was used.

Table 38: Composition of the modified *Murashige Skoog* (*MS*) media

Solution	Composition
Macronutrients (10x)	187 mM KNO_3
	30 mM $CaCl_2$
	15 mM $MgSO_4$
	12.5 mM KH_2PO_4
Micronutrients (100x)	13 mM $MnSO^4$
	10 mM H_3BO_3
	3 mM $ZnSO_4$
	0.1 mM Na_2MoO_4
	10 µM $CuSO_4$
	10 µM $NiCl_2$
Iron sulphate (100x)	10 mM $FeSO_4$
	10 mM Na_2EDTA
	0.05% 2-(N-morpholino)ethansulfonic acid (MES)

KNO_3 was added as the only nitrogen source by a separate stock solution. For preparation of *MS* plates 0.8% phytoagar per liter media were added. The pH was adjusted with KOH to pH 5.7.

2.2.26 Stable Transformation of *A. thaliana Mutant* Lines

For the generation of stable expression lines in *A. thaliana*, the transformed *A. tumefaciens* were grown as in Chapter 2.2.10 described. The *A. thaliana* plants of the desired genotype were grown up to the reproductive phase under long day conditions with full nutrient supply. Suitable plants had several shoots and flowers for the infiltration procedure. 100 ml of *YEB* media with corresponding antibiotics were inoculated with 10 loops of cells and incubated over night at 28°C. The agrobacteria were harvested by centrifugation at $3,000g$ for 15 minutes at room temperature and the cell pellet was resuspended in 5% sucrose solution. The OD_{600} was measured and the cells were diluted with sucrose solution to an OD_{600} of 0.6 - 0.8 in a total volume of 200 ml. Additionally 0.02% Silvet-L77 (Spiess-Urania) were added to the cells prior to infiltration. The plants were dipped upside down into the agrobacteria solution and incubated for 30 seconds followed by a consecutive up and down movement for 1 minute. This procedure was repeated three times per plant and construct. Afterwards, the dipped plants were put into a plastic bag with a wet paper towel to ensure high humidity during the over night incubation. The plants were kept for 24 hours away from any light source and afterwards placed back into

the growth chamber under long day conditions. The plants were watered with 1 : 1,000 *FertyMega3* (Planta Düngemittel GmbH) fertilizer for full nutrient supply, prior to the dipping procedure and the seeds were harvested, after complete drying of the plants.

After the seeds were dried and harvested the F1 generation was sown on soil and grown up to two leaf stage followed by a *Basta* (Bayer) selection with a 1 : 1,000 diluted *Basta* solution. The selection was repeated at least three times and surviving plants were transferred to single pots and leaf samples were taken, protein was extracted and a immunoblot was performed to assess the level of the protein production. The F2 generation was harvested from plants with different protein production levels.

From lines with proven protein production, F2 generation seeds were sown on soil and grown under long day conditions until the two leaf stage and again selected by spraying the seedlings with *Basta* solution. Lines were kept which showed a 75% survival rate according to the mendelian laws to proof the presence of only one trans gene. Of those lines seeds for the F3 generation were harvested. Seeds of the F3 generation of lines with single insertion were sown on MS agar plates (Chapter 2.2.25) and grown up to seedling stage for 10 days. The plates were sprayed with sterilised 1 : 1,000 *Basta* solution three times within 10 days and plants from those lines with nearly 100% of surviving plants were kept as homozygous stable expression line.

2.2.27 Germination Analysis of *A. thaliana* Seeds

To assess the germination rate of different mutant lines of the purine nucleoside degradation pathway, plates with 0.8% phytoagar dissolved in double distilled water were prepared without any additional nutrient supply. More than 100 seeds of the different *A. thaliana* knock out lines, including Col-0 as a wild type control were sterilized with 70% ethanol for 10 minutes and sown on the plates in alternating order (Figure 11).
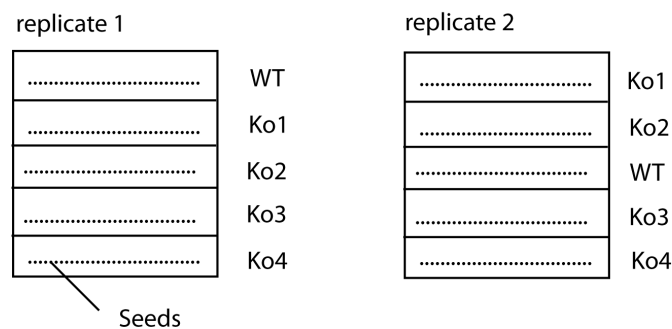
Figure 11: Determination of the germination rate of *A. thaliana* lines, WT: wild type (Col 0), Ko1 - Ko4: knock-out line number one to number four.

The seeds were vernalised at 4°C for 24 hours and afterwards transferred into the plant growth chamber operated at long day conditions. The seeds were examined daily with a

binocular microscope and counted as "germinated", if the endosperm was ruptured. The examination was performed always at the same time of the day for up to 3 consecutive days .

2.2.28 Isolation of Mesophyll Protoplasts

For the extraction of protoplast from *A. thaliana* or *N. benthamiana* leaves the enzyme solution 1 (Table 39) was prepared and warmed up to 55°C for 10 minutes for better solubilisation of the components. The solution 1 was let to cool down to room temperature and was then mixed with enzyme solution 2. The final enzyme solution is slightly brown in colour and was filtered through a 45 µm syringe filter.

Table 39: Name and ingredients of the solutions used for mesophyll protoplast isolation

Name	Content
Enzyme solution 1	20 mM MES (pH 5.7)
	1.5% (w/v) cellulase
	0.4% (w/v) macerocyme
	0.4 M mannitol
	20 mM KCl
Enzyme solution 2	10 mM $CaCl_2$
	0.1% bovine serum albumine (BSA)

0.5 - 1 mm leaf stripes were cut from plant leaves. The stripes were transferred into the prepared enzyme solution 2 (Table 39) and totally submerged into the solution. The leaf stripes were vacuum infiltrated for 30 minutes. During this infiltration the desiccator was covered by a black cloth to shield the samples from light. Afterwards the vacuum was released and the samples were incubated in the dark for at least 3 h without shaking. Following to the incubation in the dark the prepaired protoplast solution was used for subcellular localisation analysis.

2.2.29 Subcellular Localisation Analysis by Confocal Laser Scan Microscopy

The proteins of interest fused to an eYFP tag were transiently produced in *N. benthamiana* (Chapter 2.2.14). Protoplasts were isolated as described in Chapter 2.2.28 prepared for the subcellular localisation analysis. Confocal images were acquired by a Leica TCS-SP8 confocal laser scanning microscope equipped with a HCX PL APO 40 x 1.20 UV water immersion objective together with the *Leica Application Suite Advanced Flourescence Software.*

2.2.30 Dark Stress and PAM Measurement

A. thaliana seedlings were sown on white peat soil in 8 cm pots and grown under full nutrient supply for four weeks before the starting point of the reproductive phase under long day conditions. The plants were covered with a 2-tray-system like shown in Figure 12 for 3 - 6 days.
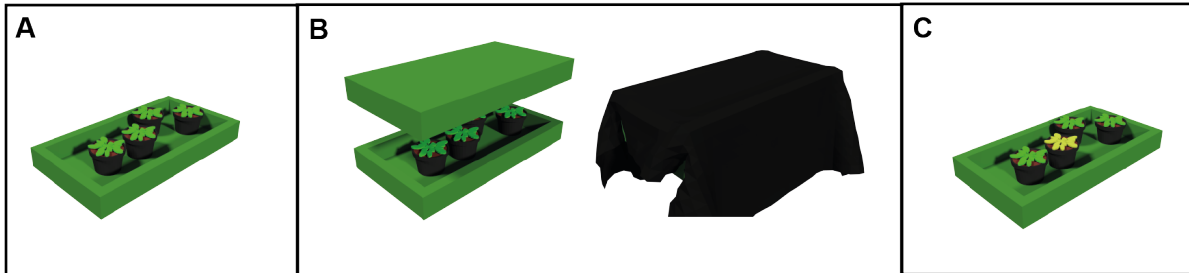
Figure 12: Experimental design of the dark stress experiment: The plants were grown under long day conditions (16 h light, 8 h dark) (A). For the experiment the plants were put into a two plant tray system and covered by a black cloth surrounding the double trays (B). The plants were shielded from photosynthetic usable light for three to six days and phenotypical abnormalities were recorded regularly (C).

The photosynthetic activity was was determined daily during the treatment. For this the Walz *Imaging PAM M-Series* was used and the F_v/F_m of whole rosettes were calculated by the *ImagingWinGigE* (Walz) software. Daily plants where removed from the cover and used for metabolite analysis. Until the end of the experiment harvested plants were stored at -80°C. Prior to the metabolite analysis by LC-MS, the plant material was freeze dried due to the unequal loss of water during the dark stress treatment. The metabolite content was normalized to the dry weight used for metabolite extraction.

2.2.31 *A. thaliana* Shaking Cultures for Pulse Chase Experiments

To evaluate if ribose is transported into the chloroplast by the pGLCT transporter a pulse chase experiment was designed feeding uridine to *A. thaliana* seedlings and measuring the quantity of D-ribose after 24 h of exposure to uridine.
50 - 55 *A. thaliana* seeds of different genotypes were transferred into an 50 ml Erlenmeyer beaker with 10 ml of shaking culture media (Table 40) and stratified at 4°C over night. The beakers were transferred into a shaker with floral light and shaken at 50 rpm for 3 days at 22°C and at 80 rpm for additional 4 days. At day 7, the media was exchanged with fresh shaking culture media to avoid nutrient depletion. The samples were split into two groups per genotype and for on of the two groups 0.1 mg ml^{-1} of sterilized uridine were added to the media whereas the other group was the control group. The shaking cultures were incubated for 24 h after the feeding pulse with uridine. In preparation for

the LC-MS measurement of the D-ribose, the seedlings were washed with ddH_2O prior to making 100 mg aliquots of the plant material. The samples were frozen in liquid nitrogen and stored at -80°C the metabolites were extracted with the organic extraction method described in Chapter 36.

Table 40: Nutrient solutions of the shaking culture media.

Number	Name	Content
1	macro nutrients	2 mM KNO_3
		1 mM NH_4NO_3
		1 mM glutamine
		1 mM $MgSO_4$
2	micro nutrients	60 µM H_3BO_3
		14 µM $MnSO_4$
		1 µM $ZnSO_4$
		0.6 µM $CuSO_4$
		0.4 µM $NiCl_2$
		0.3 µM $HMoO_4$
3	iron solution	40 µM $Na_2FE\text{-}EDTA$
4	calcium solution	4 mM $CaCl_2$
5	phosphate solution	3 mM KH_2PO_4/K_2HPO_4 (pH 5.8)
6	MES	3 mM MES (pH 5.8)
7	sugar	0.5% sucrose

3 Results

A fundamental hypothesis of this thesis was that the D-ribose, released during the degradation of ribonucleiosides by NSH1 and NSH2, might play an important role during the survival of long-term dark stress of *A. thaliana* plants. Underlining this hypothesis was the prominent dark stress phenotype shown by *GSDA* mutant plants during the characterisation of *GSDA* by Kathleen Dahncke (Dahncke 2013). Additionally, Jung *et al.* (2011) reported a necrotic phenotype of the *NSH1* mutant line after application of prolonged dark stress to the plants.

In a previous study (Schroeder 2014), the identification of a putative ribokinase (RBSK) from *A. thaliana* (*At*RBSK) and *S. cerevisiae* was achived *in silico* by protein sequence analysis. The candidate gene for *AtRBSK* was cloned C-terminally fused to proteins like YFP (X185) or a HA-StrepII tag (X184). The homologous gene from *S. cerevisiae* (*ScRBSK*) was fused C-terminally to HA-StrepII tag and included in the biochemical analysis, due to results published by Xu et al. (2013). The group suggested that this gene is not mediating the RBSK reaction despite showing a 30% identity to the *A. thaliana* homologue. Preliminary results were obtained and it was concluded that the candidate genes might encode for RBSKs, but no conclusive data for the kinetic constants could be reached. In this study, the biochemical and physiological characterisation was repeated and a comprehensive metabolomic study was conducted to give new insights into the degradation of ribonucleosides in *A. thaliana* and *S. cerevisiae*.

While conducting this study, the *At*RBSK was described in a publication by Riggs *et al.* (2016). The experiments of this study were conducted in parallel to those of Riggs and were subsequently published shortly after Riggs *et al.* (2016) in Schroeder *et al.* (2018).

3.1 *In vitro* Characterisation of the Ribokinases from *A. thaliana* and *S. cerevisiae*

In this study, *RBSK* genes from *A. thaliana* (At1g17160) and *S .cerevisiae* (YCR036W) were investigated biochemically. Regarding the plant enzyme, a physiological study was conducted, including protein generation profiles throughout the *A. thaliana* plant life cycle. Both organisms are included in the comprehensive metabolite study giving new insights into ribonulceoside degradation.

3.1.1 Ribokinase Activity Measurement by ADP Quantification with HPLC

For the biochemical analysis of the ribokinase enzymes from *A. thaliana* and *S. cerevisiae* a reliable *in vitro* assay and quantification had to be developed. In a former study (Schroeder 2014), a commercial kinase luminescence detection kit was used for the biochemical analysis. However, the results were not reproducible. Therefore, the first aim

was to develop a robust kinase assay to evaluate not only ribokinases biochemically, but as well other members of the kinase family.

The procedure of the kinase reaction is described in Chapter 2.2.20. Following the kinase reaction, the samples were placed into a HPLC system, including an ADP (adenosine diphosphate) standard for the calculation of a calibration curve. In Figure 13 a standard sample run for an ADP/ATP mixture sample is shown for a full program cycle. ADP eluted from the column 0.4 minutes earlier (retention time (R_T) = 5.856 min) than ATP (R_T = 6.208 min) allowing a clear separation of the two compounds and their quantification.
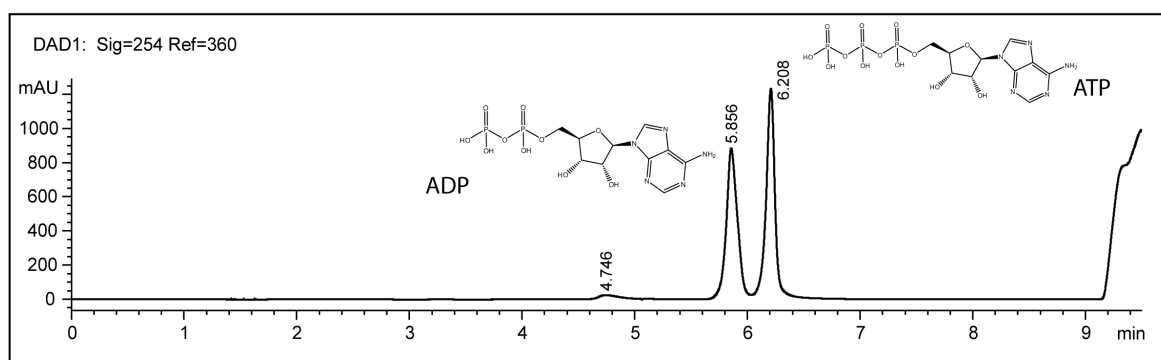
Figure 13: High Pressure Liquid Chromatography (HPLC) measurement of ADP and ATP in a mixed standard sample. ADP eluted at 5.58 minutes and ATP at 6.20 minutes.

To calculate the enzyme activity, the assay had to be performed reproducibly and correctly over a variety of substrate concentrations. Kinetic measurements included a substrate range of 0.5 K_M to at least 10 K_M (Michaelis-Menten constant). Kinases are phosphotransferases and ATP is used as a phosphate donor, resulting in ADP and the phosphorylated educt of the reaction. For the calculation of the ribokinase activity, the amount of ADP generated from different D-ribose substrate concentrations was quantified.
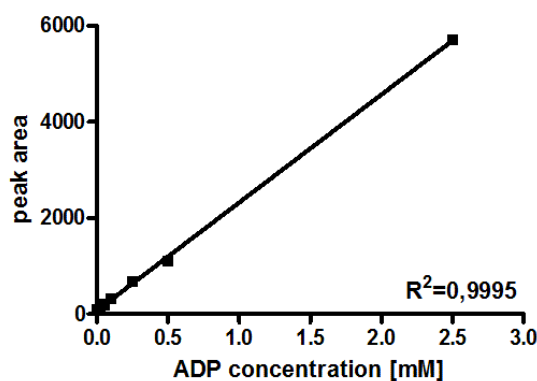
Figure 14: Correlation of ADP concentration to peak area measured by HPLC Diode array detector 1 (DAD1) at 254 nm (Ref.= 360 nm).

The ADP concentration and the detected peak area measured by the HPLC system at 254 nm (Ref.= 360 nm) displayed a linear correlation over a wide range of ADP concentrations (Figure 14). This assay could be used for not only the biochemical analysis of the RBSKs of this study, but with modifications for other potential kinases as well.

3.1.2 Affinity Purification of the Ribokinase from *A. thaliana*

For the biochemical analysis of the of the *At*RBSK, the C-terminally StrepII tagged protein needed to be purified by affinity purification. The corresponding construct (X184) was transiently expressed in *N. benthamiana* leaves (Chapter 2.2.14) and the resulting protein was affinity purified (Chapter 2.2.15). Several samples were taken during the purification process: the clarified crude extract (S1), the crude extract after incubation with the affinity matrix (S2), supernatant from the last of five washing steps (S3) and the eluted pure protein fraction combined from two elution steps (S4). Two SDS polyacrylamide gels were loaded identically with 10 µl of the samples (S1 - S4) and the proteins were separated as described in Chapter 2.2.17.
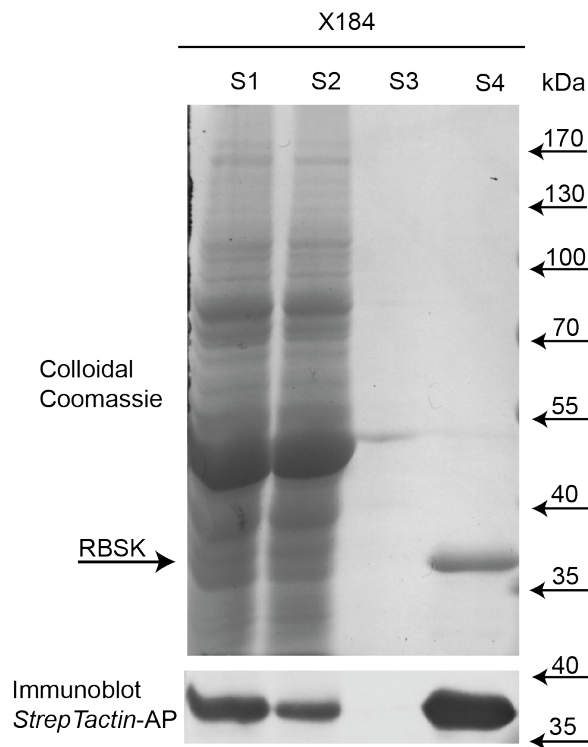
Figure 15: Affinity purification of the RBSK from *A. thaliana* with C-terminal StrepII Tag (X184) after transient protein production in *N. benthamiana* followed by an affinity purification with a *StrepTactin* matrix. 10 µl of the samples were loaded on SDS-polyacrylamide gels and stained with colloidal Coomassie blue and *StrepTactin* alkaline phosphatase conjugate after the immunoblot. S1: clarified crude extract, S2: proteins not bound to the affinity matrix, S3: residual proteins after the last washing step, S4: protein in combined elution fractions.

One gel was developed with colloidal Coomassie blue to detect the total proteins in the samples. Proteins of the second gel were transferred onto a nitrocellulose membrane and an immunoblot detection of the StrepII tag with *StrepTactin* conjugated to an alkaline phosphatase was conducted (Chapter 2.2.19).

The *At*RBSK protein has a predicted molecular mass of 42 kDa whereas the signal in the Coomassie-stained gel (S4) and on the immunoblot suggests a mass of approximately 36 kDa for the corresponding protein (Figure 15). This difference in mass is probably due to the proteolytic removal of a plastid targeting peptide with a predicted mass of 6 kDa.

3.1.3 Affinity Purification of the Ribokinase from *S. cerevsiae*

The RBSK from *S. cerevisiae* was included in this study for the biochemical analysis. The protein was C-terminally StrepII tagged (X188), transiently produced in *N. benthamiana* leaves and affinity purified similar to the plant homologue. The steps of protein purification were conducted similar as described in the previous Chapter 3.1.2.
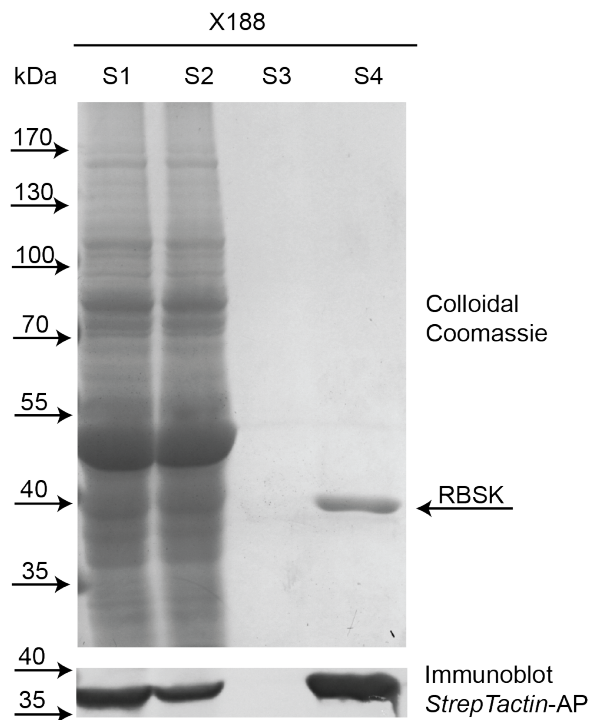
Figure 16: Affinity purification of the RBSK from *S. cerevisiae* with C-terminal StrepII Tag (X188) after transient protein production in *N. benthamiana* followed by an affinity purification with a *StrepTactin* matrix. 10 µl of the samples were loaded on SDS-polyacrylamide gels and stained with colloidal Coomassie blue and *StrepTactin* alkaline phosphatase conjugate after the immunoblot. S1: clarified crude extract, S2: proteins not bound to the affinity matrix, S3: residual proteins after the last washing step, S4: protein in combined elution fractions.

The *Sc*RBSK has a predicted size of 39 kDa and the signals in the Coomassie-stained

gel and the corresponding immunoblot matched the predicted mass (Figure 16), thus indicating a successful purification of the *Sc*RBSK protein.

3.1.4 Assessment of the RBSK activity

The HPLC ribokinase assay was utilized to assess whether the purified enzymes *At*RBSK and *Sc*RBSK show any RBSK activity. The kinase assay reactions of the two enzymes with D-ribose were prepared including controls without D-ribose, without the enzyme and without the phosphate donor ATP.
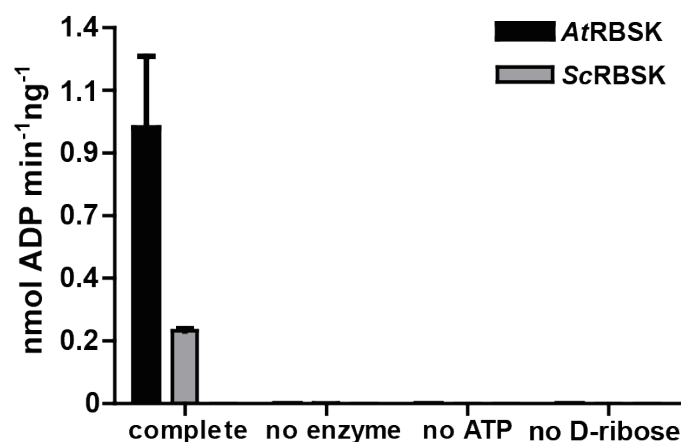
Figure 17: Confirmation of the *At*RBSK and *Sc*RBSK activity with D-ribose. The specificity of the test was demonstrated by samples excluding the enzyme, ATP or the substrate D-ribose. For the complete reaction triplicates were conducted for the three controls single reactions for each enzyme. Error bars show SD (standard deviation).

In the controls without enzyme, ATP or the substrate, no peak of ADP could be detected (Figure 17). In contrast, the samples with all substrates and the corresponding enzymes instead showed an ADP peak. For the *At*RBSK 1.0 nmol of ADP were produced per minute per ng of enzyme used in the reaction. For the *Sc*RBSK enzyme, an activity of 0.23 nmol of ADP per minute per ng of used enzyme were detected, leading to the conclusion that both of the enzymes have an activity towards D-ribose, but the enzyme from *A. thaliana* had a four times higher activity in this test. These results confirmed activity of the plant RBSK for the first time. In contrast to Xu *et al.* (2013), these results showed that also that the gene YCR036W from *S. cerevisiae* is indeed coding for a functional RBSK enzyme.

3.1.5 Determination of the Kinetic Constants for the *RBSK*s from *A. thaliana* and *S. cerevisiae*.

The kinetic constants were evaluated after transient protein production in *N. benthamiana* and affinity purification of the enzymes.
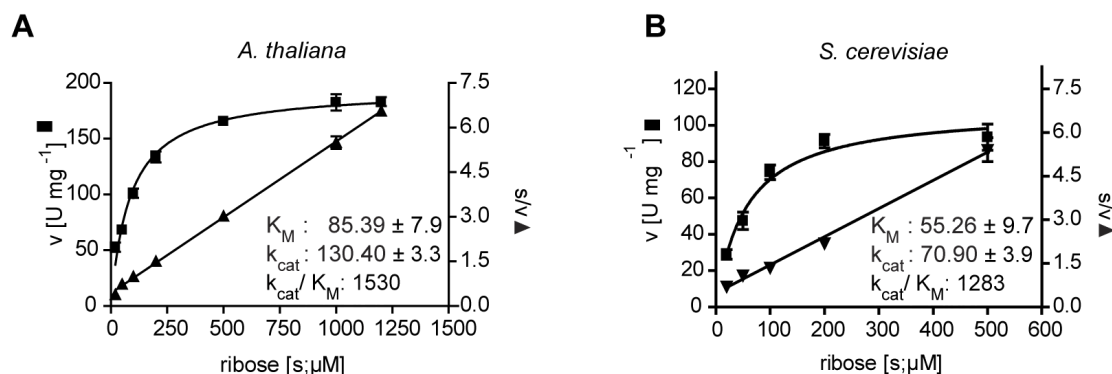
Figure 18: Kinetik constants of *At*RBSK and *Sc*RBSK for the substrate D-ribose. A: For the ribokinase from *A. thaliana*, D-ribose concentrations from 0 to 1200 µM was used. B: For the RBSK from *S. cerevisiae*, D-ribose concentrations from 0 to 500 µM were used. The Michaelis-Menten constant (K_M in µM) was determined using *PRISM Graph Pad 4*. Error bars show SD values (n = 3). k_{cat}: turnover number (sec^{-1}); k_{cat}/K_M: catalytic efficiency (mM^{-1} sec^{-1}).

The K_M values for the *A. thaliana* and the *S. cerevisiae* enzymes of 85 µM and 55 µM, respectively, showed that both enzymes can utilise D-ribose at physiological substrate concentrations (Figure 18). Riggs *et al.* (2016) reported a K_M of 150 µM for the plant RBSK. Turnover numbers of 130 s^{-1} for the *At*RBSK and 70,9 s^{-1} for the *Sc*RBSK were determined, indicating that both enzymes are highly active towards D-ribose. Compared with the study from Riggs *et al.* (2016) the *At*RBSK is 65 times more active. For the *Sc*RBSK enzyme, this was the first time this data was collected. In summary, the kinetic constants of both enzymes indicate that they are highly active RBSKs. The catalytic efficiency of the *At*RBSK was found to be significantly higher in this study than reported previously by Riggs *et al.* (2016).

3.1.6 Cofactor Analysis of the RBSK from *A. thaliana* and *S. cerevisiae*

The monovalent cation K^+ and the divalent cation Mg^{2+} are reported to be essential for the RBSK reaction in *Escherichia coli* (*E.coli*). Mg^{2+} ions stabilise the transfer of the γ-phosphate from ATP to the ribose residue, acting as an ATP chelator. K^+ ions are acting as activator for the RBSK enzyme (Anderson *et al.*, 1969). The influence of mono- and divalent ions on the RBSK reaction of *At*RBSK and *Sc*RBSK should be examined.

The ribokinase assay was performed under the same conditions as mentioned before. But the 5x stock solution was adjusted to lack either Mg^{2+} or K^+ ions.
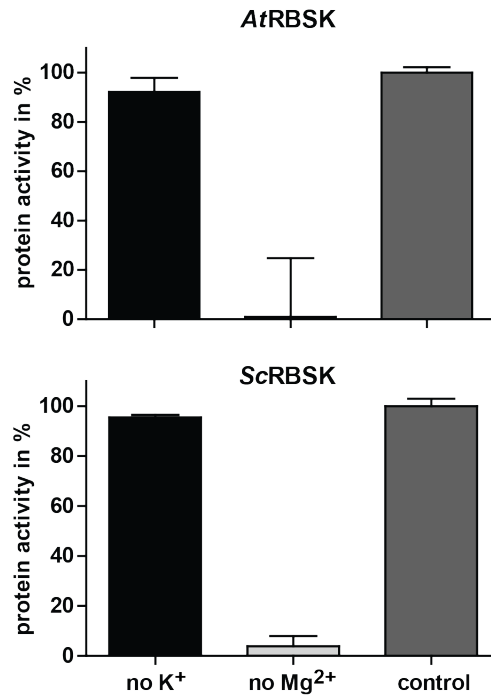
Figure 19: Assessment of the ribokinase reaction when K^+ and Mg^{2+} are not supplied. The enzyme activity was calculated in comparison to the positive control with both cations included in the reaction. The measurement was performed by HPLC and data from three biological replicates were combined and normalised for the control being 100% of possible protein activity. Error bars show SD of three replicates.

The RBSK enzymes from *A. thaliana* and *S. cerevisiae* were tested for a decrease in protein activity when the cofactors K^+ and Mg^{2+} were absent (Figure 19). In the absence of K^+ ions a decrease in activity by approximately 10% was detected for both RBSK enzymes. In contrast, the absence of Mg^{2+} ions led to a total inhibition of the *At*RBSK activity and only approximately 5 to 10% activity remained for the *Sc*RBSK enzyme. As for most kinases, Mg^{2+} ions are essential for the RBSK reaction. For the K^+ ions either their presence is not essential for the reaction in comparison to what is observed for the RBSK from *E. coli*, or the K^+ ions were tightly bound to the enzyme and co-purified with the enzyme by the StrepII-tag affinity purification. In any case the supply with additional K^+ ions does not seem to be necessary for the *At*RBSK and *Sc*RBSK enzymes.

3.1.7 Evaluation of Putative Additional Substrates for the *At*RBSK and the *Sc*RBSK

After the evaluation of the biochemical parameters of the RBSK enzymes, three other substrates in addition to the D-ribose were tested. A preliminary test of the *At*RBSK and

*Sc*RBSK activity towards the nucleosides adenosine, cytidine and uridine was performed. The aim was to provide a first insight on the substrate specificity of the RBSK from *A. thaliana* and *S. cerevisiae* and to evaluate if the these nucleosides are substrates.
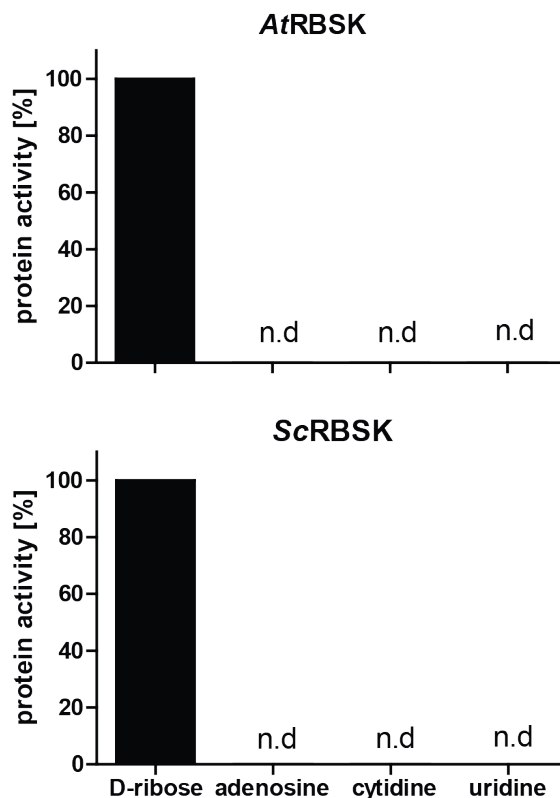
Figure 20: Substrate test of the *AtRBSK* and *Sc*RBSK withe the nucleosides adenosine, cytidine and uridine compared to D-ribose as positive control. 400 µM of the substrates were used and 400 µM of ATP as a phosphate source. The experiment was performed only once and without technical replicates leading to only a preliminary dataset. Samples with no detectable peaks were labelled n.d for not detected.

The kinase assay was prepared with 400 µM of the respective substrates adenosine, cytidine and uridine (Figure 20). Neither the *At*RBSK nor the homologous enzyme from *S. cerevisiae* showed an activity to any of the substrates whereas the enzymes were active with the positive control D-ribose. Both RBSK enzymes are highly specific towards the substrate D-ribose and not to the other nucleosides. However, it can not be excluded that other pentoses similar in structure to D-ribose, for example D-deoxyribose, might be substrates. This and the repetition of this result would have to be a subject to further tests.

3.2 *In vivo* Characterization of the Ribokinases from *A. thaliana* and *S. cerevisiae*

After the enzymatic activity as RBSKs was confirmed, the contribution of the *RBSK* to the D-ribose recycling from nucleotide degradation was investigated. Additionally, it was speculated that a *RBSK* mutant might show a phenotype of decreased stress tolerance during a treatment with prolonged dark stress similar to *NSH1* and *GSDA* mutant plants. Therefore, *A. thaliana* T-DNA lines were used for metabolite analysis by mass spectrometry (LC-MS) to evaluate the impact of the mutations on the nucleoside degradation pathway, including the impact of a *RBSK* mutation on intracellular D-ribose concentration.

3.2.1 Characterisation of the *A. thaliana RBSK* Mutant and Complementation Line.

For the analysis of the RBSK function in *planta*, a T-DNA knock out line from *NASC* was ordered (SALK005371C). For the metabolite analysis, a complementation line was needed complementing the *RBSK* mutation with a transgene.

Therefore, flowering *A. thaliana* plants were transformed with *A. tumefaciens* carrying the *RBSK*-StrepII construct X184. This construct was already used for the transient production of RBSK in *N. benthamiana* for the *in vitro* enzymatic characterisation in Chapter 3.1.2.
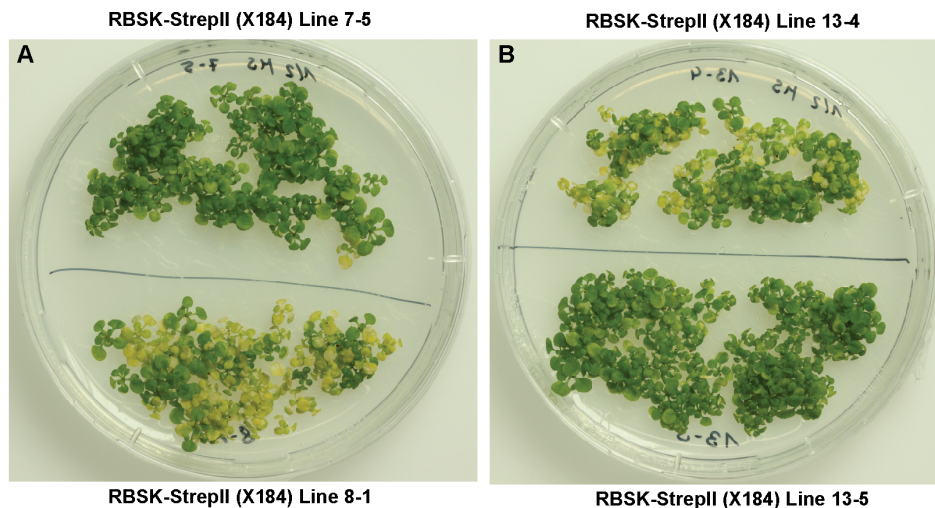
Figure 21: The F3 generation of *A. thaliana* plants transformed with *At*RBSK under control of a 35S promotor including the 3'- and 5'-UTR of the cowpea mosaic virus (CPMV) (X184) were sown on half *MS* media and grown until the two leaf stage. The plants were selected three times by *Basta* application. Lines with a 99% survival rate were selected for further analysis.

After the *Basta* (Bayer) selection of the F1 generation, the seeds of the lines 3, 7, 8 and

13 were kept. The seeds of the F2 generation of those lines were sown on soil and selected by *Basta* again. 10 plants of the lines 3, 7 and 13 were kept showing the desired ratio for a single insertion of the introduced T-DNA. F3 generation plants of 5 plants from each of the F2 lines were sown on sterile 0.5% MS plates and after 7 days of growth the plates were sprayed with filter sterilized 1 : 1,000 *Basta* solution. This selection procedure was repeated three more times (Figure 21).

A homozygous complementation line should show a 99% survival rate in this *Basta* plate screen. The lines 7-5 (Figure 21A) and line 13-5 (Figure 21B) matched the criteria, where only a few seedlings did not survive the selection procedure. The line number 7-5 was chosen as a RBSK complementation line in all following experiments. To not only show that the *rbsk* line does not produce any transcript but furthermore to show that the RBSK line 7-5 is a functional complementation line, a reverse transcriptase PCR or (RT-PCR) was performed on cDNA produced from RNA of the respective plant lines including Col-0 as wild type control.
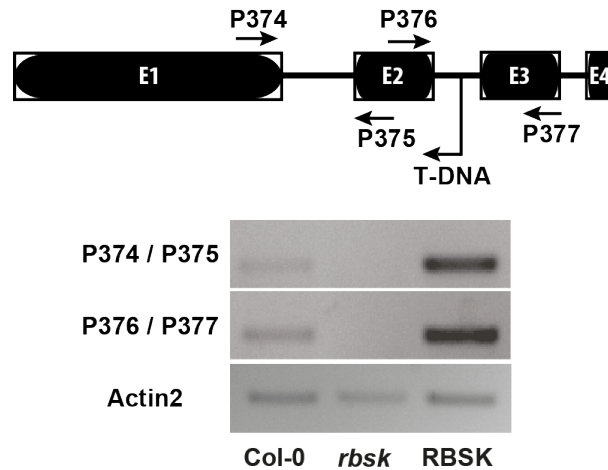
Figure 22: Characterisation of the *A. thaliana* T-DNA mutant line of *RBSK* (SALK005371C) and the complementation line RBSK (X184) by RT-PCR. The primers P374 to P377 were used for amplification from cDNA and their binding locations are marked in the overview of the gene structure. For the comparison of transcript amounts the housekeeping gene Actin2 was amplified as a control.

The RNA was extracted from adult but not yet bolting plants (20 - 25 days old) and cDNA was synthesised. The first PCR amplified the gene sequence upstream to the T-DNA insertion (P374, P375). Primers of the second PCR were designed in such a way that they flanked the T-DNA insertion site (P376, P377). Both PCRs together give an insight whether the *rbsk* plant line is a full knock-out mutant or if residual transcript is left. For the RBSK complementation line this PCRs confirmed the overexpression of the reintroduced *RBSK*.

The signals in Figure 22 show that the *RBSK* mutant line is lacking transcript upstream

and flanking to the T-DNA insertion point. In contrast, the *RBSK* complementation line is showing signals in both reactions and displays even an overexpression compared to the expression level of the control Col-0. The overexpression is due to the usage of a 35S promotor and *cowpea mosaic virus* 5'- and 3'-UTR in the vector. The *A. thaliana rbsk* line completely lacks a transcript and therefore is a null mutant plant which can be used together with the *RBSK* complementation line for functional analysis of RBSK *in vivo*. The result from the transcript analysis can be transferred on the protein concentration, because in the *rbsk* line no RBSK protein could be detected. In contrast to the RBSK complementation line, where a strong overexpression could be detected (Figure 23).
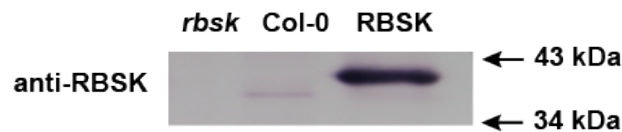
Figure 23: Immunoblot of crude protein extracts from Col-0, *rbsk* and the complementation line RBSK. 8 µl of protein were loaded and the two step detection was performed with a RBSK antibody from rabbit (1 : 400). As secondary antibody an anti-rabbit IgG from goat conjugated to an alkaline phosphatase was used (1 : 30,000).

From the three *A. thaliana* lines shown in Figure 22, leaf material was harvested and a total protein extraction was performed as described in Chapter 2.2.15. The crude extract was mixed 1 : 4 with 5x SDS loading buffer and 10 µl loaded onto a SDS polyacrylamide gel (Chapter 2.2.17). The RBSK was detected by an antibody made in rabbit against an RBSK antigen. No RBSK-signal was detected in the *rbsk* line, but the wild type control (Col-0) and the complementation line RBSK showed a signal between 34 kDa and 43 kDa (Figure 23). The signal in the RBSK line was running higher, because the protein is C-terminally fused to a HA-Strep tag increasing the size of the detected protein compared to the detected wild type RBSK. The increase in signal in this complementation line is due to a strong 35S promotor driving the expression of the *RBSK* transgene.
In summary, it could be shown that the *A. thaliana rbsk* line is a null mutant on transcript and on protein amount. The introduction of the Strep tagged RBSK protein into the *rbsk* line is leading to a higher abundance of transcript and a protein of the expected mass.

3.2.2 Characterisation of the *S. cerevisiae RBSK* Mutant and *RBSK* Complementation Line.

There was not only an interest in the *A. thaliana RBSK* function but as well in the homologous gene from *S. cerevisiae*. Xu *et al.* (2013) investigated the nucleotide catabolism and the ribose salvage in *S. cerevisiae*, including a *RBSK* mutant line. They concluded that the *ScRBSK* was not a ribokinase because the incorporation rate of labelled ribose did

not differ between the investigated mutant line and the wild type. Due to the homology in the characteristic sites for the PfkB ribokinase protein family of the *A. thaliana* and the *S. cerevisiae* RBSK sequence the enzyme from yeast was included in this study.
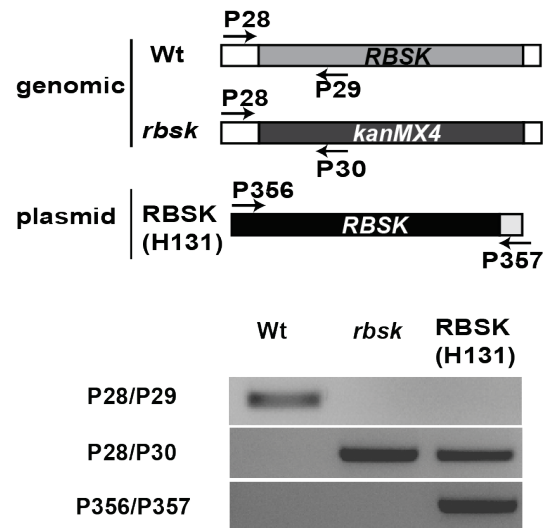
Figure 24: PCR on yeast genomic DNA extracted from the parental wild type line, the *rbsk* line and the *RBSK* complementation line. The primers P28 - P30 were suggested by *transomics* for detection of the kanMX4 casette. The primer P356 and P357 bind to the H131 construct of *RBSK*

A mutant line and a corresponding wild type (YCR06W) line were obtained from Transomics. The lines were examined at the DNA and protein level for the *RBSK* production. Additionally, a *ScRBSK* complementation line was produced by cloning the *ScRBSK* C-terminally tagged with a HA-StrepII tag, into a yeast expression vector under the control of a Cyc1 promotor.

In a PCR analysis, the parental (Wt) line showed a band in the reaction for the wild type *RBSK* (P28/P29), whereas neither the *rbsk* nor the *RBSK* complementation line showed a band in the wild type reaction (Figure 24). The *rbsk* showed the only band in the reaction for the kanMX4 cassette whereas the *RBSK* complementation line transformed with the H131 construct showed a positive result for the kanMX4 cassette and the H131 construct due to the *rbsk* background.

To address, whether the RBSK can be detected on protein level, total protein was extracted from *S. cerevisiae* over night cultures of these three yeast lines (Chapter 2.2.16).

Figure 25: Western blot after total protein extraction from the three yeast lines (Wt (parental line), *rbsk*, RBSK (H131)). 8 µl of protein were loaded and the detection was performed by an StrepTactin alkaline phosphatase conjugate.

The RBSK protein could not be detected in the parental wild type line, because the immunoblot was developed with StrepTactin-AP conjugate (Figure 25). Unfortunately, the antibody used in the immunoblot in Figure 23 to detect the *A. thaliana* RBSK, is not detecting the *S. cerevisiae* homologue. In conclusion no information regarding the protein production levels of the RBSK in wild type yeast cells could be obtained. The successful production of the RBSK protein was confirmed by detection of the C-terminally StrepII tagged recombinant RBSK.

In summary, the availability of a wild type, a null mutant and a complementation line in *S. cerevisiae* raised the possibility of a full analysis of the impact of the RBSK on the D-ribose concentration in yeast.

3.2.3 D-ribose Accumulates in *RBSK* Mutant Lines

For a comprehensive metabolomic analysis, seeds from *rbsk*, the complementation line RBSK, and the wild type Col-0 were sown on 1/2 *MS* plates and grown for 10 days under long day conditions. The samples were extracted by organic phase extraction and prepared for LC-MS analysis (Chapter 2.2.22).

This and the following LC-MS analyses were conducted in collaboration with Anting Zhu to accelerate the analysis.
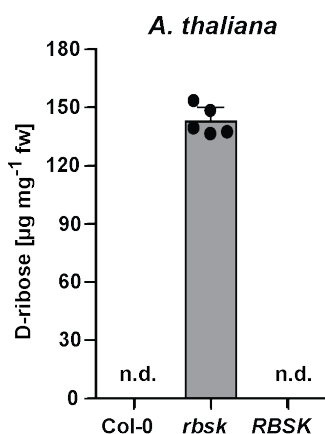
Figure 26: Quantification of the D-ribose concentration in 10-day-old seedlings in the wild type (Col-0), the *rbsk* line and the complementation line *RBSK*. Error bars show SD values (n = 5). Individual are data point shown by black circles. n.d.: not detected.

In the LC-MS analysis of 10-days-old seedlings, we detected a D-ribose accumulation in the *rbsk* line compared to the Col-0 wild type line and the RBSK complementation line (Figure 26). This shows that the *At*RBSK is required for the phosphorylation of D-ribose to ribose-5-phosphate *in vivo*. A mutation of *At*RBSK leads to an accumulation of D-ribose already at early developmental stages.
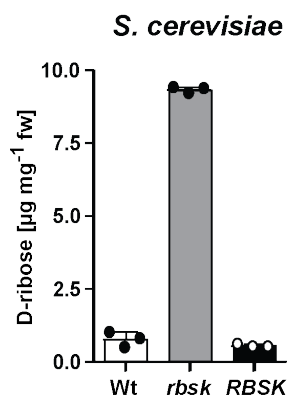
Figure 27: D-ribose quantification in *S. cerevisiae* lines. Comparing the parental wild type line (Wt) with the mutant line *rbsk* and the complementation line *RBSK* (H131). Error bars show SD values (n = 3). Individual are data point shown by black and white circles.

After the enzyme activity was evaluated for the *Sc*RBSK enzyme *in vitro*, the question arose whether *in vivo* a D-ribose accumulation could be observed in the *RBSK* mutant line. The *S. cerevisiae rbsk* showed a nine times higher concentration of ribose compared to the wild type (Wt) line and the RBSK (H131) complementation line overexpressing a functional *RBSK* gene (Figure 27).

In summary, the gene YCR06W of *S. cerevisiae* does not only code for an active RBSK, as shown by our *in vitro* kinase assay (Chapter 3.1.4), but also leads to a D-ribose accumulation *in vivo*. Our data strongly suggests, that the gene YCR06W encodes a yeast RBSK *in vivo*, in contrast to the conclusion of Xu *et al.* (2013).

3.2.4 The Nucleoside Catabolism Contributes to the D-Ribose Pool in *A. thaliana*.

The RBSK phosphorylates D-ribose released by the nucleoside hydrolase 1 and 2 (NSH1; NSH2) from the nucleosides, coming either from purine nucleotide degradation as guanosine, xanthosine, and inosine or pyrimidine nucleotide degradation as cytidine and uridine. To analyse the contribution of purine nucleoside degradation to the ribose pool, double mutant lines between *rbsk* and *gsda* (guanosine deaminase) were generated. For the contribution of the pyrimidine degradation to the D-ribose pool, *rbsk* was crossed with *cda* (cytidine deaminase). To evaluate the contribution of the total nucleoside degradation to

the ribose pool, *rbsk* was crossed with *nsh1*. The mutation of *NSH1* leads to biochemical inactivity of NSH2 and thus to a null mutant for cytosolic nucleoside hydrolase activity (Baccolini and Witte, 2019). Therefore, a *rbsk nsh2* double mutant is not necessary. The latter double mutant line (*rbsk nsh1*) should show whether there is an unknown contribution to the D-ribose accumulation in the *rbsk* line, apart from nucleoside hydrolysis.
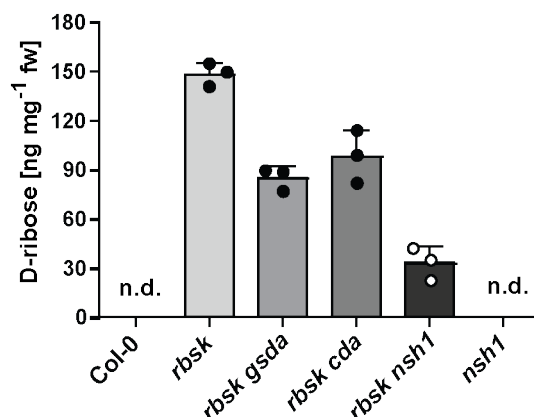
Figure 28: Quantification of D-ribose in 10 days old seedlings of Col-0 and double mutants of *rbsk* with *gsda*, *cda*, and *nsh1* by LC-MS. Included in this measurement was the *nsh1* single mutant line. Error bars show SD values (n = 3) indicated by the black or white circles. n.d.: not detected.

The double mutant line *rbsk nsh1* accumulated only one fifth of the D-ribose observed in the *RBKS* single mutant line (Figure 28). This shows that the majority of the D-ribose accumulating in the *RBSK* mutant is derived from the degradation of ribonuleosides. The residual D-ribose detected in this double mutant line might be the result of spontaneous hydrolysis of the N-glycosidic bond between nucleobase and the D-ribose residue. Another possibility is that, in a *nsh1* background, nucleosides escape into the apoplast, due to the high nucleoside accumulation in this mutant. In the apoplast this purine nucleosides can be hydrolysed by the apoplastidic NSH3 (Jung *et al.*, 2011). This result shows that the nucleoside hydrolysis is contributing most significantly to the D-ribose pool, with the possibility that D-ribose is exclusively generated by the hydrolysis of nucleosides.

The D-ribose concentrations in the double mutant lines *rbsk gsda* and *rbsk cda* were approximately 50% of the total D-ribose accumulation, respectively (Figure: 28). Therefore, it appears that the purine and pyrimidine degradation are contributing nearly equally to the D-ribose pool in the *rbsk* line.

In a further metabolite analysis, the nucleosides guanosine, xanthosine, cytidine and uridine and the nucleobase xanthine were quantified in the *rbsk* double mutant lines and the corresponding single mutant lines.
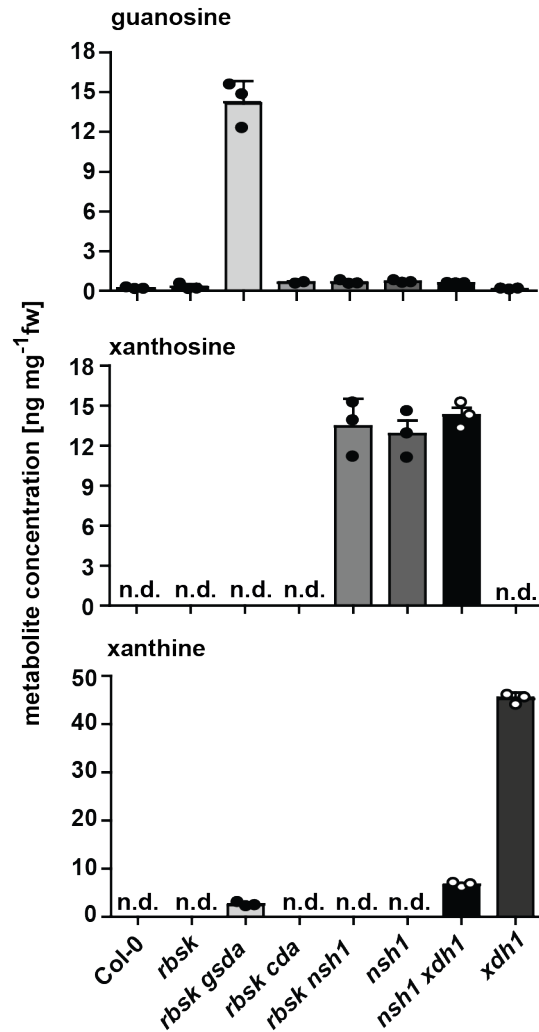
Figure 29: Quantification of metabolites from purine nucleotide degradation. Included in the measurement were 10-day-old seedlings of the lines Col-0 as wild type control, the single mutants *rbsk*, *nsh1* and *xdh1* and the double mutants *rbsk gsda*, *rbsk cda*, *rbsk nsh1* and *nsh1 xd1*; Error bars show SD of three biological replicates.n.d.: not detected

.

Guanosine accumulated up to 14 ng mg^{-1} fw only in the *rbsk gsda* line but was still detectable in all of the other tested lines. Xanthosine, as a substrate of the NSH1/NSH2 complex, accumulated in the single mutant line *nsh1* and in double mutant lines with *nsh1*, such as *rbsk nsh1* and *nsh1 xdh1* (14 ng mg^{-1} fw). Xanthosine is exclusively hydrolysed by the NSH1/NSH2 complex, leading to D-ribose and xanthine as a result. However, the nucleobase xanthine Was not only accumulating in the *xdh1* line, but as well in the double mutant *nsh1 xdh1* (8 ng mg^{-1} fw). This showed that an additional way of hydrolysing xanthosine without the influence of NSH1 exists. Nucleosides that accumulate could hydrolyse spontaneously or another nucleoside hydrolase like NSH3, which is located in

the apoplast (Jung *et al.,* 2011), hydrolyses xanthosine if it is transported out of the cell into the apoplastidic space.
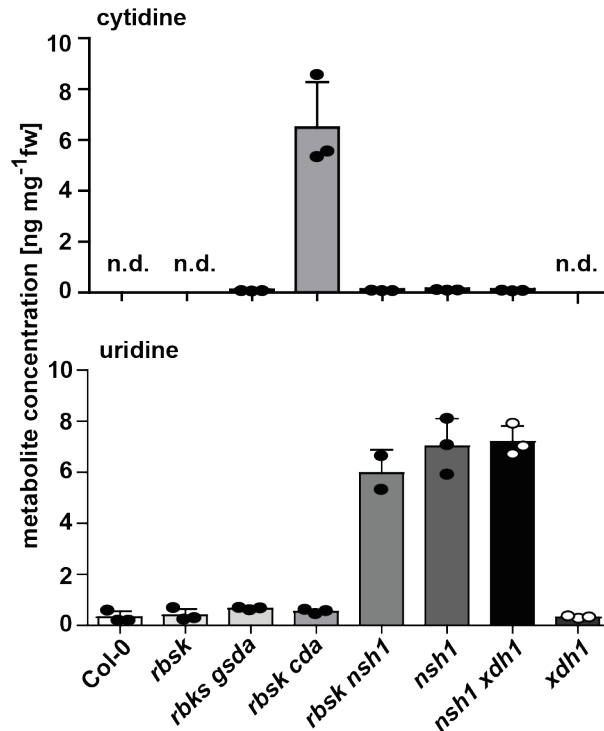
Figure 30: Quantification of cytidine and uridine in 10-days-old seedlings from nucleoside degradation mutants by LC-MS. Included in the measurement were the lines Col-0 as wild type control, the single mutants *rbsk, nsh1* and *xdh1* and the double mutants *rbsk gsda, rbsk cda, rbsk nsh1* and *nsh1 xd1*; Error bars show SD of three biological replicates. n.d.: not detected.

For the quantification of pyrimidine nucleosides, cytidine and uridine were extracted from the same plant lines used in the previous experiment and measured by LC-MS (Figure: 30). Cytidine only accumulated in the *rbsk cda* double mutant (7 ng mg^{-1} fw) whereas uridine accumulated in all lines with a *nsh1* background (*rbsk nsh1, nsh1, nsh1 xdh1*) up to 8 ng mg^{-1} fw. In the *nsh1* background, a higher accumulation of uridine could be expected, similar to the 13 ng mg fw detected for xanthosine. But in contrast to xanthosine, uridine can probably be salvaged to UMP, resulting in a weaker accumulation with up to 8 ng mg^{-1} fw.

Overall it appears that purine and pyrimidine nuleoside degradation contribute equally to the D-ribose accumulation in the *rbsk* line. Smaller quantities of D-ribose might result from hydrolysis of xanthosine by NSH3 or by spontaneous hydrolysis. Furthermore, an additional source for D-ribose, apart from nucleoside degradation cannot be excluded, the contribution to the D-ribose pool will be minor in comparison to the nucleoside degradation.

3.2.5 Physiological Characterisation of *A. thaliana RBSK* Mutants.

To assess the phenotype of the *RBSK* mutant, *A. thaliana* plants were grown on soil for 42 days under long day conditions (16 h light, 8 h darkness). The plants were cut between the root and the rosette above the soil and the shoot was separated into rosette leaves, cauline leaves and the siliques. The *rbsk* plants were visually compared with the Col-0 wildtype and the complementation line (line 7-5) overexpressing the *AtRBSK*.
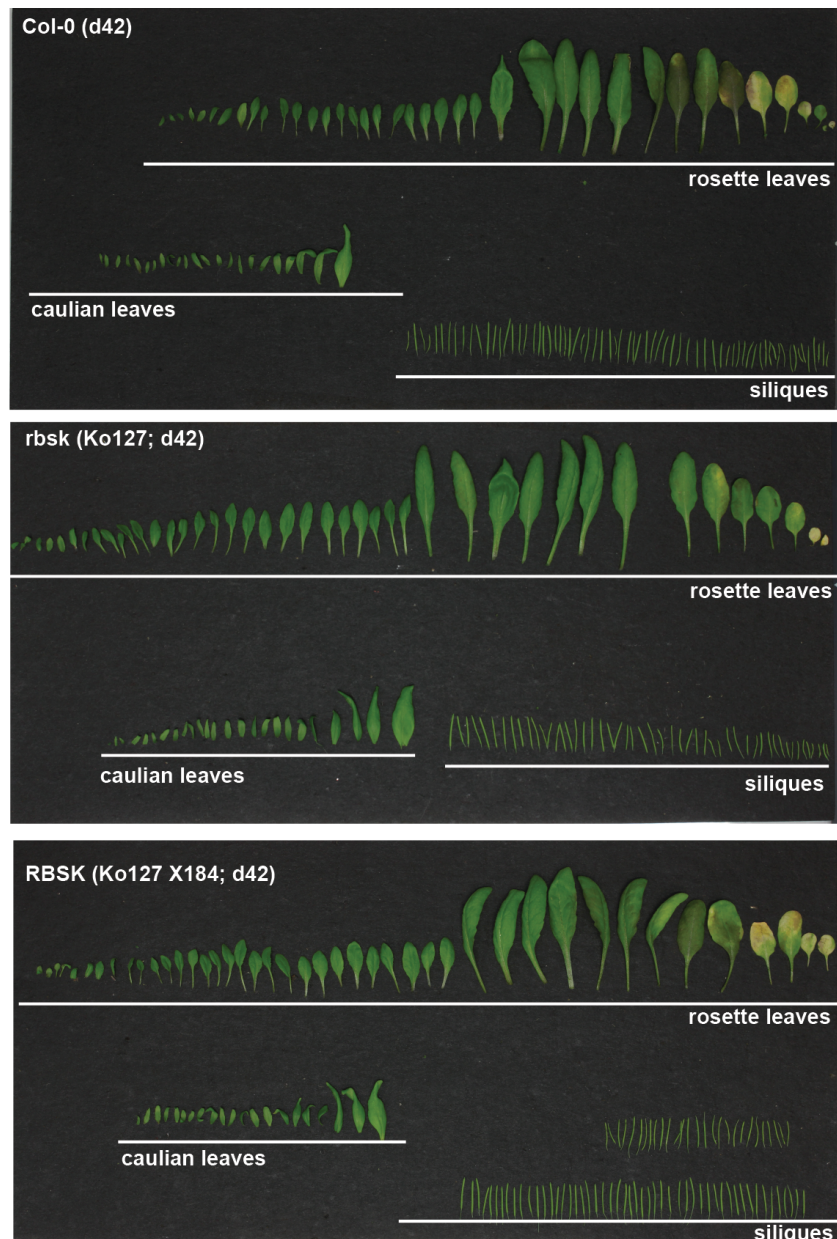
Figure 31: 42 days old plants from Col-0, *rbsk* and the complementation line *RBSK* (X184 line 7-5) were cut above the soil.The rosette leaves, cauline leaves and siliques were cut and ordered by size for phenotypical analysis. Five biological replicates were included for each genotype.

The wildtype Col-0, the *RBSK* mutant and the complementation line *RBSK* (X184) were

compared in leaf number and appearance (Figure 31). The *rbsk* plants did not differ from the wild type plants or from the complementation line *RBSK*. To investigate a possible reduced biomass production, due to the lack of ribose recycling in the *rbsk* plants, the weight of shoot and rosette was compared for the three genotypes. For this measurement, 42-days-old plants were cut above the soil and separated at the base of the shoot from the rosette.
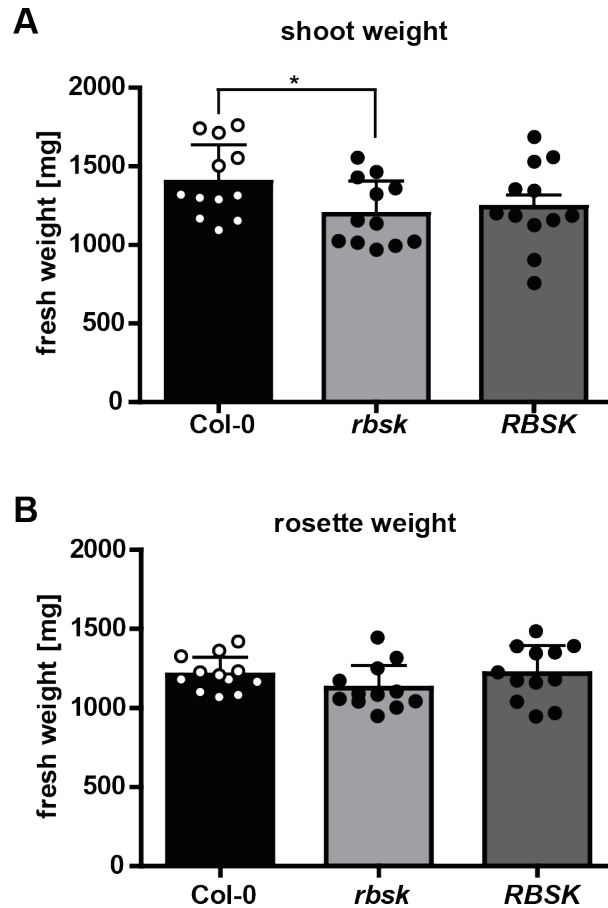
Figure 32: Assessment of differences in biomass production for the *RBSK* mutant compared to the wild type Col-0 and the complementation line *RBSK* (line 7-5). The vegetative tissue was separated into shoot material including flowers and siliques (**A**) and the plant rosette (**B**). At the time point of the harvest the plants were 42 days old. Error bars show SD (n = 12) with individual data points as circles. For statistical analysis a student's t-test was used p < 0.05.

The produced biomass was separated into rosette and shoot, including flowers and siliques. Both showed slightly less accumulated biomass for the *rbsk* and RBSK lines (Figure 32). This difference was statistically significant for the *rbsk* shoot biomass accumulation, compared to the wild type Col-0 (Figure 32A) but not for the *rbsk* rossette (Figure 32B). In conclusion, it can be said that the lack of D-ribose, coming from the nucleoside metabolism seem to have an impact on the production of shoot biomass production in *A. thaliana RBSK* mutants. During preliminary experiments, it was observed that the *rbsk* plants

were shooting earlier than the wild type Col-0 (Schroeder 2014). To re-assess this result, *A. thaliana* plants were grown for 5 weeks and the shoot length was documented for 12 plants per genotype (Figure 33).
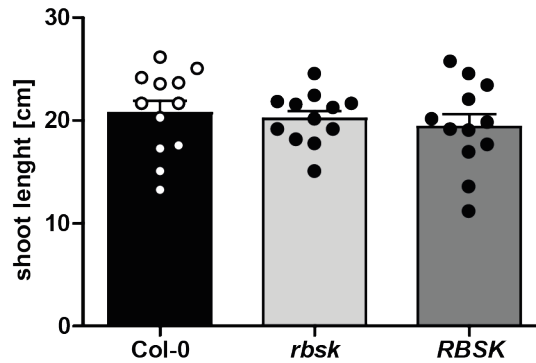
Figure 33: Shoot growth comparison between the wild type Col-0, *rbsk* and the complementation line *RBSK* (line 7-5) of 35 days old plants. Error bars are SD values (n = 12) with individual datapoints indicated as circles. For statistical analysis a student's t-test was performed ($p < 0.05$).

Under usage of a homogeneous seed batch and randomized growing conditions, no effect of RBSK was observed on bolting time or shoot height (Figure 33). Previous preliminary results could not be reproduced, giving no indications for an influence of the D-ribose on the switch between vegetative and reproductive phase.

3.2.6 Nucleoside Degradation Under Dark Stress Conditions

In a previous study about the guanosine deaminase (*GSDA*, Dahncke 2014) of *A. thaliana*, it was discovered that if the knock out mutant of *GSDA* was exposed to a prolonged period of darkness, the plants were showing a chlorotic phenotype. If the period of incubation without photosynthetically usable light was prolonged up to six days the damage by the extensive chlorosis was lethal to the plants. Attempts to rescue the *gsda* plants failed after about three days of dark exposure, whereas the wild type Col-0 recovered, even after one week of dark stress.

Additionally, Jung *et al.* (2011) described an increased susceptibility of the (*NSH1*) mutant under similar dark stress conditions. The NSH1 is hydrolysing the bond between the nucleobase and the D-ribose in several nucleosides and thus creates the substrate for the RBSK reaction.

A working hypothesis was, that the mutations in *GSDA* and *NSH1* leading to reduced D-ribose release might cause more severe sugar starvation under dark stress conditions, resulting in the documented phenotypes. Then a mutation in RBSK might result in a stronger dark stress phenotype. To test this hypothesis, a comprehensive dark stress ex-

periment was conducted, including the *RBSK* mutant and other mutants from the nucleoside degradation pathway such as nucleoside hydrolase 1 (*nsh1*), hypoxanthine guanine phosporibosyl transferase (*hgprt*), xanthine dehydrogenase (*xdh1*) and a double mutant from *gsda* and *hgprt* (C68). The double mutant was included in this study because preliminary data from Dahncke (2014) showed a decreased accumulation of guanosine and an increased accumulation of the nucleobase guanine in double mutant plants, allowing to test for a possible contribution of guanosine and guanine accumulation to the phenotype of the *gsda* single mutant.

Figure 34: Overwiev over 5-weeks-old *A. thaliana* plants after 6 days exposure to continuous darkness including the wild type Col and the mutants *rbsk, gsda, hgprt, nsh1, xdh1* and the double mutant line *gsda hgprt*. For each genotype five biological replicates were used labelled #1 to #5.

At day six of the experiment, a visual examination of the *A. thaliana* plants was performed. Additionally, the photosynthetic activities of the rosettes from all involved plant lines were measured daily by PAM (Chapter 2.2.30). The F_v/F_m values were obtained for six days of the dark stress experiment as a quantitative value for the PSII efficiency (Figure A1 -A7). The average F_v/F_m value of a healthy plant with sufficient access to light is 0.83 (Bjoerkman *et al.*, 1987). The *gsda* plants displayed an extensive chlorotic phenotype compared to the wild type Col-0 plants (Figure 34), whereas the *rbsk* plants showed no visually distinguishable phenotype compared to Col-0. This data indicates that the inability to recycle D-ribose from purine nucleoside degradation is not the cause of the *gsda* chlorotic phenotype. Surprisingly, the *NSH1* mutants did not show a chlorotic

phenotype although this was previously reported (Jung et al., 2011). However, this is consistent with the data from *rbsk*, indicating that impaired D-ribose metabolism does not aggravate the dark stress phenotype. Consistently, neither the *rbsk* nor the *nsh1* plants show a statistically significant difference in the F_v/F_m values over the course of the experiment compared to Col-0 (Figure 35). Excluding an impact on the dark stress survival due to the lack of D-ribose.
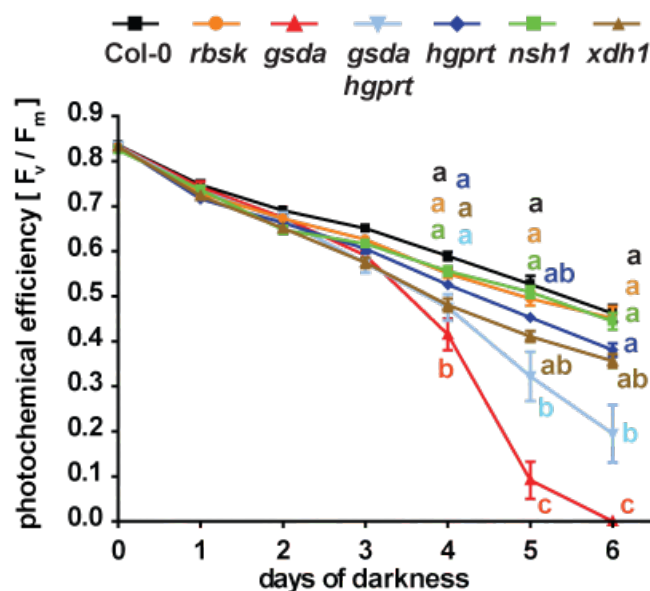
Figure 35: Quantification of the photochemical efficiency (F_v/F_m) of the visible darkstess phenotype in Figure 34 by PAM (pulse-amplitude-modulation). For each time point, five biological replicates per genotype were measured. The error bars represent the standard deviation (SD) and the statistical analysis were performed by a 2-way ANOVA with a Bonferroni post-test. Different letters indicate statistical differences at $p < 0.01$.

In contrast, the *gsda* plants show a significant decrease in the photosynthetic activity between day three and four which is further decreasing to zero at day six. Generally, the *gsda* plants are dead by day five. Interestingly, the double mutant *gsda hgprt* showed an intermediate phenotype between the *GSDA* single mutant plants and the wild type. From the visual examination, there was no noticeable difference between Col-0 the *xdh1* plants although in the measurement of the photosynthetic activity there were significant differences at day five and six.

3.2.7 Metabolic Analysis of Dark Stressed Plants by LC-MS

To examine the rate of nucleoside degradation during a six-day dark stress experiment, a metabolic analysis of the mutant lines in Chapter 3.2.6 was performed.
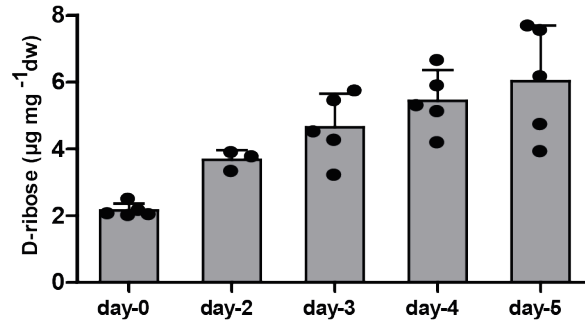
Figure 36: Measurement of D-ribose in *RBSK* mutant plants during 5 days of darkstress treatment. Error bars show SD of 3 or 5 biological replicates, indicated by the black circles.

Over the time of five days, samples were harvested and extracted for LC-MS analysis. The *RBSK* mutant line showed a steady increase in ribose over the time course of this experiment. A more than two-fold increase in D-ribose concentration from the day zero to day three was observed and a three-fold increase up to day five was detected (Figure: 36).
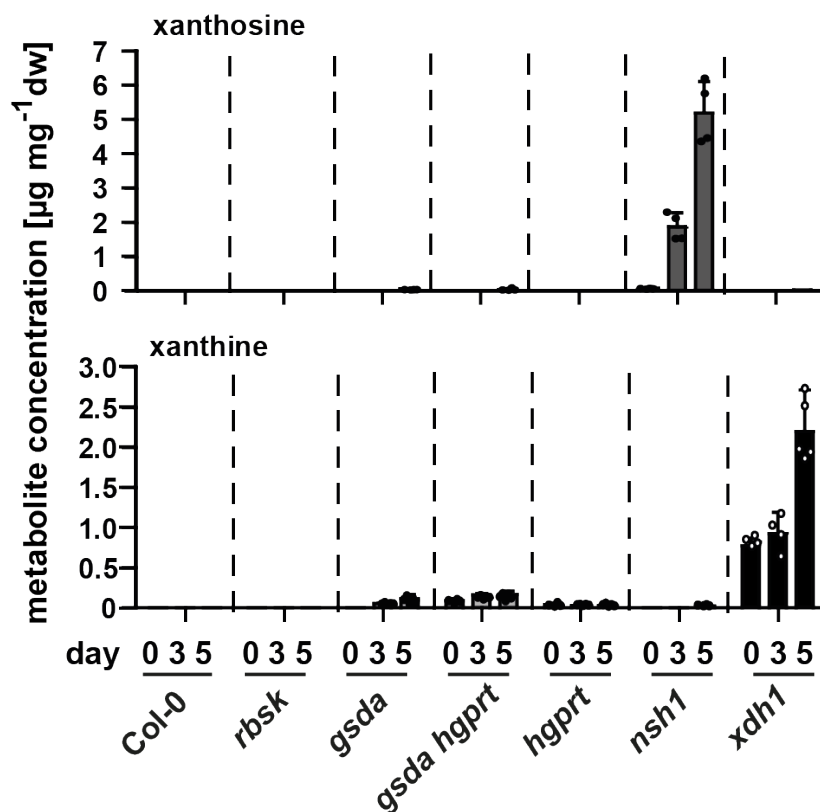
Figure 37: Measurement of xanthosine and xanthine in *A. thaliana* rosette leaves at day 0, day 3 and day 5 of the dark stress treatment. Plant lines testes involved: Col-0 as wild type control, *rbsk*, *gsda*, *hgprt*, the double mutant *hgprt gsda*, *nsh1* and *xdh1*. Error bars show SD of 4 - 5 biological replicates.

.

With the RBSK located downstream of the purine and pyrimidine nucleoside degradation, the question arose whether the degradation of the purine and pyrimidine nucleosides is the only source for ribose during the dark stress treatment. Xanthosine is only detectable in the *nsh1* mutant line (Figure 37). Whereas xanthine, the product of the NSH1 reaction is detectable in the *xdh1* line and in smaller quantities as well in *gsda*, *hgprt* and the *gsda hgprt* double mutant. During the hydrolysis reaction catalysed by NSH1, equal amounts of the nucleobase xanthine of D-ribose are produced. 2.5 µg mg^{-1} dw xanthine resulted from the purine side of nucleoside degradation (Figure 37) at day 5 of the experiment and 2.5 µg mg^{-1}dw uridine from the pyrimidine degradation (Figure 38) resulted out of the NSH1 reaction. Those quantities match approximately the amount of D-ribose measured at day 5 with 5.5 µg mg^{-1}dw. These values indicate, that the degradation of purine and pyrimidine nucleosides contribute equally to the amount of D-ribose accumulating during the dark stress. The values are slightly different if one adds the xanthosine (about 5 µg mg^{-1}dw) to the uridine (about 2.5 µg mg^{-1}dw) in nsh1 background, but still the resulting 7.5 µg mg^{-1}dw nucleosides are close to the observed 5.5 µg mg^{-1}dw D-ribose at day 5. The data indicate that nucleosides are the exclusive source of D-ribose in planta.
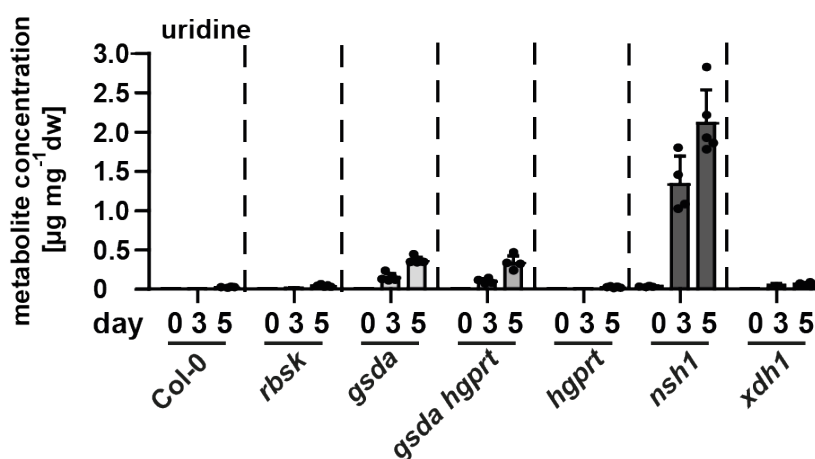
Figure 38: Measurement of uridine in *A. thaliana* rosette leaves at day 0, day 3 and day 5 of the dark stress treatment. Plant lines testes involved: Col-0 as wild type control, *rbsk*, *gsda*, *hgprt*, the double mutant *hgprt gsda*, *nsh1* and *xdh1* Error bars show SD of 4 - 5 biological replicates.

To elucidate other reasons for the *gsda* phenotype, guanosine and guanine were measured by LC-MS in all of the genotypes used in this experiment. The results for the *gsda hgprt* double mutant line confirm previous results. This double mutant line accumulates less guanosine but more guanine, than the *gsda* line at the respective days (Figure 39). In contrast, *hgprt* only accumulated small amounts of guanine and no guanosine. This leads to the conclusion that in the *gsda* background, guanosine is partially converted to guanine producing as well D-ribose. Guanine is then converted back to GMP (guanosine-monophosphate) by HGPRT using 5-phosphoribosyl-pyrophosphate as sugar phosphate

donor.
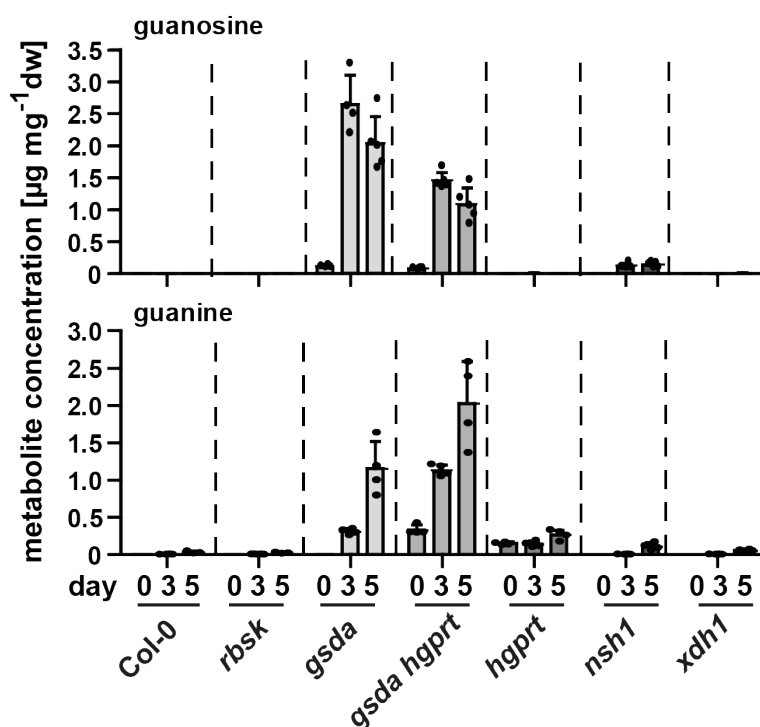
Figure 39: Quantification of guanosine and guanine in *A. thaliana* rosette leaves at day 0, day 3 and day 5 of the dark stress treatment by LC-MS. Plant lines testes involved: Col-0 as wild type control, *rbsk*, *gsda*, *hgprt*, the double mutant *hgprt gsda*, *nsh1* and *xdh1*. Error bars show SD of 4 - 5 biological replicates.

This constant generation of GMP to maintain GMP homoeostasis is filling the guanosine pool. The double mutant has less guanosine and more guanine because this cycle is interrupted in the absence of HGPRT (Figure 39). Overall, one can conclude that the high guanosine concentration in *gsda* causes the increased dark stress phenotype in this genetic background.

The blockage of the purine nucleoside degradation had side effects on other enzymes in the pathway. Guanosine and guanine accumulate slightly in the *nsh1* mutant line (Figure 39), and in the *gsda* and the double mutant *gsda hgprt* small quantities of xanthosine and xanthine are accumulating (Figure 37). It appears that in the *gsda* background the function of the NSH1 is partially impaired as well, maybe because if guanosine competitively inhibits the NSH1/NSH2 heterocomplex.

3.2.8 Impact of Nucleoside Accumulation on the *A. thaliana* Germination Rate

When seeds germinate on media lacking any nutrients to support seedling establishment they have to rely on their internal storage compounds. The mother plant is transferring nutrients from the source organs, like leaves, to the sink organs, like seeds.

The accumulation of guanosine in the *GSDA* mutant (Figure 39) has been shown to

have an effect on the germination rate of the seeds (Dahncke, 2014). To evaluate if the accumulation of other purine nucleosides and nucleobases has an influence on the germination rate of *A. thaliana* seeds, the purine nucleoside degradation mutants *gsda*, *nsh1*, the double mutant *gsda hgprt* and additionally the lines *hgprt* and *xdh1* were tested and compared with the wild type Col-0. Additionally, the *rbsk* line was included to investigate the influence of the accumulated D-ribose on the seed germination rate.
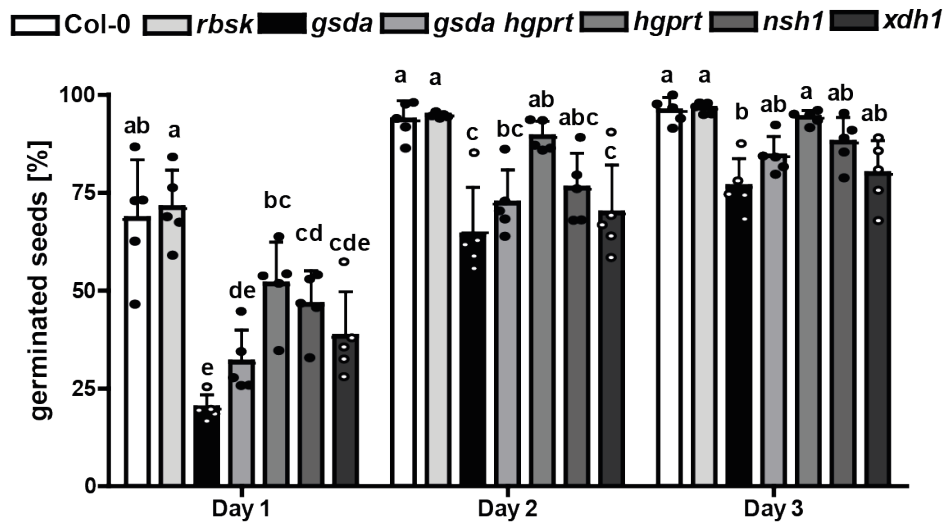
Figure 40: Germination time course of *A. thaliana* purine nucleotide degradation mutants and the *hgprt* line compared to the wild type Col-0. The seeds originated from 5 independent parent plants (n = 5) sown on 1% Agar with no additional nutrients supplied. Error bars are SD. Seeds were counted as germinated when the seed coat was ruptured . For the statistical analysis a 2-way ANOVA with Bonferroni post test was conducted. Differences in letters indicate a statistical difference p < 0.05.

The accumulation of D-ribose seems to have no effect on the germination rate of *A. thaliana* seeds (Figure 40), because the germination rate of the *rbsk* seeds is identical to the Col-0 wild type. Similarly, the *hgprt* line shows no difference to the wild type Col-0. The other mutant lines, especially the *gsda* line, displayed significantly delayed germination. In the *gsda* line, the effect is so strong that within the first 24 h only approximately 20% of the seeds germinated increasing up to 70% by day 3. The double mutant *gsda hgprt* showed an intermediate germination phenotype compared to the single mutant parents *gsda* and *hgprt*. The data indicates that factors leading to high guanosine concentrations enhance germination delay, presumably because guanosine is toxic for this process. The importance of the ability to metabolize purine nucleosides during germination is underlined by the general delayed germination rates of *gsda*, *gsda hgprt*, *xdh1* and *nsh1*.

3.2.9 Ribose Concentration During Different Stages of *A. thaliana* Ontogenesis.

During the different developmental stages of an *A. thaliana* plant life, the metabolism changes according to the developmental requirements. During the reproductive stage nutrients are withdrawn from the vegetative tissue, transported to the reproductive organs, and later into the seeds. In Jung *et al.* (2011), it was shown that nucleotide metabolism accelerates during the reproductive phase leading to an early senescence phenotype in *NSH1* mutants. Since RBSK acts downstream of NSH1, one may speculate that the RBSK protein production might be increased at later development stages.
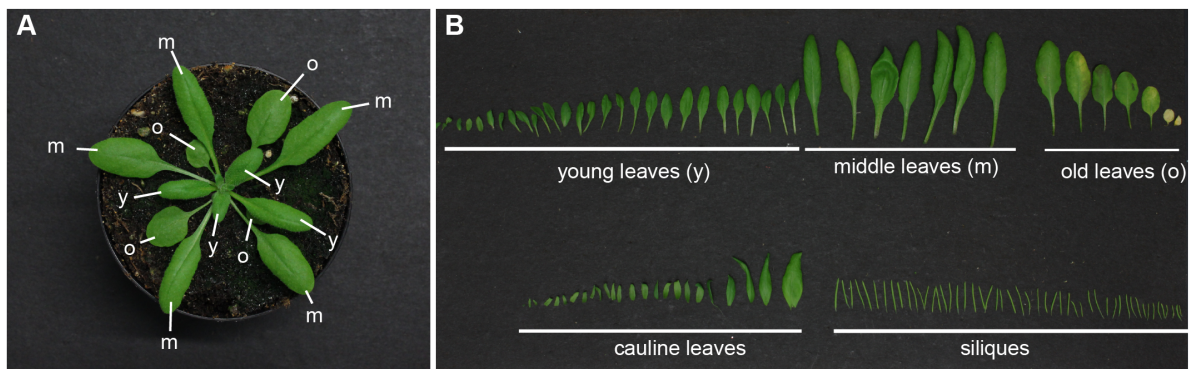
Figure 41: Determination of *A. thaliana* plant material for separation into young (y), middle (m) and old (o) prior to D-ribose quantification of 24-day-old plants (A). From 45 days old plants, apart from the rosette samples, siliques, flowers and cauline leaves were included into the measurement (B).

To obtain an overview of the RBSK production and the D-ribose concentration during the ontogenesis of *A. thaliana*. The plants were grown under long day conditions on soil until the day of harvest. Only the seedlings were grown on 0.5 MS medium for up to 10 days. The plants were either grown for 24 days, just prior to the start of the reproductive stage (before bolting, Figure 41A). Or up to 45 days to produces flowers and siliques (after bolting, Figure 41B). The different samples harvested were: 10 days old seedlings, leaves from rosettes before bolting, flowers, siliques, cauline leaves and rosette leaves during the reproductive phase. The rosette material was further separated into young, middle and old leaves to obtain a detailed overview over the D-ribose concentrations across the rosette.
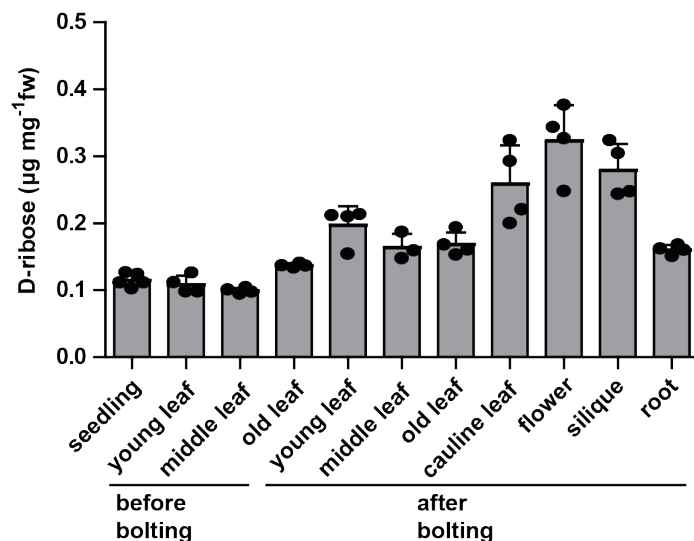
Figure 42: D-ribose quantification of different developmental stages. The tissues are: 10 days old seedlings, leaves of plants before the begin of the reproductive phase and plants after bolting with several shoots and fully developed siliques. The rosette leaves were separated into young, middle and old leaves. Additionally root sample tissues were taken. fw, fresh weight. Error bars show SD of 4 - 5 biological replicates.

The concentrations of D-ribose range in plants before bolting, including seedlings, from about 100 ng mg^{-1} fw to 130 ng mg^{-1} fw (Figure 42) in older leaves. In plant tissue after bolting, the concentration of D-ribose range from 180 ng mg^{-1} fw in middle and old rosette leaves up to 320 ng mg^{-1} fw in flowers. The higher D-ribose concentration in the reproductive phase might be explained with a potentially higher nucleoside turnover during senescence and reproduction.

Additionally, to the D-ribose profile the RBSK protein production profile was recorded in distinct tissues of plants from different developmental stages. Total protein was extracted from different tissues of Col-0 plants grown in parallel to the *rbsk* plants used for LC-MS analysis. The harvest of the material was performed similar as described before and 10 µl of the protein samples, obtained from equal fresh weight, were loaded on an SDS polyacrylamide gel for subsequent immunoblotting. For the detection of the RBSK protein, background the RBSK antibody was used.

35 kDa

seedling | young leaf | middle leaf | old leaf | young leaf | middle leaf | old leaf | cauline leaf | flower | silique | root

before bolting   **after bolting**
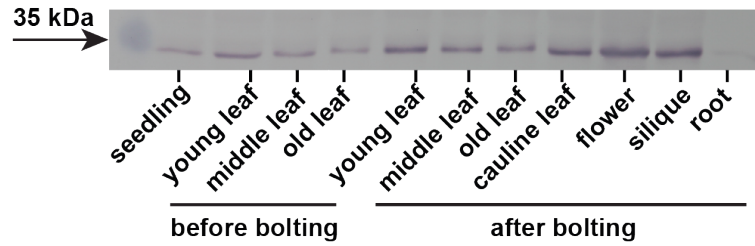
Figure 43: Western Blot of Col-0 protein extracts detected with an RBSK-antibody. 8 µl of protein extract, obtained on equal fresh weight basis, were loaded and transferred onto a nitrocellulose membrane. For the development of the membrane an RBSK-antibody (1:400) was used as primary antibody followed by an rabbit-IgG antibody conjugated to an alkaline phosphatase. Due to the viscosity of the root sample tissue it was diluted 1 : 4 prior to use. The other samples were used undiluted.

The protein production pattern of the RBSK matched the D-ribose profile found in the *rbsk* from the LC-MS analysis, showing that a higher D-ribose accumulation coincides with a stronger RBSK production in the different tissues of bolting plants to plants before bolting or 10-day-old seedlings (Figure 43). Contrary to expression data available from *eFP browser*, a *RBSK* signal was detected in root tissue, leading to the conclusion that the *RBSK* is expressed in roots.

3.3 Investigation of a Putative D-ribose Permease

The nucleoside hydrolysis by the NSH1 and NSH2 heterocomplex is localised in the cytosol, whereas the RBSK reaction is localised in the chloroplast (Riggs et al.,2016; Schroeder *at al.,* 2018). Therefore, the D-ribose has to be transported from the cytosol into the chloroplast, for further use in the RBSK reaction. However, a plastidic D-ribose transporter is unknown up to date.

Due to the limited amount of described D-ribose permeases, a new approach was chosen to identify suitable candidate genes for a plastidic D-ribose transporter. Ureides are catabolic intermediates derived from purine ring degradation, which are used in tropical legumes for the export of fixed atmospheric nitrogen from nodules to the shoot. It was estimated in such legumes, that genes involved in the nucleotide biosythesis, will be upregulated in the nodules versus roots of ureide exporting plants compared to homologous genes expressed in nodules of amide exporting legumes. Therefore, could this analysis lead to yet unknown candidate genes involved in the ureide biosynthesis.

3.3.1 Comparative RNAseq Analysis of Ureide and Amide Exporting Legumes

RNAseq data from ureide exporting legumes like *Glycine max* (L.) and *Phaseolus vulgaris* (L.) were compared with amide exporting legumes *Lotus japonicus* (L.) and *Medicago truncatula* (L.). The RNAseq data from publicly available sources were combined and statistically evaluated by Marco Herde as the *P.vulgaris* data set had the best statistical coverage, it was chosen as a starting point for the database assembly. Based on the similarity scores to *P. vulgaris* sequences, orthologues of the other three species were assigned. As major pre-selection criterion, transcripts of candidate genes needed to be up-regulated at least 1.5 times in *P. vulgaris*. Subsequently all expression patterns were statistically evaluated and a corrected p-value was assigned. Those candidates which showed no statistically significant upregulation were not excluded from the list. However, the absence of statistically significant regulation were denoted with a "no" in Table 41. In cooperation with Katarina Winkel the orthologs of genes from the monosaccharide transporter-like gene family (MST-like) characterised by Büttner *et al.* (2007) in *A. thaliana* were assessed for specific upregulation in the ureide exporting legumes *P. vulgaris* and *G. max* compared to the amide exporting legumes *L. japonicus* and *M. truncatula*. For all the genes in the MST-like subfamily *At*pGLCT/*At*SGB1 orthologs in the four legumes could be found by homology analysis choosing the candidates with the best E-value starting from the *A. thaliana* sequence.

Table 41: RNAseq analysis of the *At*pGLCT/*At*SGB1 family homologues (subfamily of MST-like family) in ureide and amide exporting legumes. The *A. thaliana* gene numbers are listed with the expression data of their *P. vulgaris*, *G. max*, *L. japonicus* and *M. truncatula* orthologues. The values represent the fold changes of gene expression in nodules versus roots by the algorithm *edgeR* (including Bonferroni correction $p < 0.05$) as reported by McCarthy *et al.* (2012). not matching pre-selection criteria: regulation criteria of at least a 1.5 fold change is not matched in *P. vulgaris*; no: no upregulation after p-value correction. *RBSK*: ribokinase *pGLCT*: plastidic glucose transporter; *pGLCT-LIKE*: plastidic glucose transporter like; *SGB1*: suppressor of G protein beta1; *SGB1-LIKE*: suppressor of G protein beta1 like.

Name	*Arabidopsis thaliana* gene number	*Phaseolus vulgaris*	*Glycine max*	*Lotus japonicus*	*Medicago truncatula*
RBSK	At1g17160	-3,2575	-1,532	no	no
pGLCT	At5g16150	-4,7970	-1,929	no	no
pGLCT-LIKE	At1g05030	no	no	no	no
SGB1	At1g79820	not matching pre-selection criteria			
SGB1-LIKE	At1g67300	not matching pre-selection criteria			

From all candidates out of the MST-like transporter family described by *Büttner et al.* (2007), only the *A. thaliana* gene At5g16150 orthologue in *P. vulgaris* showed the expected expression pattern. The homologue of this gene shows a five-fold up-regulation in *P. vulgaris* and a two-fold upregulation in *G. max*, in nodules compared to root tissue. By contrast, the homologues of the amide exporting legumes do not show any expressional changes.

Matching the expected expression criteria, the gene At5g16150 (*pGLCT*)could be involved in the ureide biosynthesis and therefore be a putative D-ribose transporter. But the gene At1g05030, with the highest similarity towards *pGLCT*, does not show any up-regulation in either of the legumes.

In summary, the gene At5g16150 showed the expected expression pattern to be involved in the ureide synthesis in ureide exporting legumes and therefore might be involved in D-ribose transport. This transporter is described previously as a plastidic glucose transporter and therefore was studied in more detail.

3.3.2 Cloning of the Putative D-ribose Permease *pGLCT* of *A. thaliana*

The coding sequence (cds) without stop codon of At5g16150 was amplified from *A. thaliana* leaf cDNA by PCR with the primers P1012 and P1013. This cloning led to the constructs

H390 and H391, in which the pGLCT protein was fused C-terminally to a HA/StrepII tag (H390) and an eYFP tag (H391). In parallel the cds was amplified with the primers P1014 and P1012 from cDNA, to include the native stop codon (H392) for protein production without a tag.

3.3.3 Subcellular Localisation of the pGLCT-YFP after Transient Production in *N. benthamiana*

The pGLCT transporter was already described as a plastidic glucose exporter by *Weber et al.,* (2000) and *Cho et al.* (2011). However, subcellular localisation by confocal laser scaning microscopy (CLSM) was never conducted before. The H391 (pGLCT-YFP) construct was transformed into *A. tumefaciens* cells and transiently produced in *N. benthamiana* leaves as described in Chapter 2.2.14.

In the CLMS analysis, the YFP signal shows a clear circular shape (Figure 44A) surrounding the chloroplast autofluorescence (Figure 44B). This indicates chloroplastidic localisation for the pGLCT-YFP fusion protein, confirmed by the overlay of both channels in picture 44C. The immunoblot shows a signal at approximately 66 to 68 kDa in the crude protein extract of pGLCT-eYFP infiltrated leaves compared to the uninfiltrated wild type sample (Figure 44D). Interestingly, the size of the fusion protein differs from the predicted size of 84 kDa and was approximately 16 kDa smaller than expected. Reasons for this variation in size could be that the predicted protein includes the organellar targeting peptide, directing the protein to the chloroplast membrane. *Weber et al.* (2000) reported that the mass of the processed pGLCT protein is 43 kDa, when combined with the 25 kDa of YFP leads to a mass of 68 kDa for the processed fusion protein.
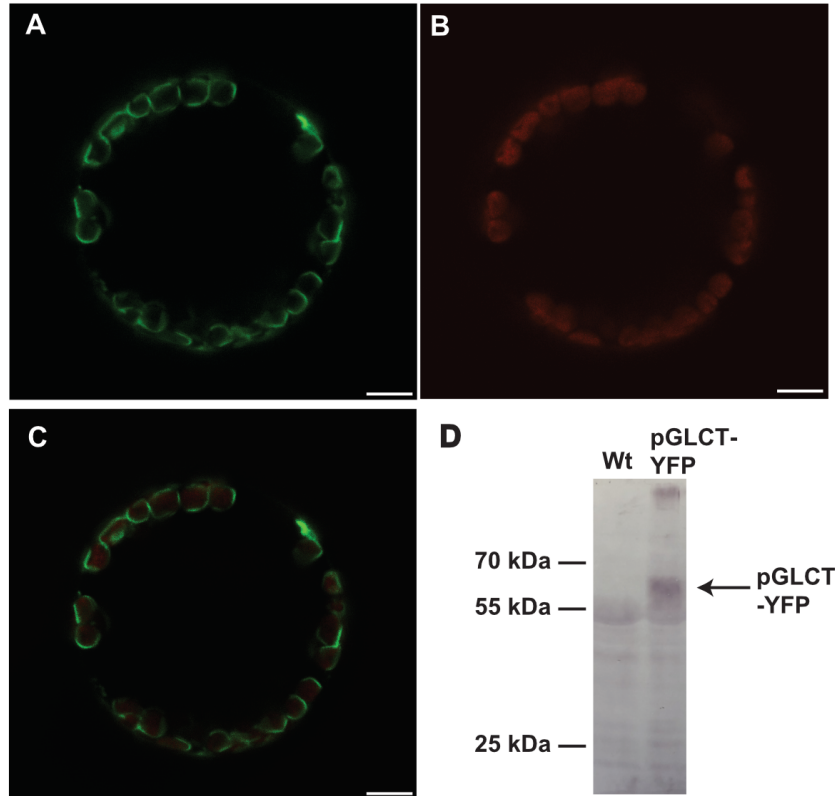
Figure 44: CLMS analysis of a *N. benthamiana* mesophyll protoplast after transient expression of the pGLCT-YFP fusion protein in (H391). A: YFP channel; B: chloroplast autoflourescence; C: Overlay of prictures A and B; D: immunoblot of 10 µl clarified crude protein extract from infiltrated *N. benthamiana* leaves. A monoclonal anti-YFP-antibody from mouse and an goat-anti-mouse IgG-antibody conjugated to AP were used for detection. The expected size of the fusion protein is 84 kDa. The scale marks 7.5 nm.

The marked band (P) in the immunoblot in Figure 44C corresponds to a protein of less than 70 kDa. Free YFP was not detected, demonstrating that the fusion protein was stable.

In summary, the subcellular localisation of the pGLCT protein at the chloroplast membrane was shown for the first time by CLMS confirming previous biochemical data, indicating a plastidic localisation (Weber *et al.,* 2000).

3.3.4 Selection of a *pGLCT* Complementation Line

The transporter pGLCT was described by *Weber at al.*(2000) and *Cho et al.* (2011) to be a plastidic glucose exporter. Cho *et al.* characterized the *A. thaliana* mutant lines *pglct-1* and *pglct-2* (Figure A8) and confirmed that both lines are null mutants on transcript and protein level. For the investigation of the D-ribose transport in *A. thaliana*, the mutant lines characterised by *Cho et al.* were obtained from NASC and the genetic status was confirmed by PCR.

To examine a putative D-ribose transport function for pGLCT, a thorough metabolite analysis was conducted, including not only the *pGLCT* mutant lines, but as well a functional pGLCT complementation lines. To generate these, *pglct-2* plants were transformed with the pGLCT-YFP construct or alternatively with pGLCT constructs which does not have a tag (H391, H392). Seeds of the transformed T0 generation were harvested, sown on soil and selected with *Basta* as described in Chapter 2.2.26. Survivors of this selection procedure were propagated. In the F2 generation, the *Basta* selection was repeated, and leaf material was harvested from the surviving plants. The pGLCT production was examined in the pGLCT-YFP line by CLSM.
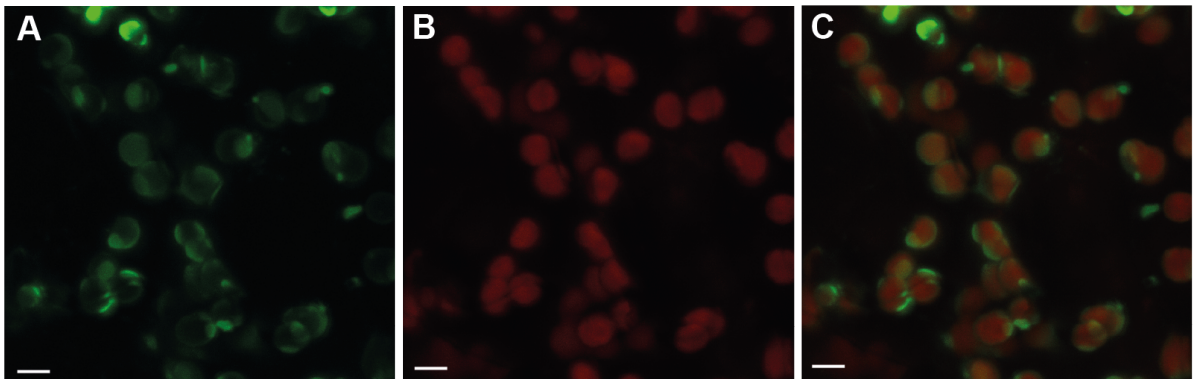
Figure 45: CLSM analysis of H391 (pGLCT-YFP) stable expression line (F2 generation) in rosette leaves. A: YFP signal, B: chloroplast autofluorescence, C: overlay of channel A and B. Scale bar: 5 nm.

For the line H391, a strong YFP signal was detected (Figure 45A) in the periphery of mesophyll chloroplasts, surrounding the chloroplast autofluorescence (Figure 45B and 45C). This shows a strong production of the pGLCT-YFP fusion protein in the *A. thaliana* plants.

In parallel to the pGLCT-YFP complementation line, a line producing pGLCT without a tag was propagated. Because a detection via a tag is impossible in this line, a semi-quantitative RT-PCR was conducted, using primers specifically binding to the introduced transgene.
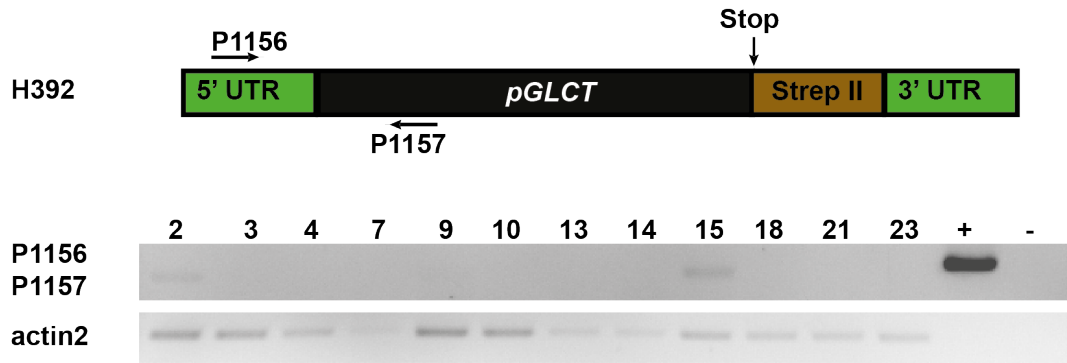
Figure 46: RT-PCR on cDNA from 12 plants of the stable complementation line of pGLCT in *A. thaliana pgclt-2* background. The pimers P1156 and P1157 only generate a PCR product on the transgene introduced from construct H392. As a positive control H392 plasmid DNA was used. As quality control of the synthesised cDNA, the *ACTIN2* gene was amplified.

From the 12 plants tested in the RT-PCR, a signal was detected only for three of the plants. Signals from plant number 2 and number 15 are clearly visible in the agarose gel (Figure 46). For a third plant, number 9, a very faint signal was detected, suggesting a weak transcript amount in this line. The three plants selected by expression in this experiment were propagated further to generate seeds. The following offspring of line number two were used for the metabolite analysis.

3.3.5 Assessment of the D-Ribose Concentration in *pglct-2* Plants Compared to *rbsk* and the wild type.

The hydrolysis of nucleosides by NSH1 and NSH2 and the phosphorylation of D-ribose to D-ribose-5-phosphate are consecutive reactions in the D-ribose metabolism. The *RBSK* mutant is accumulating high amounts of D-ribose. So it was assumed that, if the D-ribose cannot be activated due to the lack of a functional transport mechanism in the *pglct* lines, D-ribose might accumulate as well. Dark stress conditions were used to increase the flux through nucleoside hydrolysis, potentially boosting any effects.
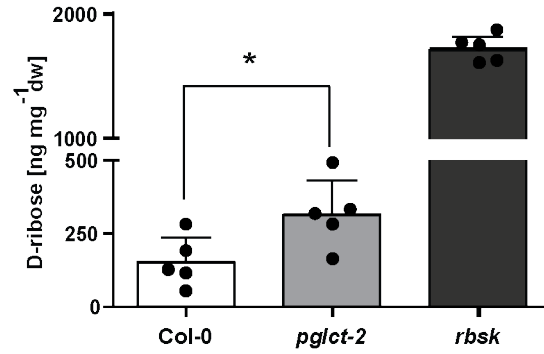
Figure 47: D-ribose quantification of 29-days-old *A. thaliana* rosettes after three days of dark stress. Error bars show SD (n = 5). Individual values of the replicates are shown as black circles. For statistical analysis, a student t-test was used indicating statistical significance at p < 0.05.

For the *pglct-2* line about 300 ng mg^{-1} dw D-ribose were detected, which is significantly more D-ribose compared to the wild type Col-0 (Figure 47). This result shows, that the pGLCT transporter might be involved in the transport of D-ribose at the plastid membrane. However, compared to the *rbsk* line the *pGLCT* mutant line accumulated 15 times less D-ribose. The discrepancy in the D-ribose accumulation between the mutant lines led to the question, whether other transporters might as well be involved in transporting D-ribose in cooperation with pGLCT.

3.3.6 D-Ribose Quantification by LC-MS in Seedling Shaking Cultures Supplied with Uridine

Uridine is a pyrimidine nucleoside and a substrate of NSH1, which hydrolyses the bond between the nucleobase (uracil) and the D-ribose residue. It was speculated that a supply of nucleosides in form of uridine might lead to an increase in D-ribose accumulation in mutants blocked in the metabolism or internal transport of this sugar if pGLCT and RBSK actually work consecutively in the D-ribose recycling pathway, the D-ribose pool should increase in both corresponding mutants in the same way, when uridine is supplied as an extra D-ribose source.

Liquid media cultures with 50 seeds were grown for 6 days as described in Chapter 2.2.31. At the 7th day, 0.1 mg ml^{-1} uridine was added to the fresh media for 24 h, followed by the seedling harvest and metabolite extraction.
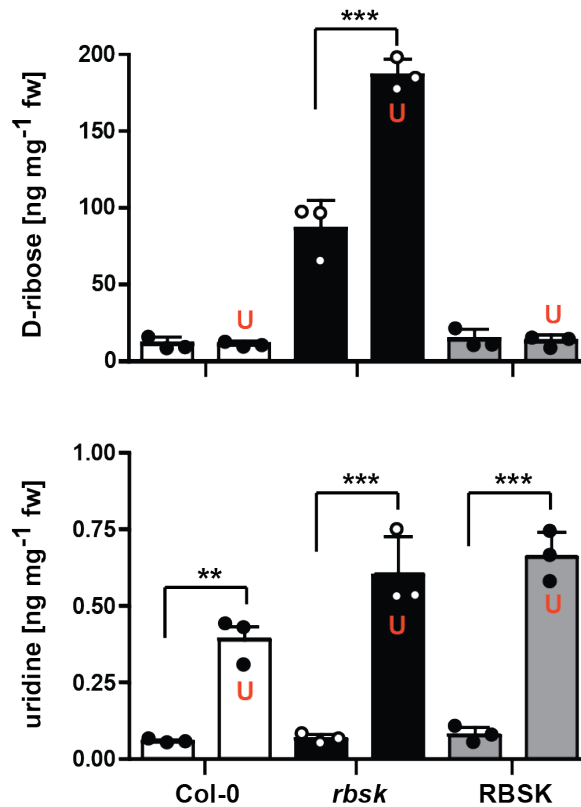
Figure 48: D-ribose quantification (upper panel) and uridine quantification (lower panel) in 7-days-old seedlings. After incubation for 24 h with media containing 0.1 mg ml^{-1} uridine. The samples supplied with uridine are marked with a red U. Circles show individual data points. For statistical analysis a One-way-ANOVA was used with Bonferroni post test. ($p < 0.05$ = *; $p < 0.01$ = **; $p < 0.001$ = ***)

First, an experiment with the wild type, an *rbsk* line and the RBSK complementation line in *rbsk* background was conducted. If uridine was supplied to 7-days-old seedlings, the uridine concentration in plants exposed to uridine was significantly higher as in plants not supplied with additional uridine (Figure 48). Ample washing of the seedlings at harvest insured that uridine from the medium was fully removed before the measurement. The supplied uridine was taken up by the seedlings and increased the uridine pool by four-fold in Col-0 within 24 h and up to six-fold in the *rbsk* and RBSK line. The exposure to uridine led to a significant increase of D-ribose in the *rbsk* seedlings but not in Col-0 or the RBSK complementation line. The D-ribose accumulation was twice as high as in *rbsk* plants supplied with uridine compared to plants without additional uridine. A total amount of 1.5 mg of uridine was supplied to 50 seedlings and approximately 0.6 ng mg^{-1} fw total uridine could be measured in the *rbsk* samples. The reason for this difference in uridine supply and incorporation might be uridine salvage to UMP and further use by the plant, for example in nucleic acids, or that the uridine is not taken up entirely within the 24 h of the experiment. In summary, the supply of uridine is, a suitable way to increase the input to the D-ribose pool in *A. thaliana* seedlings.

The *pGLCT* mutant lines (*pglct-1* and *pglct-2*) and the corresponding wild type lines isolated from the segregating mutant populations were analysed in a second uridine shaking culture experiment it was hypothesised, that the mutant lines might show an increase in the D-ribose concentrations similar to the *rbsk* line when uridine was supplied.
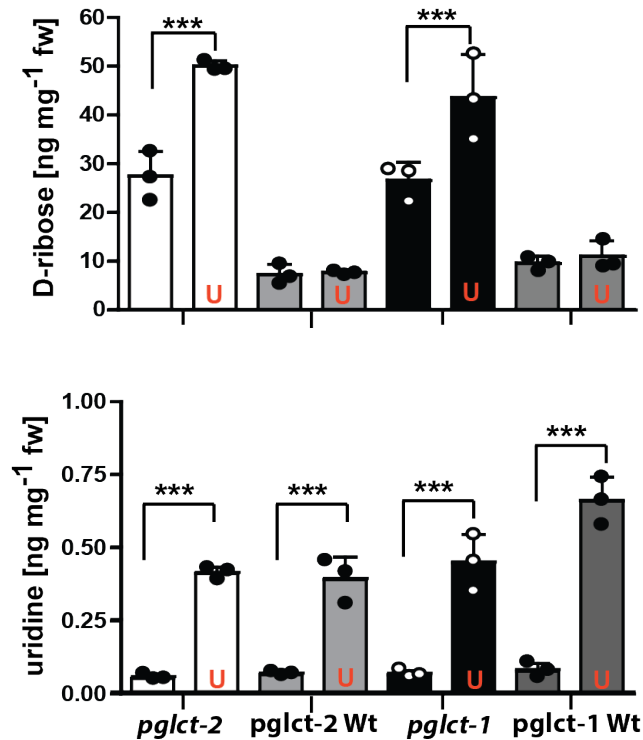
Figure 49: Quantification of D-ribose (upper panel) and uridine (lower panel) in 7-days-old seedlings of a shaking culture after incubation with 0.1 mg ml^{-1} uridine for 24 h. The corresponding wild type lines, isolated from the segregating mutant populations, were included as controls (pglct-2 Wt, pglct-1 Wt). The samples supplied with uridine are marked with a red U. For statistical analysis a One-way-ANOVA with Bonferroni post test was used. ($p < 0.05$ = *; $p < 0.01$ = **; $p < 0.001$ = ***)

The uridine concentration in the samples supplied with uridine is significantly higher than the untreated samples throughout all lines (Figure 49 lower panel). The concentrations of uridine, ranging 0.45 to 0.60 ng mg^{-1}fw, match the amount measured in Col-0 before (Figure 48 lower panel). The *pGLCT* mutant lines, but not in the corresponding wild type lines, the D-ribose concentration was significantly increased after uridine treatment (pgclt-1 Wt; pglct-2 Wt; Figure 49 upper panel). Without any supply of uridine, the D-ribose concentration was already higher in the *pGLCT* mutants than in the corresponding wild type lines. This concentration is increased up to approximately 50 ng mg^{-1}fw D-ribose in the *pGLCT* mutants with the supply of uridine. The about two-fold increase of D-ribose concentration in the *pGLCT* mutant lines upon uridine feeding, matches the increase

observed in the *rbsk*. However, the *rbsk* line still accumulated five times more D-ribose than *pglct-2*. This result strongly suggests, that the pGLCT transporter is transporting D-ribose. Furthermore, the similarity in fold chance in D-ribose concentration of the *rbsk* and the *pglct* line, shows that both proteins are linked in the D-ribose recycling pathway.

3.3.7 Investigation of Possible D-Ribose Transport Into the Cholorplast Stroma by a pGLCT-LIKE Transporter

The accumulation of D-ribose in the *pglct* lines differs significantly from the accumulation in the *rbsk* lines. This leads to the question, whether an additional permease is transporting D-ribose, which may explain why the total accumulation of D-ribose detected in the *pGLCT* mutant lines is less than expected. Büttner *et al.* (2007) showed that in *A. thaliana* the pGLCT transporter has a paralogous gene, called *pGLCT-LIKE* (At1g05030). Although, this gene is not up-regulated in ureide exporting legumes compared to amid exporting legumes (Table 41), we included the *pGLCT-LIKE* gene in our analysis as well, to evaluate its contribution to the D-ribose transport in *A. thaliana*.

Because *pGLCT-LIKE* is not characterized up to now, a first CLSM analysis was conducted to assess, whether the protein is located as well in the chloroplast membrane. The pGLCT-LIKE, comprising a C-terminal YFP tag, was transiently produced in *N. benthamiana*, for this subcellular localisation analysis.

After the transient protein production of pGLCT-LIKE-YFP (H439) in *N. benthamiana* for three days, leaf material was harvested and protoplasts were prepared as described in Chapter 2.2.28. In the CLMS analysis, a strong YFP signal was detected from pGLCT-LIKE-YFP (Figure 50A), which co-localised with the chloroplast autofluorescence (Figure 50 B) in the overlay of both channels (Figure 50C). To confirm the protein stability an immunoblot was performed with crude extracts of pGLCT-LIKE-YFP including the controls pGLC-YFP and uninfiltrated *N. benthamiana* leaves (Figure 50D). The immunoblot is showing a pGLCT-LIKE-YFP signal at the mass of 70 kDa, although the predicted size is 84 kDa. This indicates proteolytic cleavage of the full-length protein for the translocation into the chloroplast.
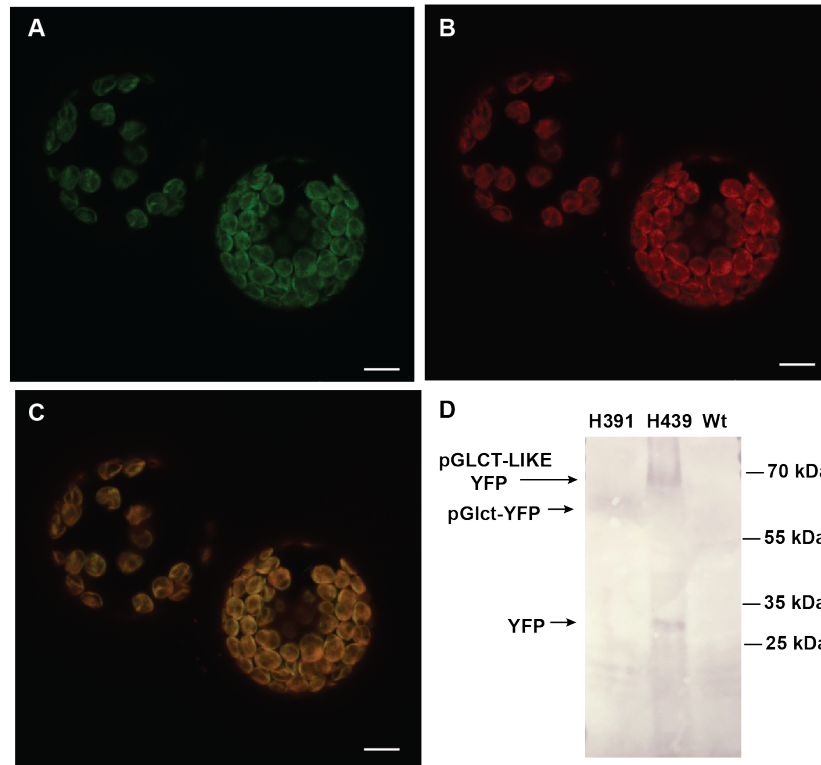
Figure 50: Subcellular localisation of pGLCT-LIKE-YFP (H439) after transient protein production in *N. bethamiana* and preparation of mesophyll chloroplasts. A: YFP signal, B: signal of the chloroplast autofluorescence, C: overlay of the channels A and B, D: immunoblot detection with anti-YFP antibody from mouse and goat-anti-mouse IgG conjugated to AP as secondary antibody. 10 µl clarified crude extract from *N. bethamiana* were loaded from pGLCT-LIKE-YFP (H439), pGLCT-YFP (H391) and uninfiltrated *N. benthamiana* leaves (Wt) as controls. The scale size is 10 nm.

This result indicates that the pGLCT-LIKE-YFP fusion might become unstable after import into the chloroplast, so free YFP accumulated after proteolytic cleavage in the chloroplast stroma. Furthermore, this result raises doubts about the functional similarity towards the pGLCT transporter, but a definitive conclusion however, can not be drawn from this CLSM analysis.

3.3.8 Characterisation of the *pGLCT-LIKE* Mutant Line

For the evaluation of the pGLCT-LIKE contribution to the D-ribose transport into the chloroplast, a further metabolic analysis was conducted. The D-ribose accumulation was measured in a *pGLCT-LIKE* mutant background. The mutant line Ko172 (Table 14) was obtained from NASC and was analysed by PCR and RT-PCR.
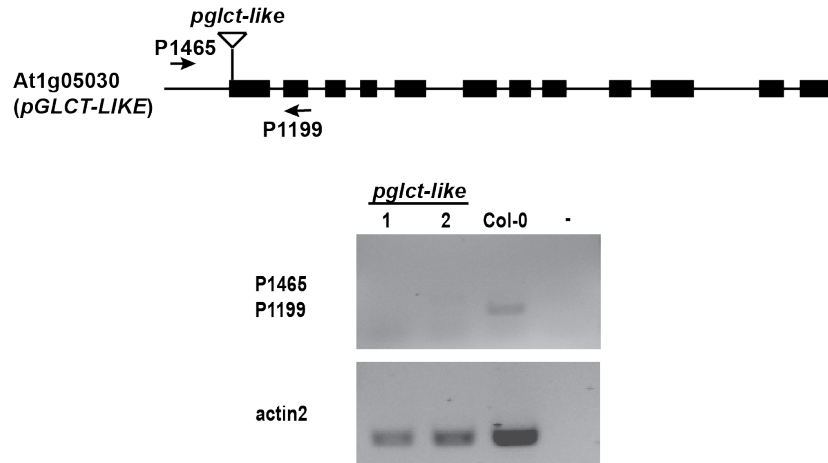
Figure 51: Trascript analysis of the *pGLCT-LIKE* mutant by RT-PCR. The primers P1465 and P1199 are flanking the T-DNA insertion in the first exon of the *pGLCT-LIKE* gene. As control an *ACTIN2* PCR was included to show the presence of amplifyable cDNA. The cDNAs fom two individual mutant plants, as well as from Col-0 and a control without cDNA were analysed.

The insertion point of the T-DNA was confirmed by sequencing prior to the transcription analysis. Two primers (P1465, P1199) were designed flanking the insertion point of the T-DNA (Figure 51). The amplification of the cDNA from two independent *pglct-like* plants did not lead to a signal with primers flanking the T-DNA insertion, whereas the Col-0 control shows a band at 300 bp. The presence of amplyfiable cDNA is shown by the *actin2* signal in the lower agarose gel picture (Figure 51). In conclusion, it could be confirmed that the *pglct-like* line is a null mutant with no residual transcript.

The *pglct-like* line was examined for phenotypic differences compared to a wild type line obtained from the segregating mutant line (pglct-like Wt) (Figure 52). After 30 days, no difference was visible between the *pglt-like* and the corresponding wild type line (Figure 52). At 48 days after germination, the plants were again visually compared and showed no difference compared to the wild type line (pglct-like Wt) for five replicates each. The biomass generation of both lines was determined for the rosette and the combined shoot tissues. In both, rosette and shoot weight measurements, the *pglct-like* line showed minimal less weight in comparison to the wild type line (Figure 52). The mutation of *pGLCT-LIKE* might have an impact on the shoot biomass generation, although the differences were not statistically significant at $p < 0.05$.
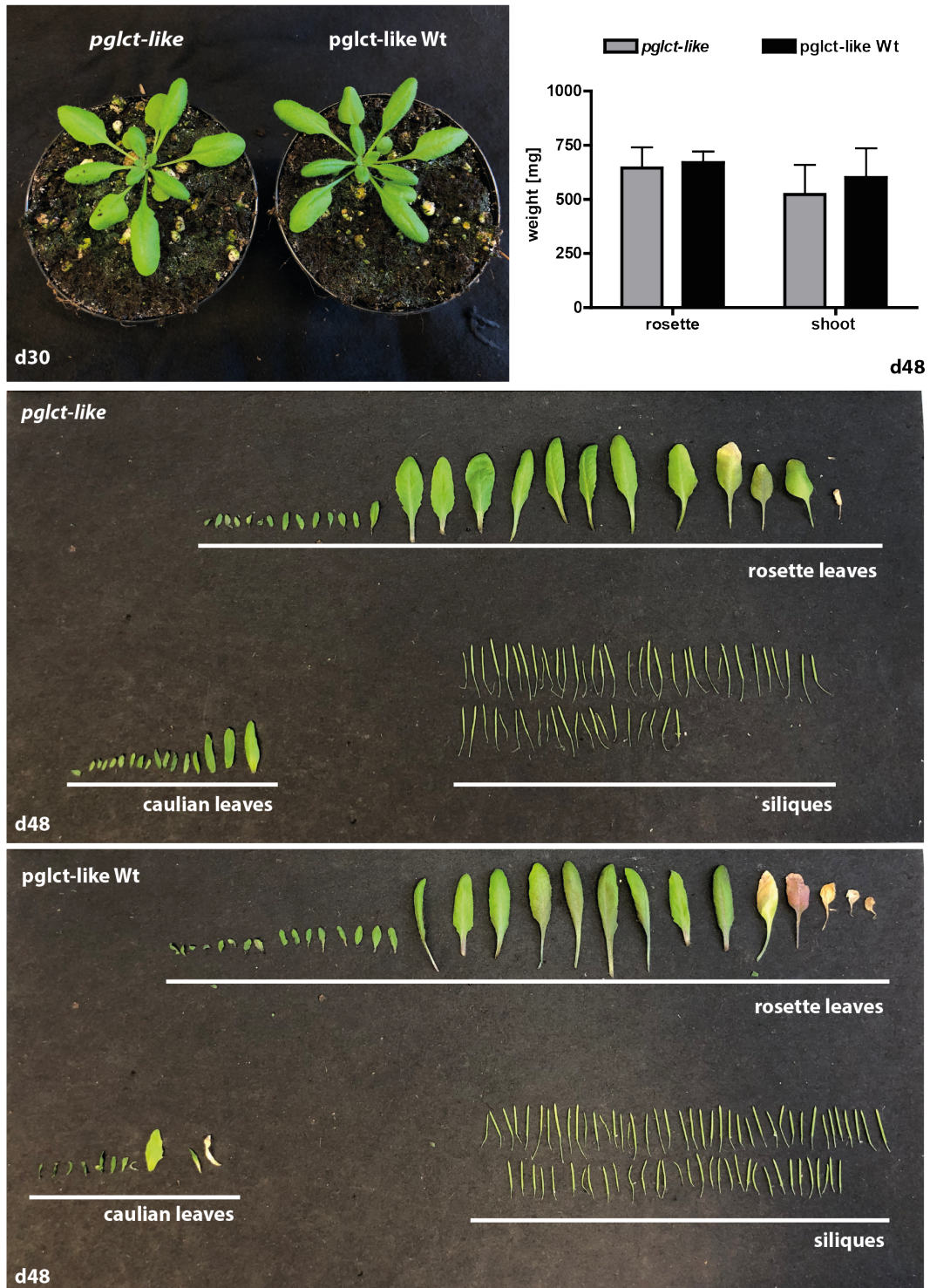
Figure 52: Phenotypical examination of the *pglct-like* line compared to the pglct-like wild type line obtained from a *pglct-like* segregating population. The plants were compared at 30 days after germination (d30) during the vegetative phase and at day 48 (d48) during the reproductive phase. Shoots and rosettes of five biological replicates of each line were analysed for their fresh weight (d48). Statistical analysis using a Student's t-test was used at p < 0.05. Error bars show SD (n = 5).

3.3.9 Evaluation of the pGLCT-LIKE Contribution to the D-Ribose Recycling in *A. thaliana* Mutant Lines

To examine, if the pGLCT-LIKE transporter is contributing to the D-ribose transport in *A. thaliana* plants, leaf material of five biological replicates after three days of dark stress was harvested. The metabolites were extracted and quantified as described in Chapter (2.2.22).
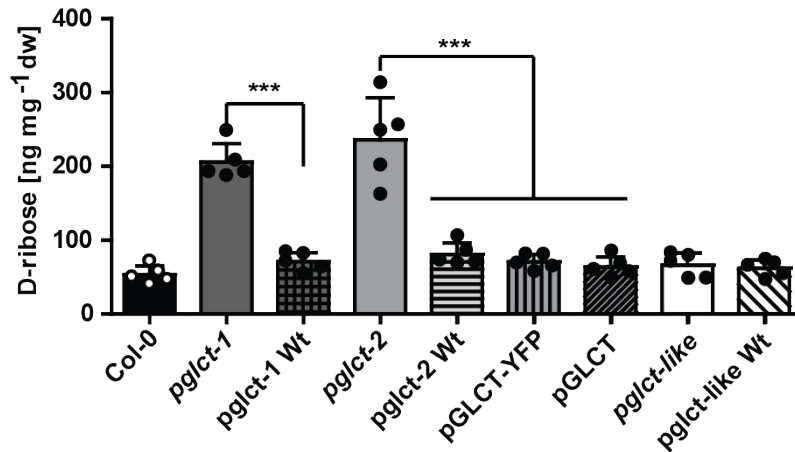
Figure 53: LC-MS quantification of the D-ribose concentration in 28-days-old plants after three days of dark stress. Included in the analysis were the corresponding wild type lines to the mutant lines *pglct-1, pglct-2* and *pglct-like* marked with *Wt*. Furthermore the stable complementation lines pGLCT-YFP (H391) und pGLCT without a tag (H392) were included. For statistical analysis a one-sided ANOVA with Bonferroni post test was used (p < 0,001 = ***). The error bars show SD (n = 5), indicated by the black or white circles.

The D-ribose concentration in dark stressed *A. thaliana* plants is more than doubled in the *pGLCT* mutant lines *pglct-1* and *pglct-2* compared to the corresponding wild type lines pglct-1 Wt and pglct-2 Wt (Figure 53). In the complementation lines pGLCT-YFP and pGLCT (in *pglct-2* background) D-ribose concentrations were as low as in the wild type. Additionally, the *pglct-like* line and the corresponding wild type line were included in this analysis. In both, the D-ribose concentrations are not higher than in Col-0 or other Wt-controls, which indicates that pGLCT-LIKE is not involved in D-ribose transport into the chloroplast. Further evidence could be obtained by the analysis of a *pglct pglct-like* line. This double mutant would exclude the possibility that possible lack of a pGLCT-LIKE D-ribose transport function by the functional pGLCT transporter is masked in the *pglct-like* background.

3.3.10 D-Ribose Quantification in a 24 h Time Course

Cho *et al.* (2011) showed that the *pGLCT* mutant slightly accumulated glucose during the night time (8 h dark). A possibility is that this permease has a dual transport function, exporting glucose from the chloroplast at night to support starch degradation and importing D-ribose during the day time, for phosphorylation by the RBSK in the chloroplast. To evaluate the circadian changes in the D-ribose concentration, samples from *pglct-2* plants and the corresponding wild type (pglct-2 Wt) were harvested in 6 h intervals during 24 h.
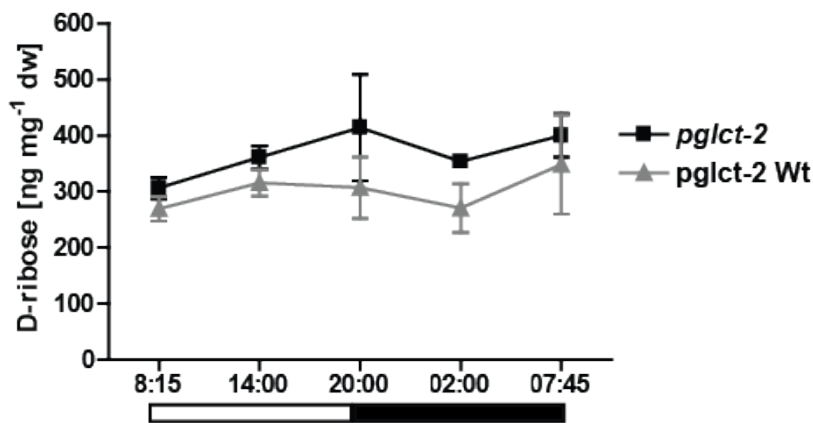
Figure 54: D-ribose quantification in 42-days-old rosettes. The harvest points were spread equally over the time course of the experiment. Plants were grown in 12 h day/night conditions for at least one week prior to harvest. For the statistical analysis, a two-way ANOVA with Bonferroni post test was used. The error bars show SD values (n = 4).

If the proposed dual function as a glucose exporter at night and a D-ribose importer by day is correct for pGLCT, D-ribose should accumulate naturally in the wild type by night, because the transporter is occupied with glucose transport at that time and cannot import any D-ribose.

Indeed, an apparent increase in D-ribose concentration from the middle towards the end of the night was observed in the pglct-2 Wt (Figure 54). The *pglct-2* mutant is showing the same tendency. However, the increase is not statistically significant in neither of the lines. Over all, a higher D-ribose concentration was measured in the *pglct-2* line throughout the experiment, compared to the pglct-2 Wt, which already contained 250 ng mg^{-1}dw, due to the age of the plants. It was suggested that D-ribose accumulated in the night, will be depleted over the day, because the pGLCT transporter might not export glucose during the day. This seems to be a very efficient process because the quantities of D-ribose decreased by about 20% in the pglct-2 Wt line. Next morning the value of the previous morning is reached again. Furthermore, the D-ribose concentration is more or less steady over the day in the wild type.

In summary, dual transport function of pGLCT was obtained in this experiment. A repetition will be required, due to the high standard deviations and the advanced age of the plants, resulting in a high background concentration of D-ribose. The second wild type line from the segregating population of *pglct-1* might be included in a new the analysis as an independent line. Additionally, glucose should be quantified to estimate whether the D-ribose and glucose concentrations change antagonistically.

3.3.11 Impact of the pGLCT Transporter on the D-Ribose Transport During *A. thaliana* Onthogenesis

The D-ribose accumulation is increased during the reproductive phase of the *A. thaliana* life, shown for the *rbsk* line (Figure 42). Here the effect of pGLCT abrogation on D-ribose concentration during different stages of plant life was evaluated.
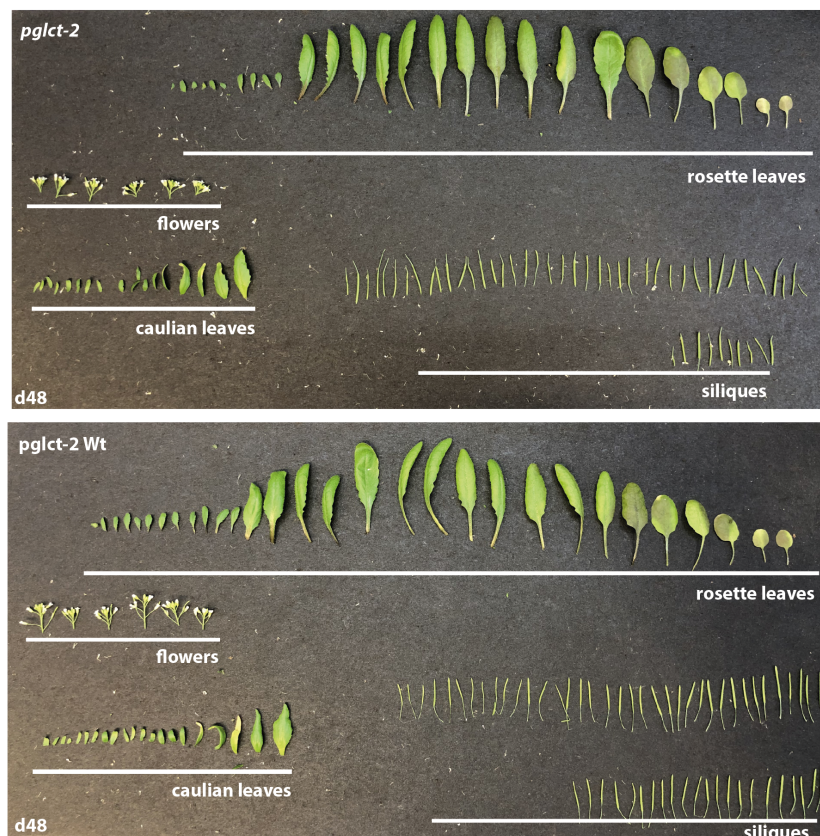
Figure 55: Phenotypical evaluation of 48-days-old plants of *pglct-2* and the corresponding wild type (pglct-2 Wt). Five plants for each genotype were separated in the different tissues: rosette leaves, cauline leaves, flowers and siliques.

The *rbsk* line did not show a phenotype under optimal growth conditions (Figure 31). The *pglct-2* line compared to the corresponding wildtype did (Figure 55). Apparently are defects in D-ribose metabolism not overly critical for *A. thaliana*.

In a metabolite analysis, the effect of *pGLCT* mutation during *A. thaliana* onthogenesis

was evaluated. Plant material from plants before bolting (27-days-old) was harvested including seedling (11-days-old) and rosette leaves separated into young, middle and old leaves, as shown in Figure 41. From plants in the reproductive phase (48-days-old), rosette leaves (separated into young, middle and old leaves), cauline leaves, flowers and siliques were harvested. Furthermore ,root material was included from bolting plants (48-days-old).
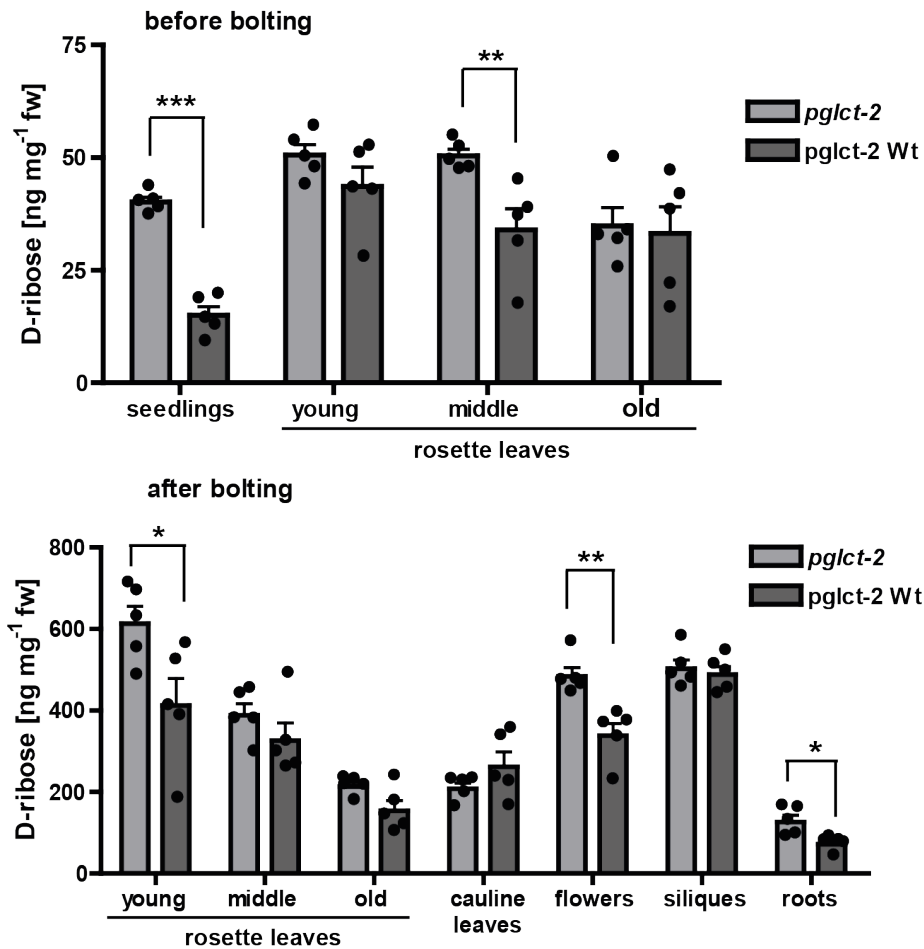
Figure 56: D-ribose quantification during the vegetative and reproductive phase in *pglct-2* and the corresponding wild type. Tissues of 11-day-old seedlings, young, middle and old rosette leaves of 27-day-old plants were used. Furthermore the rosette leaves of 48-day-old plants separated into young, middle and old leaves, cauline leaves, flowers, siliques and roots were used. Error bars represent SD values (n = 5) and black circles show individual data points.

The D-ribose concentration in *pglct-2* plants was higher in all tissues compared to the pglct-2 wild type line, except in cauline leaves (Figure 56). The seedlings showed the highest D-ribose concentration, with a 2.5 fold higher concentration of D-ribose in the mutant line compared to the wild type. In roots and flowers, the D-ribose accumulation is, 1.5 fold increased in *pglct-2*.

In general, does *A. thaliana* accumulates more D-ribose during the reproductive phase. Between 2-fold and 10-fold more D-ribose accumulated when shoots, including flowers, siliques and cauline leaves were developed. This correlates with increased ribonucleotide catabolism in later stages of the plants life.

3.3.12 Enhancement of *S. cerevisiae* Growth Using D-Ribose as the Only Carbon Source.

S. cerevisiae consumes hexoses as a main carbon source for growth and proliferation. The most common hexose used is glucose, which is abundant in the normal growth media (*YPD*) at about 2% (w/v). If the carbon source is exchanged with a pentose sugar, like D-ribose, *S. cerevisiae* show a strong reduction of growth. The *S. cerevisiae* line overexpressing *ScRBSK* was compared to the wild type line for the ability to grow on 2% D-ribose.
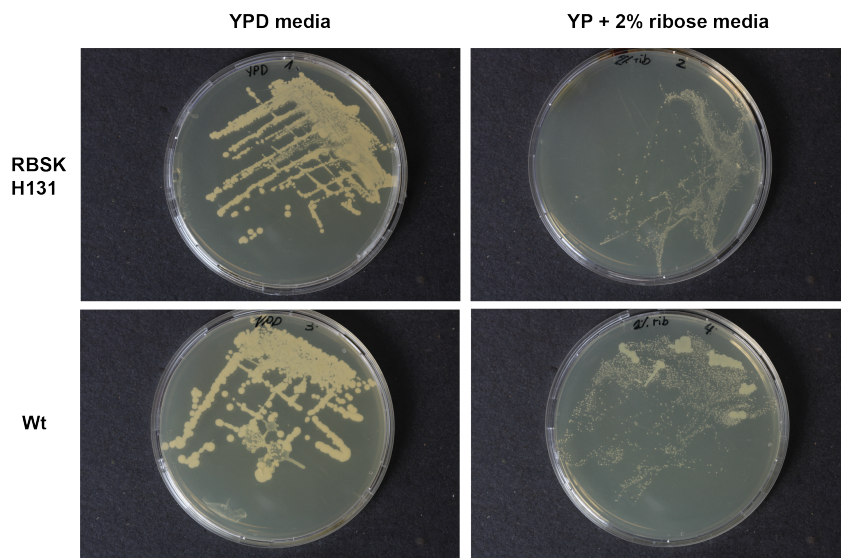
Figure 57: Growth of *S. cerevisiae* cells overexpressing *ScRBSK* (H131) on YPD full media, containing 2% glucose or 2% D-ribose compared to the growth of the parental wild type control (WT). The cells were spread on the plates from a glycerol culture and incubated at 30°C for 2 days.

Neither the parental wild type line (WT) nor the RBSK line grew well on D-ribose containing media compared to YPD media with 2% glucose (Figure 57). Although the amount of cells was not quantified prior to the spreading on the plates, it can be concluded that neither of the two *S. cerevisiae* strains was growing well, compared to the full media. This result shows that the overexpression of the *RBSK* did not improve the growth of the *S. cerevisiae* cells on D-ribose, indicating that the lack of D-ribose transport into the cells might be the reason for the poor growth on D-ribose. Because there is no D-ribose

transporter known in *S. cerevisiae*, transport of D-ribose might be improved by transformation of *S. cerevisiae* cells with the *pGLCT* from *A. thaliana*.

The *pGLCT*, was cloned into a yeast expression vector, for expression with a C-terminal YFP tag or without a tag, leading to the constructs H610 (pGLCT-YFP) and H611 (pGLCT-noTag). *S. cerevisiae* wild type cells (BY4743) were transformed with both constructs. A similar plate assay, as shown in Figure 57, was repeated including the lines H610, H611 and the wild type control.
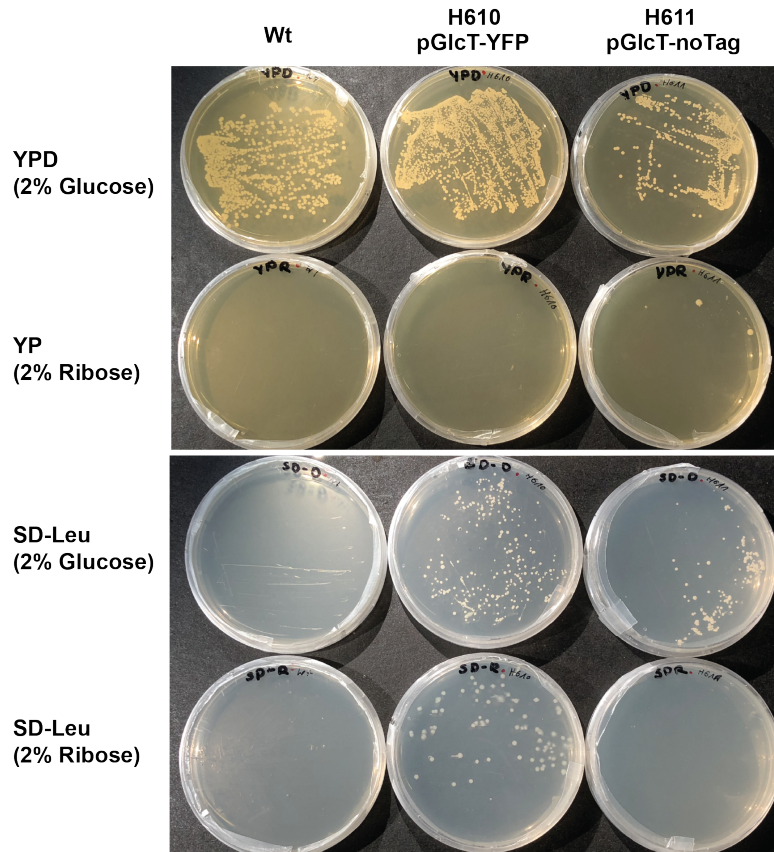
Figure 58: Yeast growth assay of two pGLCT *S. cerevisiae* complementation lines on YP or SD-Leu media with either 2% glucose or 2% D-ribose. As control the wild type line (Wt) was used and compared to pGLCT-YFP (H610) and pGLCT-noTag (H611). The cells were spread from glycerol cultures and incubated at 30°C for two days.

On full YPD (2% glucose) media, all of the three genotypes grew equally, but when glucose was exchanged with 2% D-ribose neither of the genotypes grew. H611 (pGLCT-noTag) developed two colonies (Figure 58). The SD media lacking leucine and containing 2%-glucose or 2% D-ribose were included to show the presence of the constructs which carries the *LEU2* gene as selection marker for the transgene.

On SD-leu media with 2% D-ribose only the pGLCT-YFP construct (H610) developed colonies. This indicates that this construct might produce a functional transporter for

the uptake of of D-ribose into *S. cerevisiae* cells. On the other hand, the pGLCT-noTag (H611) construct did not show any growth on SD-Leu plates with D-ribose. The YFP-tag might stabilize the protein or the initial density of cells with construct H610 was by chance higher which led to better growth on D-ribose plates. To assess the production of pGLCT-YFP (H610), *S. cerevisiae* cells from a liquid culture were investigated by CLSM (Figure 59).
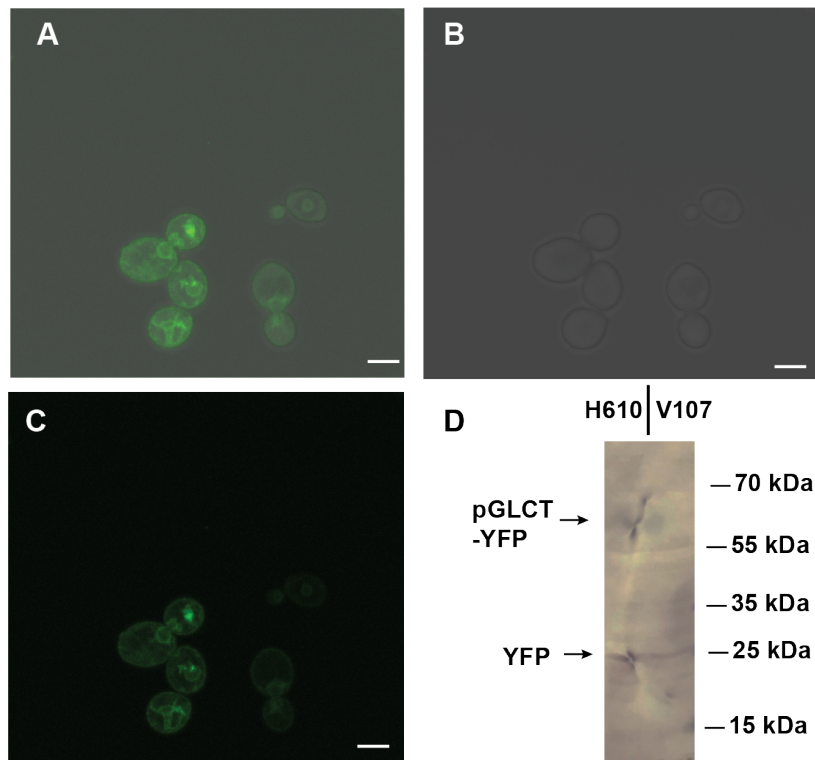
Figure 59: *S. cerevisiae* cells producing H610 (pGLCT-YFP) investigated by CLSM. A: overlay of B: bright field and C: YFP signal; D: immunoblot with 10 µl total protein extracts from *S. cerevisiae* liquid cultures of a pGLCT-YFP line and a line transformed with the empty vector as wild type control. The scale bar shows 5 nm.

The overlay in Figure 59A is a combination of the bright field signal (Figure 59B) and the YFP signal (Figure 59C), showing YFP signal inside the yeast cells. The subcellular localisation of the fusion protein is unclear, because an adequate yeast subcellular marker was not available to us. The pGLCT-YFP does not seem to be located exclusively in the plasma membrane, but as well in other subcellular structures. The immunoblot showed a faint signal at 68 kDa was detected matching the molecular mass previously detected for the pGLCT-YFP fusion protein (Figure 59D). On the other hand, a band of free YFP is visible at 25 kDa, which shows that the protein is partially unstable.

In summary, the pGLCT-YFP fusion protein is produced in very low amounts in the *S. cerevisiae* cells that the fusion protein is unstable. Additionally, the localisation of the YFP signal appears to be inside the yeast cells, not on the outer membrane. A reason for

the low expression and the localisation might be that *A. thaliana* pGLCT was produced as full-legth protein including the chloroplast targeting peptide, which might not be properly processed in yeast. This result raises as well doubts about the growth of the pGLCT-YFP line on SD-Leu minimal media containing 2% D-ribose (Figure 57). This growth might be an artefact, potentially caused by a high cell number transferred from the glycerol stock on the plates as inoculum. A new growth experiment with controlled inoculum strength was set up. The strain carrying an empty vector (V107) functioned as a wild type control on the SD-LEU media, because the wild type strain is not able to grow on this minimal media lacking leucine.
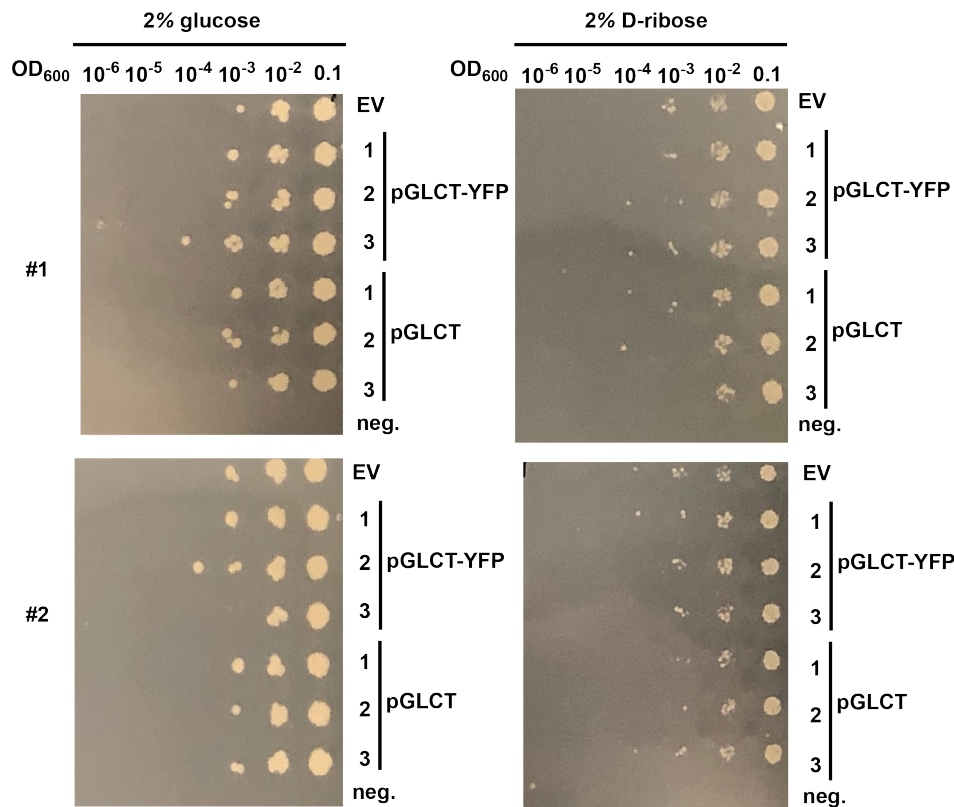
Figure 60: *S. cerevisiae* growth assay including strains carrying the empty vector (EV) and three independent lines of pGLCT-YFP and pGLCT were adjusted to an OD_{600} of 0.1 and then diluted by up to five orders of magnitude. One drop of each culture was transferred by a stamp onto plates, containing minimal medium (SD-Leu) and 2% of either glucose or D-ribose. The plates were incubated at 30°C for three days. Two independent replicates were produced (#1 and #2).

On 2% of glucose the *S. cerevisiae* lines generally showed a growth up to an OD_{600} of 10^{-3} (Figure 60). For the growth on D-ribose it can be concluded that the expression of *pGLCT* in *S. cerevisiae* is not improving in the growth on 2% D-ribose media. It is possible that this result was obtained because pGLCT was either mislocalised, produced too low, or simply not functional in *S. cerevisae*.

4 Discussion

Plants are stationary organisms, which rely on efficient nutrient remobilisation to grow and proliferate. One of the most important nutrients is nitrogen (N), of which the majority is bound in proteins. About 10%, however are bound in the nucleobases and nucleic acids (DNA or RNA). During the course of purine nucleotide catabolism, two cytosolic nucleoside hydrolases (NSH1 and NSH2) hydrolyse the N-glycosidic bond of the nucleosides, releasing D-ribose and a nucleobase. The biochemistry of the N recycling pathways is well understood in *A. thaliana*, but the fate of the D-ribose released during nuceotide degradation is not well understood up to now.

Agranoff *et al.* (1956) were the first to describe a functional ribokinase (RBSK) from calf liver extracts. But it took 60 more years until the first RBSK from plants was described in 2016 by Riggs *et al.*, followed shortly later by our own study in 2018 (Schroeder *et al.*). The RBSK is catalysing a reaction at an important crossroad between the degradation of purine and pyrimidine nucleotides and the recycling of D-ribose. The phosphorylation of D-ribose to D-ribose-5-phosphate in the plastids, reintroduces the pentose into general carbon metabolism for example the non-oxidative pentose phosphate pathway (non-ox. PPPW) and the production of activated D-ribose (PRPP) for nucleotide *de novo* synthesis and salvage

In this work the RBSKs from *A.thaliana* and *S. cervevisiae* were characterised *in vitro* and *in vivo* and an extensive metabolite analysis of multiple mutant lines gave new insights into the possible links between nucleoside catabolism and carbon metabolism in *A. thaliana*. A second focus of this work was to elucidate the transport of D-ribose from the cytosol, into the chloroplast. The hydrolysis of nucleosides is localised in the cytosol whereas the RBSK reaction is localised in the chloroplast. A plastitic D-ribose transporter has not been described up to now. Candidate genes for such transporter were identified and mutant lines of the most promising candidate, *pGLCT*, were analysed in respect to an alteration of D-ribose concentration under different conditions and at distinct developmental stages.

4.1 Characterization of a Functional Ribokinase in *A. thaliana* and *S. cerevisiae*

4.1.1 Establishment of a Non-Radioactive Kinase assay

For the measurements of ATP dependent kinases, radioactively labelled ATP is frequently used. Hereby, either the depletion of labelled phosphate donor or the increase in phosphorylated product is measured (Witt *et al.*, 1975; Hastie *et al.*, 2006). For this study a alternative approach was established in out laboratory.

During a kinase reaction, in most cases ATP is converted to ADP and γ-phosphate for the

phosphorylation of the substrate. The nucleoside tri- and diphosphates can be detected photometrically after a chromatographic separation by HPLC. The ATP and ADP peak could be clearly separated on a C18 column with a difference in retention time of 0.4 minutes and detected by the diode array detector at 254 nm and 360 nm reference (Figure 13). This detection method is in generally suitable for all kinase reactions involving tri-, di- or even mono-phosphate nucleotides.

For the measurement of kinetic constants, a range of 0.5 to at least 10 fold of the expected K_M should be assessed. The literature describes that K_M values of characterised RBSKs can differ greatly. For the RBSK of *Bos taurus* a K_M of 22 µM was described and for the RBSK from *Salmonella enterica* a K_M of 2 mM was found (Agranoff and Brady 1956; Torneux *et al.,* 2000). Due to the fact that D-ribose is not detectable by the diode array detector, only the peaks of ATP and ADP could be quantified. The kinase assay showed a linar correlation between the ADP concentration and the detected peak area in a range from 50 µM up to 2.5 mM (Figure 14). The requirements for testing the kinetic constants of the RBSKs.

4.1.2 Biochemical characterisation of the RBSK from *A. thaliana* and *S. cerevisiae*

For the evaluation of the kinetic constants of the *At*RBSK and *Sc*RBSK, the proteins were transiently produced in *N. benthamina* including a C-terminal Strep-tag and purified by affinity purification with *StrepTactin*. Both proteins were successfully produced in *N. benthamiana* and purified for further analysis (Figures 15 and 16).

To show the enzymatic activity of the RBSKs from *A. thaliana* (*At*RBSK) and *S. cerevisiae* (*Sc*RBSK), the purified enzymes were tested in a preliminary experiment with D-ribose (Figure 17). For both enzymes the formation of ADP was detected in the samples containing D-ribose but not in the controls. This result indicated for the first time that both genes code for functional RBSKs. The plant RBSK was discovered in parallel by Riggs *et al.,* (2016). For the *Sc*RBSK, Xu *et al.,* (2013) firstly had claimed that it is not a RBSK, because they observed no difference in limited D-ribose usage of an *ScRBSK* mutant and the wild type.

The determination of the kinetic constants showed, that the K_M values of both enzymes are of similar magnitude with 85 µM for the *At*RBSK and 55 µM for the *Sc*RBSK (Figure 18), which is also similar to the K_M values of the RBSK from *E. coli* with 110 µM (Maj and Gupta, 2001), and of *Homo sapiens* with 120 µM (Quiroga-Rodger *et al.,* 2015). For *At*RBSK the K_M was evaluated shortly prior to our study by Riggs *et al.* (2016) who described an about two fold higher K_M (150 µM) as determined in our study (Schroeder *et al.,* 2018). We measured the turnover numbers (k_{cat}) of 130,4 s^{-1} for the *At*RBSK and 70,9K s^{-1} for the *Sc*RBSK (Figure18), indicating, that the *A. thaliana* enzyme is nearly twice as

processive as the homologue from *S. cerevisiae.* Only three k_{cat} values are described in the literature for the other RBSK enzymes, for *A. thaliana* (2 s^{-1}), *H.sapiens* (10,4 s^{-1}), and *Leishmania major* (*L.major*) (10,8 s^{-1}) (Ogbunude *et al.,* 2007; Quiroga-Roger *et al.,* 2015; Riggs *et al.,* 2016). The reported k_{cat} value for the *At*RBSK by Riggs and colleges is 65 times lower than the turnover number we determined. A plausible cause for the different turnover numbers, could be the distinct expressions system used in the study from Riggs and our study. We produced the full-length protein in *N. benthamiana* , whereas a N-terminally truncated protein was produced in *E. coli* in the other study. The importance of the correct N-terminus for catalytic activity was recognised by Riggs and colleges, but the N-terminal chloroplast targeting sequence needed to be artificially removed for the expression in *E. coli.* The prediction of the correct sequence to be removed may have been problematic (Riggs *et al.,* 2016). Indeed, sequencing after transient protein production in *N. benthamiana,* indicated a 20 amino acid long protein sequence of the putative transit peptide was still detectable after the proteolytic processing of the protein (Schroeder *et al.,* 2018).

RBSKs require monovalent and divalent ions for the phosphorylation reaction. Magnesium (Mg^{2+}) mediates the transfer of the γ-phosphate from ATP to the C_5-atom of the D-ribose by acting as an ATP chelator in *B. taurus, E. coli* and *H. sapiens* RBSKs (Agranoff *et al.,* 1956; Maj *et al.,* 2001; Quiroga-Roger et al., 2015). Potassium (K^+) is reported to activate the *E. coli* RBSK enzyme and is therefore necessary for protein activity (Andersson *et al.,* 2002).

In our hands, the activities of both RBKs were reduced in a reaction without Mg^{2+} by about 95% and without K^+ by only 10% (Figure 19), suggesting that K^+ might not be essential for the RBSK reaction. The recently reported *At*RBSK crystal structure also emphasises the importance of Mg^{2+} for the enzymatic reaction in compliance with our data (Kang *et al.,* 2019). A possibility for our high RBSK activity without any added K^+ is, that the ions were possibly co-purified with the RBSK proteins during the Strep-tag affinity purification.

Additionally, phosphate was reported to have an influence on the K_M of the *E. coli* RBSK for the substrate D-ribose. 20 mM of phosphate decreased the K_M from 610 µM to 110 µM according to Maj *et al.* (2001). It can be argued, that 20 mM phosphate is not a reasonable amount to be found in *E. coli in vivo* and therefore the decrease in K_M might just be relevant *in vitro* . We did not add phostphate to the*At*RBSK or the *Sc*RBSK. An independence from organic phosphate addition was shown by Riggs *et al.* (2016) for the *At*RBSK.

We additionally assessed whether compounds containing a D-ribose residue, like ribonucleosides, might be an additional substrate for the RBSKs. Apart from the adenosine kinases (ADK1 and ADK2) and the uridine kinases (UKL1 and UKL2) other nulcoside kinases, producing nucleoside monophosphates are not known in plants (Moffat et al.,2000;

Chen and Thelen, 2011). It is conceivable that RBSK might also possess nucleoside kinase activity. Adenosine, cytidine and uridine were tested in a preliminary substrate screen experiment compared to the enzyme activity with D-ribose (Figure 20). Neither with adenosine, nor cytidine or uridine any kinase activity was detected for any of the enzymes. It can be concluded that even though the RBSKs are part of the PfkB kinase protein family, as are the adenosine kinases, the RBSKs do not use nucleosides as a substrate. Even though the RBSKs are forming a distinct phylogenetic group apart from other sugar kinases of the PfkB members (Schroeder et la., 2018), other sugars similar to D-ribose might be a suitable substrates. D-deoxyribose from DNA nucleosides for example, were reported to be phosphorylated by the RBSKs from *Bos taurus, E. coli, Salomonella enterica, and Lactobacillus plantarum* (Agranoff *et al.*, 1956; Cuvikovsky *et al.*, 2007; Ginsburg 1959; Tourneux *et al.*, 2000). Therefore, D-deoxyribose might be an additional substrate for *At*RBSK and *Sc*RBSK, but this has not yet been tested. For the RBSK of *E. coli* the additional substrates D-fructose, D-xylose and D-arabinose were reported (Chuvikovsky *et al.*, 2006). The RBSK from *H. sapiens* did not show any activity towards neither D-fructose, D-xylose nor D-galactose and only minor activity for D-arabinose (Park *et al.*, 2007).

4.1.3 *In vivo* Characterization of the *A. thaliana* and *S. cerevisiae* RBSKs

An *in vivo* analysis was conducted to evaluate the impact of *RBSK* abrogation an overexpression on the physiology and the metabolism of *A. thaliana* and *S. cerevisiae*. Mutant lines for *RBSK* and complementation lines overexpressing *RBSK* were obtained for both model organisms, *A. thaliana* and *S. cerevisiae*. All lines were evaluated for their transcript and protein production (Figures 21 to 23, 24 and 25).

The plant and yeast mutant lines were included in a first metabolite analysis. In metabolite extracts of 10-day-old *A. thaliana* seedlings D-ribose was detected in the *rbsk* line and not in the complementation line *RBSK* or the wild type (Figure 26) In *S. cerevisiae* D-ribose was only detected in the *RBSK* mutant line but not in the wild type and the complementation line (*RBSK*) (Figure 27). This demonstrates, that the RBSK is required for D-ribose phosphorylation *in vivo*, not only in *A. thaliana*, but as well in *S. cerevisiae*. This result disproves as well the conclusion of Xu *et al.* (2013), that the gene YCR036W might not be a RBSK. A metabolite analysis was conducted with these RBSK variants investigating as well the metabolic source of D-ribose. For this purpose double mutant lines of *rbsk* with *gsda, cda* and *nsh1* were produced to to evaluate the contribution of purine and pyrimidine nucleoside catabolism and the overall contribution of nucleoside degradation to the D-ribose pool *in planta*.

The about 78% lower concentration of D-ribose in the *rbsk nsh1* line shows, that the nucleotide catabolism is the major contributor to the D-ribose pool (Figure 28). The residual 22% could result from non-enzymatic hydrolysis of the N-glycosidic bond be-

tween the sugar and the nucleobase. A second possibility is, that nucleosides which accumulate in the *nsh1* background, might be transported into the apoplast and hydrolysed there by NSH3 (nucleoside hydrolase 3), which is only true for purine nucleosides (Jung *et al.,* 2011).

The hypotheses, which both assume that nucleosides are also the major source for the residual D-ribose observed in *nsh1*, are supported by the xanthine accumulation in the *nsh1 xdh1* double mutant line (Figure 29). In which, although the cytosolic nucleoside hydrolysis are blocked. A possible nucleoside instability had been observed in a *nsh1 cda* double mutants before. This line accumulates cytidine although the deamination reaction from cytidine to uridine was blocked. It also accumulated the nucleobase cytosine, although generally there is no cytidine hydrolase in plants and other cytosolic hydrolase activities are absent as well in *nsh1* (Figure 30) (Chen *et al.,* 2016). If the D-ribose is resulting from the NSH3 mediated hydrolysis of purine nucleosides, it could then be directed back into the cell by the *A. thaliana* polyol transporter 5 (AtPLT5) (Klepek *et al.,* 2005). The contribution of purine and pyrimidine nucleoside catabolism to the D-ribose pool, appears to be nearly equal (Figure 28). The D-ribose concentration, derived from purine catabolism, is 44% lower in the *rbsk gsda* mutant line compared to the *rbsk* line (Figure 28). In the *rbsk cda* line a decrease of D-ribose accumulation down to 64% of the wild type concentration was observed. Keeping in mind, that up to 20% of the D-ribose can be hydrolysed from the nucleobases without the contribution of the cytosolic nucleoside hydrolases, purines and pyrimidines contribute to 42% and 49%, respectively to the D-ribose accumulation in *rbsk* background.

4.1.4 Impact of *RBSK* Mutation on the Growth of *A. thaliana* Plants

In purine and pyrimide catabolism, D-ribose is released by nucleoside hydrolysis and accumulates in the *rbsk* (Figure 26). Especially in the reproductive phase where nutrients from source tissues (rosette leaves) is remobilised to the sink tissues like flowers and seeds (Koch *et al.,* 2004) D-ribose could be crucial. Therefore it was evaluated whether the *RBSK* mutation leads to a phenotype in *A. thaliana* plants.

RBSK, *rbsk* and Col-0 plants were grown for 42 days were visually compared, leading to the conclusion that there is no difference between the lines tested (Figure 31). This indicates that the lack of D-ribose, which is not available for the plant, might not essential for growth or seed production under normal growth conditions. This is similar to the *NSH1* mutant line, where Riegler *et al.* (2011) reported no impact on growth and development under normal growth conditions. In the *rbsk* line however, the biomass quantification showed a significant difference for the shoot weight (Figure 32A), but not for the rosette weight (Figure 32B) between the examined genotypes. This result indicates that although there was no visible difference in the *rbsk* line compared to the wild type, the remobilisation of D-ribose might be more important during the reproductive phase than previously

thought. In a following experiment the shoot biomass should be investigated more into detail and a comparison of seed weight, seed number, and the seed metabolic status could explain the decreased biomass production in the *rbsk* line and in which part of the shoot this effect might occur. During this experiment, different environmental conditions could be included to enhance the effect.

Other mutants of the nucleotide catabolism pathway, like *nsh1*, *gsda*, and *xdh1*, did also not show an aberrant phenotype under normal growth conditions (Brychkova *et al.,* 2008; Jung *et al.,* 2009/2011; Dahncke *et al.,* 2013). In contrast the *CDA* mutant clearly showed a decreased biomass accumulation, due to intermediates of the pyrimidine catabolism accumulating in this mutant line and interfering with the plant metabolism (Chen *et al.,* 2016). In a preliminary experiment, the *rbsk* line showed an early flowering up to 1 week prior to the wild type. It was postulated that the accumulation of D-ribose might influence the sugar pools during the transition from the vegetative phase to the reproductive phase and thereby influence shoot induction. Such an influence was described for the mutation of a trehalose-6-phosphate synthase in *A. thaliana*, which led to a decreased trehalose-6-phosphate concentration in the shoot apical meristem (SAM) and thereby to delayed bolting and flowering (Wahl *et al.,* 2013). However, in a thorough repeat of this experiment with *rbsk*, no significant differences between the wild type and the mutant were detected for the time of shooting and the shoot length (Figure 33). Therefore, it must be concluded that the nucleoside catabolism and the resulting D-ribose is not influencing neither the timepoint of bolting, nor the biomass production in *A. thaliana rbsk* plants. A reason for this might be that D-ribose 5-phosphate can be generated by the D-ribose 5-phosphate isomerase (RPI) of the non-ox. PPPW. This pathway is used for the conversion of C5-sugars into fructose 6-phosphate and triose phosphate, which then can be used for glycolysis or gluconeogenesis (Stincone *et al.,* 2015). A mutation in the cytosolic *RPI2* gene however, affects the photosynthetic activity of the chloroplast and the mutants accumulate less starch and flower later as the wildtype (Xiong *et al.,* 2009). This indicates that the majority of D-ribose 5-phosphate is produced by the PPPW, and that the RBSK reaction might have a minor impact on the D-ribose 5-phosphate pool.

4.1.5 D-ribose Recycling is not Contributing to the Dark Stress Phenotype of Purine Nucleoside Catabolism Mutants

Although the *rbsk* line and most of the mutants of the nucleoside catabolism look phenotypically like the wild type under full nutrient supply, under extreme situations like prolonged dark stress, a defect in purine nucleotide catabolism seems to have an impact on plant fitness. For *nsh1*, extensive chlorosis was reported after five days of dark stress (Jung *et al.,* 2011), which somehow matches with the phenotype of *xdh1* line, showing accelerated senescence under prolonged dark stress conditions (Brychkova *et al.,* 2008). Furthermore, the *gsda* line displayed a senescence phenotype under dark stress conditions

with accelerated chlorosis and no survivals beyond day three of the treatment (Dahncke 2014; Schroeder *et al.,* 2018).

It was speculated, that maybe the lack of energy from D-ribose-5-phosphate produced by the blockage of the purine catabolism in the *gsda* background, causes the lethal phenotype of this mutant. To clarify whether defective D-ribose recycling might increase the severity of dark stress symptoms, *rbsk* was included in a dark stress study, in addition to the wild type Col-0, the *gsda*, *gsda hgprt* double mutant, *hgprt*, *nsh1*, and *xdh1*. The *rbsk* line did not show any sign of chlorosis, neither in visual comparison nor in quantification of the photosynthetic activity (Figures 34, 35). This demonstrates clearly, that carbon starvation cannot be the reason for the *gsda* phenotype. The *rbsk*, *nsh1* and *hgprt* line did not show any difference to the wild type control. However, though the D-ribose content is increased constantly throughout the dark stress treatment (Figure 36) indicating that the purine nucleoside catabolism was induced during this stress (Brychkova *et al.,* 2008; Jung *et al.,* 2011).

For *nsh1* the lack of any increased stress phenotype is in contrast to the findings of Jung *et al.* (2011), who showed that *NSH1* mutants develop chlorosis during prolonged dark stress periods. In *xdh1*, a slight decrease in photochemical efficiency by day five was visible, indicating that cellular degradation processes are in progress. Brychkova *et al.,* (2008) proposed, that the ureides, intermediates downstream of XDH1, are scavenging reactive oxygen species (ROS) produced during dark stress treatment. They claimed, that a lack of ureides leads to a ROS induced phenotype of chlorosis, which can be seen in *nsh1* and *xdh1*. Uric acid, the direct product of the XDH1 reaction, was postulated to quench ROS in mesophyll cells upon a powdery mildew infection (Ma *et al.,* 2016) and might as well play a role in the survival of prolonged darkness. In our hands however, we could only confirm a slight decrease in photochemical efficiency in the *XDH1* mutant (Figure 35). For neither the *nsh1* nor the *xdh1* line a visually obvious abnormality compared to the wild type was observed (Figure 34). It appears probable that the growing conditions influence whether stress phenotypes are observed or not. It needs to be tested which parameters of the growing conditions provoke the more severe stress phenotypes reported for *nsh1* and *xdh1* by others.

Even though there was no visual stress phenotype in *nsh1*, the methabolic analysis clearly showed an accumulation of xanthosine, uridine and small quantities of guanosine and guanine in this mutant. This accumulation increased during the dark stress treatment (Figures: 37, 38, and 39). Confirming that nucleotide degradation is induced during prolonged darkness.

The strong phenotype for *gsda*, manifested by a rapid decrease in photochemical efficiency from day three on, coincides with the start of increased nucleotide degradation shown by the xanthosine accumulation in *nsh1* (Figures 37, 39). As carbon starvation, due to a lack of D-ribose is not the cause of *gsda* phenotype, the *hgprt* mutant and the *gsda hgprt*

double mutant were included in this experiment. From previous experiments it was known that *gsda hgprt* contained less guanosine but more guanine that *gsda*. By investigating these mutants, the effects of guanosine and guanine accumulation on the phenotype could be assessed. The double mutant line showed in the visual comparison and in photochemical efficiency analysis an attenuated *gsda* phenotype, whereas the *hgprt* shows a wild type phenotype. AS expected *gsda hgprt* accumulated more guanine and less guanosine during the dark stress experiment as *gsda* (Figure 39). It appears that guanosine is toxic when accumulating to hight concentrations as in *gsda*. The guanosine amounts are reduced in *gsda hgprt*, which ameliorates the phenotype. Guanine, on the contrary, seems to be less toxic that guanosine. Why is there less guanosine and more guanine in *gsda hgprt* compared to *gsda*? As guanosine accumulates in the *gsda* background, it partially decays to guanine, most likely by non-enzymatic hydrolysis. If the guanine is then phosphorylated by HGPRT to GMP, guanosine will be produced again by dephosphorylation of GMP, because GMP homoeostasis needs to be maintained. This leads to a futile cycle of the GMP degradation, guanosine decay, and salvage of guanine to GMP.

Furthermore the accumulation of guanosine seems to have an inhibitory effect on NSH1, indicated by the slight accumulation of uridine (Figure 38) and on XDH1, indicated by some xanthine accumulation in the *gsda* background (Figure 37).The accumulation of nucleosides can have pleiotropic effects on the organisms shown for example by Chen *et al.* (2016) with the accumulation of cytidine. A high concentration of certain downstream products of purine catabolism, in particular of uric acid, a substrate of urate oxidase (UOX), leads to a drastic phenotype in *A. thaliana* seedling establishment (Hauck *et al.* 2014).

4.1.6 Nucleoside Accumulation has an Impact on *A. thaliana* Germination Rates

Purine nucleotide salvage is strictly required for the germination of *A. thaliana* seedlings and is preferred in the early days of germination over the *de novo* synthesis (Stasolla *at al.,* 2003). Additionally, the export of newly synthesized adenylates from the chloroplast is necessary for germination. The mutation of *BRITTLE1*, an nucleotide exporter, is embryo lethal in *A. thaliana* (Kirchberger *et al.,* 2008). Jung *et al.* (2009) concluded, that the balance of nucleoside *de novo* synthesis and salvage from seed storage compounds is crucial for efficient seed germination.

Here we tested different mutants including *rbsk, gsda, hgprt, gsda hgprt, nsh1* and *xdh1* compared to the wild type to examine potential effects on the germination efficiency. The lines *rbsk* and *hgprt* showed no difference to the wild type. But the mutants deficient in enzymes of the purine catabolism are delayed in germination (Figure 40). For *xdh1* and *nsh1* this is in line with the literature (Brychkova *et al.,* 2008; Jung *et al.,* 2011). The *gsda* line showed the most pronounced delay with inly 20% germinated seeds within the first 24 h. Up to day three, *gsda* did not reach the wild type level of germination (Figure 40). Again the *gsda hgprt* double mutant line showed an attenuated phenotype

compared to *gsda*, indicating that the accumulation of guanosine in the *gsda* background might slow down seed germination. The *GSDA* mutant displays a more pronounced dark stress phenotype and a stronger germination delay than the *GSDA HGPRT* double mutant, strongly suggesting, that the hight amounts of guanosine are the cause of these defects in *gsda*. *CDA* mutants, which contain high amounts of cytidine and cytosin, even display developmental defects under non stress conditions (Chen *et al.*, 2016). However, it has so far not been investigated whether germination is also compromised in *cda*.

The *rbsk* line is showing no difference to the wild type, leading to the conclusion that the lack of D-ribose recycling is not essential for germination. The degradation of storage compounds, mainly oil in *A. thaliana*, seems to be sufficient to allow germination (Büttner *et al.*, 2010).

4.1.7 D-Ribose Accumulation as an Indicator for Ribonucleotide Catabolism in Different Developmental Stages of *A. thaliana*

Although the *rbsk* line did not show a visible phenotype, a metabolic phenotype (the accumulation of D-ribose), was detected by LC-MS. The concentration of D-ribose can probably serve to quantify ribonucleoside catabolism, because nucleoside hydrolysis is likely the only source of D-ribose. We were interested in the importance of ribonucleotide catabolism during the onthogenesis of *A. thaliana*. Therefore, *A. thaliana* tissues from different developmental stages, ranging from 10-day-old seedlings to the reproductive phase (42-days-old), were analysed for the D-ribose concentrations (Figure 41).

The results showed that the D-ribose concentration in young tissues of *rbsk*, like seedlings and leaves of rosettes before bolting, is approximately at the same level. At the transition from the vegetative state to the reproductive state, the amount of D-ribose accumulated in the rosette leaves is 1.5 fold higher as in the corresponding tissues before bolting. This corresponds well to the RBSK production, which is induced upon bolting (Figure 43).

In conclusion nucleoside catabolism leads to D-ribose generation at all developmental stages, but the extend of purine and pyrimidine catabolism apparently increases during the reproductive phase, leading to higher D-ribose concentrations in *rbsk* at this stage. Interestingly, *RBSK* is not expressed in roots, according to public transcriptome databases, which is contrary to the expression pattern of the *NSH1* to be expressed highest in the roots. By contrast, here it was shown, that the RBSK protein is present in roots and that the *rbsk* line is accumulating high amounts of D-ribose in this tissue (Figure 42 and 43).

4.2 Investigation of Putative Candidate Genes for a Plastidic D-Ribose Permease, Linking Nucleotide Degradation and D-Ribose Recycling

To recycle nitrogen from nucleobases, transport mechanisms across several membranes are important. The conversion of uric acid to allantoin, for example, takes place in the peroxysome, while the turnover into allantoate by allantoinase is located in the endoplasmatic reticulum.

The hydrolysis of nucleosides, catalysed by NSH1 or the NSH1-NSH2 complex occurs in the cytosol. The following RBSK reaction however, is located in the chloroplast, as are the downstream reactions to PRPP and parts of the oxidative pentose phosphate pathway (Figure 8) (Riggs *et al.,*2016; Schroeder *et al.,*2018). Due to their polarity, pentoses cannot diffuse freely into the chloroplast, but need to be transported by suitable permeases. For *E. coli* an ABC-type transporter, encoded in the *rbsDACBK* operon, has a high affinity towards extracellular D-ribose (Lopilato *et al.,* 1984; Shimida *et al.,* 2013). Six genes are part of this operon with the *rbsA* encoding an ATPase, *rbsB* is annotated as an periplasmatic D-ribose binding protein, and *rbsC* codes for a membrane located permease (Park *et al.,* 1999). RbsD catalyses the conversion between the pyranose and the furanose form of D-ribose while*rbsK* is annotated as the actual kinase. Furthermore, a Lac-I type repressor *rbsR* is located in a seperate operon downstream of the *rbsDACBK* operon (Lopilato et *et al.,* 1984; Park *et al.,*1999). In plants, a D-ribose ABC transporter similar to the one from *E. coli* is not known.

The *A. thaliana* polyol transporter 5 (AtPLT5) was described in 2005 by Klepek *et al.* to transport D-ribose from the apoplast into the cytosol. AtPLT5 is the first permease in plants for which D-ribose transport was described.

Database searches for homologues *E. coli* rbskABC in *A. thaliana* of for other members of the polyol transporters did not identify promising candidate genes for further analysis.

4.2.1 Search for Suitable D-Ribose Transporter Candidates

For plants in general, atmospheric nitrogen (N_2) is not accessible. Legumes however can embark on a symbiotic relationship with nitrogen fixing rhyzobia bacteria, which supply N-containing compounds in exchange for carbon compounds (Udvardi *et al.,* 2013). Legumes can be distinguished in two groups, the ureide exporting (*G.max*, *P.vulgaris*) and amide exporting legumes (*L.japonicus*, *M.truncatula*) (Sheoran *et al.,* 1982). Ureides like allantoin and allantoate are derived from purine nucleotide metabolism. And genes involved in ureide synthesis are upregulated in the infected *G.max* or *P.vulgaris* nodule cells.To identify unknown genes in purine biosynthesis and purine catabolism a comparative RNAseq analysis, comparing the induction of genes in nodules of ureide and amide exporting legumes, was undertaken in our laboratory.

The production of ureides starts with the assimilation of N to amino acids like glycine, glutamine and aspartate, of which in several reactions IMP is produced. IMP is converted in several steps to xanthosine, which is a central metabolite of the ureide biosynthesis. The hydrolysis of xanthosine leads to xanthine and D-ribose, and xanthine is turned into the ureides allantoin and allantoate by further reactions (Zrenner *et al.,* 2006; Werner and Witte 2011). Because of the intense ureide production upon nitrogen fixation in ureide-exporting legumes, there is a high flux through purine catabolism in these plants, but not in amide-exporting legumes. Based on this, a bioinformatic analysis was conducted by Marco Herde and Katharina Winkel, comparing gene expression data and selecting genes which are upregulated in roots versus nodules of ureide exporting legumes compared to amide exporting legumes. This resulted in a database of genes potentially involved in ureide biosynthesis and related pathways.

RBSK expression is upregulated in nodules compared to roots of ureide-exporting plants but not in amide-exporting plants (Table 41). This indicates that the rate of D-ribose recycling is increased in ureide-exporting plants and and induction of the cytosol to plastid D-ribose transport might also be required. Members of the monosaccharide transporter family (MST) described by Büttner *et al.,* (2010) were included in the RNAseq analysis. The *pGLCT* homologues of *P. vulgaris* and *G. max* showed, as the only member of the pGLCT/SGB1 family, an regulation pattern similar to *RBSK* (Table 41). The pGLCT homologues in both kinds of legumes show a 77 - 86% sequence identity with pGLCT from *A. thaliana* in a BLAST protein alignment analysis.

In the following, *pGLCT* (At5g16150) of *A. thaliana* was characterised, because it was the most promising candidate for a plastidic D-ribose permease.

4.2.2 pGLCT might be a Plastidic D-Ribose Transporter in *A. thaliana*

The pGLCT permease was first described by Weber *et al.* (2000) as glucose exporter in spinach chloroplasts. In 2011, Cho *et al.* included pGLCT in the analysis of starch export from *A. thaliana* chloroplasts. The data from Weber *et al.* and Cho *et al.* on pGLCT and the expression data of *pGLCT* homologues in legumes (Table 41) led to the hypothesis that pGLCT might have a dual function in transporting glucose as well a D-ribose.

In *Leishmania mexicana* (*L. mexicana*) *LmGT2* encodes for a glucose transporter with secondary D-ribose transport activity, similar to what we propose for pGLCT from *A. thaliana* (Naula *et al.,* 2010). Maybe a D-ribose transport activity is more common for glucose transporters than previously thought. The over all similarity of pGLCT and LMGT2 is only 22%. Because of the difference between the two proteins, it is not possible to use sequence comparison to identify amino acids likely involved in D-ribose recognition.

First the subcellular localisation of the *pGLCT* (At5g16150) transiently expressed in *N. benthamiana* was investigated by CLSM, showing that the fusion protein is located

in the inner membrane of the chloroplast surrounding the stroma (Figure 44). Therefore, pGLCT is localised at the correct subcellular position to potentially transport the D-ribose from the cytosol into the chloroplast.

Metabolite analysis revealed a two fold higher D-ribose concentration in the *pglct-2* line compared to the wild type, indicating that pGLCT might be involved in a D-ribose transport (Figure 47). Cho *et al.,* (2011) proposed in their study, that pGLCT might have another transport function except glucose export from starch degradation, because the transporter is expressed in heterotrophic tissues, like roots, where the plastids do not accumulate transitory starch from photosynthesis. Interestingly, the *rbsk* line accumulates five times more D-ribose than *pglct-2*, raising the question whether there is an additional gene coding for second D-ribose transporter.

If pGLCT was in fact a D-ribose transporter, D-ribose accumulation should increase in a *pGLCT* mutant, when a higher D-ribose release rate is provoked by external addition of nucleosides. Seven days old seedlings of *rbsk* and *pglct-2* showed an equal increase (two fold) in D-ribose concentration 24 h after uridine application (Figures 48 and 49). This supports the idea that pGLCT may be the plastidic D-ribose transporter. We conceptualised the following: uridine is taken up by the roots mediated by ENT3 (Cornelius *et al.,* 2012). Followed by the hydrolysis by NSH1 in the cytosol, generating uracil and D-ribose (Jung *et al.,* 2011). The D-ribose is afterwards transported into the chloroplast by pGLCT and phosphorylated by *RBSK* to D-ribose 5-phosphate.

We showed here, that the induction of D-ribose formation is possible by the supply of nucleosides to a seedling shaking culture. This system could hence be used for the investigation of D-ribose recycling in addition to the induction of D-ribose formation by prolonged darkness. By applying of stable uridine isotopes, the metabolic fate of cytosolic D-ribose could be investigated in more detail.

It is apparent that the D-ribose concentration is higher in the *rbsk* than the *pglct* line, indicating that there might be a second transporter facilitating the D-ribose transport into the plastids (Figures 48; 49). In the MST-like subfamily *pGLCT/SGB1* a possible paralogue (At1g05030) to *pGLCT* was identified (Büttner *et al.,* 2010). This putative paralogue is the most promising candidate for a further plastidic D-ribose transporter and is here referred to as *pGLCT-LIKE*. This gene has not been characterised so far and no data regarding the subcellular localisation is available. Proteomic analysis suggests that, PGLCT-LIKE is localised in the plastidic membrane (Hooper *et al.,* 2017). In a subcellular localisation analysis by CLSM the YFP signal was localised in the chloroplast stroma, not in the plastidic membrane as seen for PGLCT (Figure 50). The immunoblot showed a signal for free YFP, indicating that there is substantial proteolytic cleavage of the pGLCT-YFP fusion protein and no definitive statement about the subcellular localisation can be made. A *pGLCT-LIKE* mutant line was obtained, characterised and included in the metabolite analysis (Figure 51).

The *pglct-like* line was included in the metabolite analysis additionally to the *pglct-1* and *pglct-2* lines and the complementation lines pGLCT-YFP and pGLCT-noTag (Figure 53). Four times more D-ribose accumulated in *pglct-1* and *pglct-2* compared to the corresponding wild type lines. D-ribose accumulation is reversed in the complementation lines pGLCT-YFP and pGLCT. Demonstrating the pGLCT is a plastidic D-ribose transporter. In contrast pGLCT-LIKE does not seem to be involved in D-ribose translocation into the chloroplast, because D-ribose concentrations were unaltered in the mutant. This raises the question what the substrate of pGLCT-LIKE might be, which should be covered in a new study.

The disaccharide sucrose is the main transported sugar in many plants. Carbon compounds, produced during the day by photosynthesis are transported as sucrose into sink tissues like roots, young leaves, reproductive organs like flowers, seeds, and tubers and meristem cells for energy production and growth or are stored as transitory starch (Koch *et al.*, 2004). The transport of sucrose is facilitated by a high number of transporters, expressed in many tissues. Five sucrose importers (SUC1-SUC5) are expressed in *A. thaliana* roots (Durand *at al.*, 2018). Another example are the 17 *SWEET* (*Sugars Will Eventually be Exported Transporter*) genes, encoding for sucrose exporters in *A. thaliana* and 23 *SWEET* genes are described in rice (*Oryza sativa*) (Hu *et al.*, 2018). The high number of different sucrose transporters highlights the importance of efficient and selective sucrose transport. After the transport, sucrose can be hydrolysed by invertases to glucose and fructose for further use in the sugar metabolism. This makes glucose and fructose the most important monosaccharides in plants. For glucose alone, several transporters are described in different *A. thaliana* tissues. The glucose transporter *At*ERD6-LIKE is expressed at the tonoplast membrane, *At*STP1 is a guard cell specific glucose transporter, *At*STP3 is expressed in green leaves, and *At*STP9 in pollen (Büttner *et al.*, 2000; Scholz-Starke *et al.*, 2003; Poschet *et al.*, 2011). D-ribose however, is derived exclusively from nucleotide catabolism and requires probably far less transport capacity. This low contribution of D-ribose to the total sugar pool and the fact that D-ribose transport seems to be a secondary activity for the described D-ribose transporters *Lm*GT2 and *At*PLT5, raises the question whether putative D-ribose transporters might be identified in families with other annotated transport functions, like glucose transport. The *At*PLT5 transporter, as the first described plant D-ribose transporter and the pGLCT transporter are members of different subfamilies of the MST-LIKE protein super family (Büttner *et al.*, 2007). Therefore it is possible that D-ribose transporter may discovered in other sugar transport families.

The kinetic constants for pGLCT are so far not reported for glucose or for D-ribose (Weber *et al.*, 2000; Cho *et al.*, 2011). The D-ribose transporter *Lm*GT2 showed very similar K_M values for glucose (K_M= 109 µM) and for D-ribose (98 µM), indicating a similar affinity towards both substrates (Naula *et al.*, 2010). For pGLCT, a reduction

in glucose transport when supplied with an over excess of D-ribose could not be shown by Weber *et al.* (2000). Similar uptake rates were shown for glucose and D-ribose in extracted *Spinacia oleracea* chloroplasts with 7.4 and 6 µmol (mg Chl)$^{-1}$ h^{-1}, respectively (Schaefer *et al.,* 1977). But inhibition of glucose transport by the supply of D-ribose could not be shown in the extracted spinach chloroplasts either. The transporter needs to be expressed in a heterologous system allowing the evaluation of the kinetic constants independently from the interference of other sugar transporter.

4.2.3 Overexpression of *pGLCT* in *S. cerevisiae* does not Support Growth on D-Ribose as the Only Carbon Source.

Saccharomyces cerevisiae is a single cell eukaryotic organism, used in the production of alcohol (ethanol) by anaerobic fermentation under the consumption of carbohydrates, mainly glucose (Bisson *et al.,* 2003). Therefore, *S. cerevisiae* can be considered very important in the production of not only biofuel but as well alcoholic beverages (Ragaukas *et al.,* 2006; Young *et al.,* 2010; Steensels *et al.,* 2014).

The main carbon source for the growth of *S. cerevisiae* is glucose. For the transport of glucose from the surrounding medium into the cells, sugar transporters are required. 300 different transporters are listed in the yeast transport protein data base (YTPdb) accounting for 5% of the total *S. cerevisiae* proteome (Brohée *et al.,* 2010). In this database 20 genes are listed, encoding for monosaccharide transporter, 2 genes for disaccharide transporter, and 5 genes for polyol transporter. The annotated sugar transporters share a structure of 12 trans-membrane helices and the majority accounts for glucose or hexose transporters respectively (Bisson *et al.,* 2003). The uptake of pentoses and growth as a carbon source, however has not been described for wild type *S. cerevisiae.* Biotechnological developments in the field of biofuel generation from fermented plant material led to *S. cerevisiae* strains capable of the utilization of D-xylose and L-arabinose, the major components of hemi-cellulose (Bisson *et al.,* 2003). D-ribose, however is not described to be transported by a specific D-ribose permease in *S. cerevisiae* but in some strains of *Pichia.* In *Pichia pinus* and *Pichia fermentas*, D-ribose transport was reported (Barnett et al., 1975). In *P. fermentas*, the D-ribose transport is facilitated by a glucose transporter as a secondary transport activity. In *P. pinus* however, inhibition studies showed an independent transport of glucose and D-ribose (Barnett et al., 1975).

The overexpression of *ScRBSK* (H131) alone does not contribute to a better growth on D-ribose containing media compared to the wild type, showing that the enhancement of D-ribose conversion is not sufficient to support growth similar to glucose as a carbon source (Figure 57). The heterologous overexpression of the *pGLCT* from *A. thaliana* in *S. cerevisiae* might have given an indication whether the lack of sufficient D-ribose transport across the plasma membrane is the reason for this phenotype. The lines H610 and H611 producing pGLCT-YFP and pGLCT without a tag however did not show a significant

difference in growth compared to the *S. cerevisiae* line expressing the empty vector (V107) (Figure 60). However, it is possible for *S. cerevisiae* to grow on D-ribose in a limited fashion but neither *RBSK* overexpression nor enhanced transport by *pGLCT* overexpression is increasing the growth rates on D-ribose. There are several reasons for this negative result. First, the full *pGLCT* cds was used, including the plastid translocation signal which might have interfered with the expression in *S. cerevisiae*. The experiment could be repeated with the *A. thaliana pGLCT* sequence fused to a *S. cerevisiae* translocation signal, from a transporter known to be localised in the plasma membrane. Alternatively, the amount of energy generated from the activation of D-ribose by RBSK and direction of D-ribose 5-phosphate into the non-ox. PPPW is not enough to sustain the cellular energy demand of *S. cerevisiae* cells. The expression of *pGLCT* in other organisms, like *E. coli*, might be a suitable alternative for the evaluation of D-ribose and glucose transport. For this, an *E. coli* strain lacking the glucose and D-ribose transporters should be used.

4.3 D-Ribose Transport Model in the Context of Nucleotide Metabolism in *A. thaliana*

A model of D-ribose transport in the context of nucleotide metabolism was draw, which incorporates the findings of this study.

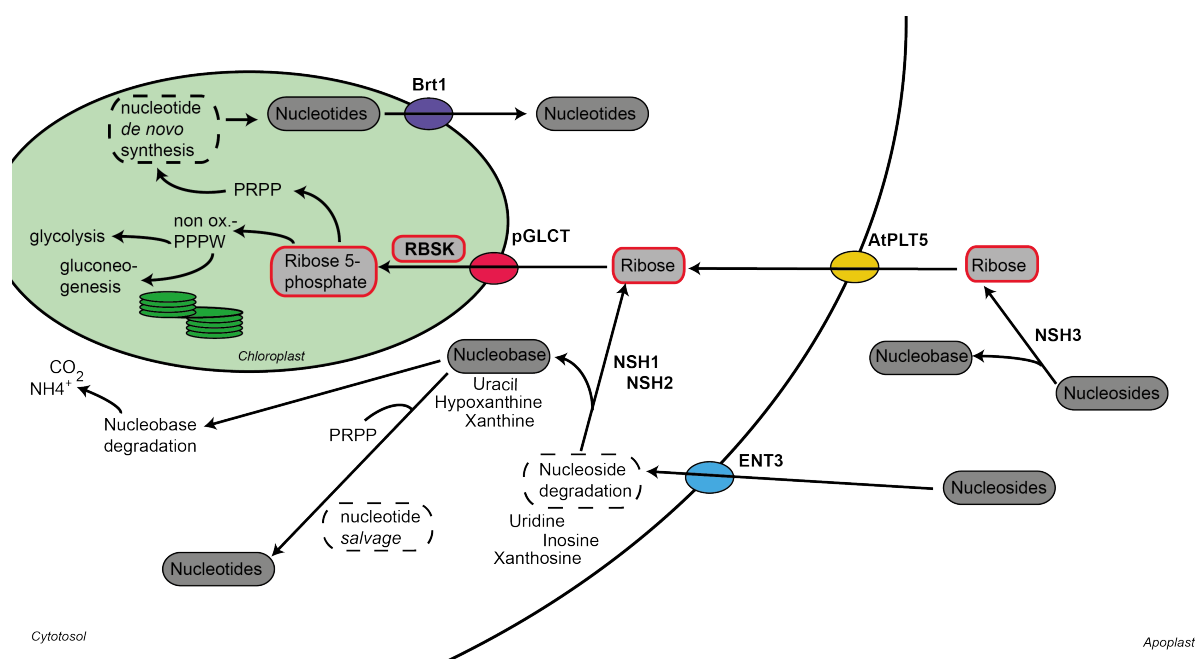Figure 61: Proposed ribose metabolism in *A. thaliana*. NSH1: nucleoside hydrolase 1; NSH2: nucleoside hydrolase 2; NSH3: nucleoside hydrolyse 3; *At*PLT5: *A. thaliana* polyol transporter 5; Brt1: brittle transporter 1; ENT3: equilibrate nucleoside transporter 3; pGLCT: glucose transporter; RBSK: ribokinase; non ox.-PPPW: non oxidative pentose phosphate pathway; PRPP: prosphoribosyl pyrophosphate.

Purine nucleosides can be hydrolysed in the apoplast by NSH3 or in the cytosol by NSH1 and NSH2, yielding D-ribose and the nucleobase (Figure 61) (Jung *et al.,* 2011; Riegler *et al.,* 2011; Baccolini and Witte, 2019). Pyrimidine nucleoside hydrolysis is performed by NSH1 in the cytosol. The extracellular D-ribose can be transported across the plasma membrane by AtPLT5 contributing to the cytosolic D-ribose pool (Klepek *et al.,* 2005). Extracellular purine nucleosides can be transported into the cytosol by the ENT3 transporter where they are hydrolysed by the NSH1/NSH2 hetero-complex (Cornelius *et al.,* 2012; Baccolini and Witte, 2019). From the cytosol, the sugar will be transported probably by the pGLCT transporter into the chloroplast, where it will be used as a substrate by the RBSK for the production of D-ribose 5-phosphate (Riggs *et al.,* 2016; Schroeder *et al.,* 2018). After this activation, D-ribose 5-phosphate can be used in the non-ox. PPPW through which it can be fed into the glycolysis or gluconeogenesis. Furthermore, D-ribose 5-phosphate can serve for the production of PRPP which is used not only in nucleobase salvage reaction but as well for *de novo* synthesis of nucleotide (Zrenner *et al.,* 2009). However, it is possible that other transporters might contribute to the D-ribose transport into the cytosol and the chloroplast. Adenylates like AMP, ADP, and ATP are exported from the chloroplast by BRITTLE1 (Kirchberger *et al.,* 2008).

4.4 Final Comments

This thesis is contributing to an improved understanding of nucleoside degradation, transport and recycling of D-ribose in *A. thaliana.*

Although, a D-ribose accumulation was shown for *pglct* plants, a thorough biochemical characterisation of the transporter should follow. It has to be verified that glucose and D-ribose are suitable substrates for pGLCT, followed by the evaluation of the kinetic constants for D-ribose and glucose, including an inhibition study. Therefore, pGLCT has to be transiently produced in *S. cerevisiae* or *E. coli* and a suitable transport assay hast to be established.

A thorough metabolic analysis of the sugar levels in the *pglct* lines could lead as well to a better insight into the function of this transporter. Therefore not only glucose and D-ribose should be included in a metabolic analysis but as well other sugars like D-ribose 5-phosphate, glucose 1-phosphate, glucose 6-phosphate, UDP-glucose, and ADP-glucose to see how the D-ribose and glucose pools are effected by the *pGLCT* mutation. Furthermore, the 24 h experiment should be repeated including the quantification of glucose to evaluate how the proposed double transport function is affecting the D-ribose and the glucose pool through a full circadian cycle.

A mutation of the *AtRBSK* homologue in ureide exporting legumes could show an impact on the ureide synthesis in the nodule, because of the high flux through the purine catabolism high amounts of D-ribose result from the purine nucleoside hydrolysis in order

to produce allantoin and allantoate. If D-ribose is not phosphorylated to D-ribose 5-phosphate the synthesis of PRPP might be impaired leading to a lower purine nucleotide biosynthesis and therefore a decreased formation of the ureides allantoin and allantoate.

References

Analysis of the genome sequence of the flowering plant *Arabidopsis thaliana*. **2000.** *Nature* **408:** 796–815.

Agranoff BW, Brady RO. 1956. Purification and properties of calf liver ribokinase. *Journal of Biological Chemistry* **219:** 221–229.

Alamillo JM, Díaz-Leal JL, Sánchez-Moran MV, Pineda M. 2010. Molecular analysis of ureide accumulation under drought stress in *Phaseolus vulgaris* L. *Plant, Cell & Environment* **33:** 1828–1837.

Alonso JM, Stepanova AN, Leisse TJ, Kim CJ, Chen H, Shinn P, Stevenson DK, Zimmerman J, Barajas P, Cheuk R, Gadrinab C, Heller C, Jeske A, Koesema E, Meyers CC, Parker H, Prednis L, Ansari Y, Choy N, Deen H, Geralt M, Hazari N, Hom E, Karnes M, Mulholland C, Ndubaku R, Schmidt I, Guzman P, Aguilar-Henonin L, Schmid M, Weigel D, Carter DE, Marchand T, Risseeuw E, Brogden D, Zeko A, Crosby WL, Berry CC, Ecker JR. 2003. Genome-wide insertional mutagenesis of *Arabidopsis thaliana*. *Science* **301:** 653–657.

Amann T, Hellerbrand C. 2009. GLUT1 as a therapeutic target in hepatocellular carcinoma. *Expert Opinion on Therapeutic Targets* **13:** 1411–1427.

Anderson A, Cooper RA. 1969. The significance of ribokinase for ribose utilization by *Escherichia coli*. *Biochimica et Biophysica Acta (BBA) - General Subjects* **177:** 163–165.

Andersson CE, Mowbray SL. 2002. Activation of ribokinase by monovalent cations. *Journal of Molecular Biology* **315:** 409–419.

Ashihara H. 2012. Xanthosine metabolism in plants: Metabolic fate of exogenously supplied C-14-labelled xanthosine and xanthine in intact mungbean seedlings. *Phytochemistry Letters* **5:** 100–103.

Ashihara H, Sano H, Crozier A. 2008. Caffeine and related purine alkaloids: biosynthesis, catabolism, function and genetic engineering. *Phytochemistry* **69:** 841–856.

Ausubel M, Brent R, Kingston RE, Moore DD, Seidman JG, Smith JA, Struhl K. 1989. Current protocols in molecular biology. *Molecular Reproduction and Development* **1**: 146.

Baccolini C, Witte C-P. 2019. AMP and GMP Catabolism in *Arabidopsis* Converge on Xanthosine which Is Degraded by a Nucleoside Hydrolase Heterocomplex. *The Plant Cell.* (in Press)

Barnett JA. 1975. The entry of D-ribose into some yeasts of the genus *Pichia. Journal of General Microbiology* **90**: 1–12.

Berg JM, Tymoczko JL, Stryer L. 2013. Stryer Biochemie. Berlin, Heidelberg: Springer Berlin Heidelberg.

Bisson LF, Coons DM, Kruckeberg AL, Lewis DA. 1993. Yeast sugar transporters. *Critical Reviews in Biochemistry and Molecular Biology* **28**: 259–308.

Bertani G. 1951. Studies on lysogenesis. I. The mode of phage liberation by lysogenic *Escherichia coli. Journal of Bacteriology* **62**: 293–300.

Bisson LF, Coons DM, Kruckeberg AL, Lewis DA. 1993. Yeast sugar transporters. *Critical Reviews in Biochemistry and Molecular Biology* **28**: 259–308.

Bjoerkman O, Demmig B. 1987. Photon yield of O2 evolution and chlorophyll fluorescence characteristics at 77 K among vascular plants of diverse origins. *Planta* **170**: 489–504.

Boer P, Sperling O. 1995. Role of cellular ribose-5-phosphate content in the regulation of 5-phosphoribosyl-1-pyrophosphate and *de novo* purine synthesis in a human hepatoma cell line. *Metabolism: Clinical and Experimental* **44**: 1469–1474.

Bork P, Sander C, Valencia A. 1993. Convergent evolution of similar enzymatic function on different protein folds: the hexokinase, ribokinase, and galactokinase families of sugar kinases. *Protein Science : A Publication of the Protein Society* **2**: 31–40.

Brinkrolf K, Ploeger S, Solle S, Brune I, Nentwich SS, Hueser AT, Kalinowski J, Puehler A, Tauch A. 2008. The LacI/GalR family transcriptional regulator UriR negatively controls uridine utilization of *Corynebacterium glutamicum* by binding to catabolite-responsive element (cre)-like sequences. *Microbiology* **154**: 1068–1081.

Brohée S, Barriot R, Moreau Y, André B. 2010. YTPdb: a wiki database of yeast membrane transporters. *Biochimica et Biophysica Acta (BBA)* **1798:** 1908–1912.

Brychkova G, Alikulov Z, Fluhr R, Sagi M. 2008. A critical role for ureides in dark and senescence-induced purine remobilization is unmasked in the *Atxdh1 Arabidopsis* mutant. *The Plant Journal : for Cell and Molecular Biology* **54:** 496–509.

Büttner M. 2010. The *Arabidopsis* sugar transporter (AtSTP) family: an update. *Plant Biology* **1:** 35–41.

Büttner M. 2007. The monosaccharide transporter(-like) gene family in *Arabidopsis*. *FEBS Letters* **581:** 2318–2324.

Büttner M, Sauer N. 2000. Monosaccharide transporters in plants: structure, function and physiology. *Biochimica et Biophysica Acta* **1465:** 263–274.

Campbell NA, Reece JB, Urry L, Kratochwil A. 2009. Biologie. München: Pearson.

Chen L-Q, Hou B-H, Lalonde S, Takanaga H, Hartung ML, Qu X-Q, Guo W-J, Kim J-G, Underwood W, Chaudhuri B, Chermak D, Antony G, White FF, Somerville SC, Mudgett MB, Frommer WB. 2010. Sugar transporters for intercellular exchange and nutrition of pathogens. *Nature* **468:** 527–532.

Chen M, Herde M, Witte C-P. 2016. Of the Nine Cytidine Deaminase-Like Genes in *Arabidopsis*, Eight Are Pseudogenes and Only One Is Required to Maintain Pyrimidine Homeostasis *in Vivo*. *Plant Physiology* **171:** 799–809.

Chen M, Thelen JJ. 2011. Plastid uridine salvage activity is required for photoassimilate allocation and partitioning in *Arabidopsis*. *The Plant Cell* **23:** 2991–3006.

Cho M-H, Lim H, Shin DH, Jeon J-S, Bhoo SH, Park Y-I, Hahn T-R. 2011. Role of the plastidic glucose translocator in the export of starch degradation products from the chloroplasts in *Arabidopsis thaliana*. *The New Phytologist* **190:** 101–112.

Chuvikovsky DV, Esipov RS, Skoblov YS, Chupova LA, Muravyova TI, Miroshnikov AI, Lapinjoki S, Mikhailopulo IA. 2006. Ribokinase from *E. coli*: expression, purification, and substrate specificity. *Bioorganic & Medicinal Chemistry* **14:** 6327–6332.

Cold Spring Harbour Protocols. 2015. Synthetic Defined (SD) Medium. *Cold Spring Harbor Protocols* **2015:** pdb.rec085639.

Cornelius S, Traub M, Bernard C, Salzig C, Lang P, Moehlmann T. 2012. Nucleoside transport across the plasma membrane mediated by equilibrative nucleoside transporter 3 influences metabolism of *Arabidopsis* seedlings. *Plant Biology* **14:** 696–705.

Dahncke K. 2014. Charakterisierung der Guanosindeaminase von *Arabidopsis thaliana* und Evaluation ihrer Bedeutung für den Purinnukleotidabbau: Freie Universität Berlin.

Dahncke K, Witte C-P. 2013. Plant purine nucleoside catabolism employs a guanosine deaminase required for the generation of xanthosine in *Arabidopsis. The Plant Cell* **25:** 4101–4109.

Deng D, Xu C, Sun P, Wu J, Yan C, Hu M, Yan N. 2014. Crystal structure of the human glucose transporter GLUT1. *Nature* **510:** 121.

Durand M, Mainson D, Porcheron B, Maurousset L, Lemoine R, Pourtau N. 2018. Carbon source-sink relationship in *Arabidopsis thaliana*: the role of sucrose transporters. *Planta* **247:** 587–611.

Edwards K, Johnstone C, Thompson C. 1991. A simple and rapid method for the preparation of plant genomic DNA for PCR analysis. *Nucleic Acids Research* **19:** 1349.

Feys BJ, Wiermer M, Bhat RA, Moisan LJ, Escobar NM, Neu C, Cabral A, Parker JE. 2005. *Arabidopsis* SENESCENCE-ASSOCIATED GENE101 stabilizes and signals within an ENHANCED DISEASE SUSCEPTIBILITY1 complex in plant innate immunity. *The Plant Cell* **17:** 2601–2613.

Frank B. 1889. Ueber die Pilzsymbiose der Leguminosen. *Berichte der Deutschen Botanischen Gesellschaft* **7:** 332–346.

Ginsburg A. 1959. A deoxyribokinase from *Lactobacillus plantarum. The Journal of Biological Chemistry* **234:** 481–487.

Guixé V, Merino F. 2009. The ADP-dependent sugar kinase family: kinetic and evolutionary aspects. *IUBMB Life* **61:** 753–761.

Harju S, Fedosyuk H, Peterson KR. 2004. Rapid isolation of yeast genomic DNA: Bust n' Grab. *BMC Biotechnology* **4:** 8.

Hastie CJ, McLauchlan HJ, Cohen P. 2006. Assay of protein kinases using radiolabeled ATP: a protocol. *Nature Protocols* **1:** 968

Hauck OK, Scharnberg J, Escobar NM, Wanner G, Giavalisco P, Witte C-P. 2014. Uric acid accumulation in an *Arabidopsis* urate oxidase mutant impairs seedling establishment by blocking peroxisome maintenance. *The Plant Cell* **26:** 3090–3100.

Hellriegel H, Wilfarth H. 1889. Erfolgt die Assimilation des freien Stickstoffs durch die Leguminosen unter Mitwirkung niederer Organismen? *Berichte der Deutschen Botanischen Gesellschaft* **7:** 138–143.

Hooper CM, Castleden IR, Tanz SK, Aryamanesh N, Millar AH. 2017. SUBA4: the interactive data analysis centre for *Arabidopsis* subcellular protein locations. *Nucleic Acids Research* **45:** D1064-D1074.

Hu W, Hua X, Zhang Q, Wang J, Shen Q, Zhang X, Wang K, Yu Q, Lin Y-R, Ming R, Zhang J. 2018. New insights into the evolution and functional divergence of the SWEET family in *Saccharum* based on comparative genomics. *BMC Plant Biology* **18:** 270.

Huck JHJ, Verhoeven NM, Struys EA, Salomons GS, Jakobs C, Van der Knaap MS. 2004. Ribose-5-phosphate isomerase deficiency: new inborn error in the pentose phosphate pathway associated with a slowly progressive leukoencephalopathy. *American Journal of Human Genetics* **74:** 745–751.

Islam MR, Kim H, Kang S-W, Kim J-S, Jeong Y-M, Hwang H-J, Lee S-Y, Woo J-C, Kim S-G. 2007. Functional characterization of a gene encoding a dual domain for uridine kinase and uracil phosphoribosyltransferase in *Arabidopsis thaliana*. *Plant Molecular Biology* **63:** 465–477.

Jung B, Floerchinger M, Kunz H-H, Traub M, Wartenberg R, Jeblick W, Neuhaus HE, Moehlmann T. 2009. Uridine-ribohydrolase is a key regulator in the uridine degradation pathway of *Arabidopsis*. *The Plant Cell* **21:** 876–891.

Jung B, Hoffmann C, Moehlmann T. 2011. *Arabidopsis* nucleoside hydrolases involved in intracellular and extracellular degradation of purines. *The Plant Journal : For Cell and Molecular Biology* **65:** 703–711.

Kang P-A, Oh J, Lee H, Witte C-P, Rhee S. 2019. Crystal structure and mutational analyses of ribokinase from *Arabidopsis thaliana. Journal of Structural Biology* **(in press)**

Katahira R, Ashihara H. 2006. Profiles of purine biosynthesis, salvage and degradation in disks of potato (*Solanum tuberosum* L.) tubers. *Planta* **225:** 115–126.

Kirchberger S, Tjaden J, Neuhaus HE. 2008. Characterization of the *Arabidopsis* Brittle1 transport protein and impact of reduced activity on plant metabolism. *The Plant Journal : For Cell and Molecular Biology* **56:** 51–63.

Kleinboelting N, Huep G, Kloetgen A, Viehoever P, Weisshaar B. 2012. GABI-Kat SimpleSearch: new features of the *Arabidopsis thaliana* T-DNA mutant database. *Nucleic Acids Research* **40:** D1211-5.

Klepek Y-S, Geiger D, Stadler R, Klebl F, Landouar-Arsivaud L, Lemoine R, Hedrich R, Sauer N. 2005. *Arabidopsis* POLYOL TRANSPORTER5, a new member of the monosaccharide transporter-like superfamily, mediates H+-Symport of numerous substrates, including myo-inositol, glycerol, and ribose. *The Plant Cell* **17:** 204–218.

Koch K. 2004. Sucrose metabolism: regulatory mechanisms and pivotal roles in sugar sensing and plant development. *Current Opinion in Plant Biology* **7:** 235–246.

Kopecná M, Blaschke H, Kopecny D, Vigouroux A, Koncitíková R, Novák O, Kotland O, Strnad M, Moréra S, Schwartzenberg K von. 2013. Structure and function of nucleoside hydrolases from *Physcomitrella patens* and maize catalyzing the hydrolysis of purine, pyrimidine, and cytokinin ribosides. *Plant Physiology* **163:** 1568–1583.

Li J, Wang C, Wu Y, Wu M, Wang L, Wang Y, Zang J. 2012. Crystal structure of Sa239 reveals the structural basis for the activation of ribokinase by monovalent cations. *Journal of Structural Biology* **177:** 578–582.

Lodwig E, Poole P. 2003. Metabolism of Rhizobium Bacteroids. *Critical Reviews in Plant Sciences* **22:** 37–78.

Lopilato JE, Garwin JL, Emr SD, Silhavy TJ, Beckwith JR. 1984. D-ribose metabolism in *Escherichia coli* K-12: genetics, regulation, and transport. *Journal of bacteriology* **158:** 665–673.

Ma X, Wang W, Bittner F, Schmidt N, Berkey R, Zhang L, King H, Zhang Y, Feng J, Wen Y, Tan L, Li Y, Zhang Q, Deng Z, Xiong X, Xiao S. 2016. Dual and Opposing Roles of Xanthine Dehydrogenase in Defense-Associated Reactive Oxygen Species Metabolism in *Arabidopsis*. *The Plant Cell* **28:** 1108–1126.

Maj MC, Gupta RS. 2001. The effect of inorganic phosphate on the activity of bacterial ribokinase. *Journal of Protein Chemistry* **20:** 139–144. **Maj MC, Singh B, Gupta RS. 2002.** Pentavalent ions dependency is a conserved property of adenosine kinase from diverse sources: identification of a novel motif implicated in phosphate and magnesium ion binding and substrate inhibition. *Biochemistry* **41:** 4059–4069.

Marschner P. 2012. Marschner's mineral nutrition of higher plants. Amsterdam, Boston: Elsevier/Academic Press.

McCarthy DJ, Chen Y, Smyth GK. 2012. Differential expression analysis of multi-factor RNA-Seq experiments with respect to biological variation. *Nucleic acids research* **40:** 4288–4297.

Moffatt B, Somerville C. 1988. Positive selection for male-sterile mutants of *Arabidopsis* lacking adenine phosphoribosyl transferase activity. *Plant Physiology* **86:** 1150–1154.

Moffatt BA, Wang L, Allen MS, Stevens YY, Qin W, Snider J, Schwartzenberg K von. 2000. Adenosine kinase of *Arabidopsis*. Kinetic properties and gene expression. *Plant Physiology* **124:** 1775–1785.

Mueckler M, Caruso C, Baldwin SA, Panico M, Blench I, Morris HR, Allard WJ, Lienhard GE, Lodish HF. 1985. Sequence and structure of a human glucose transporter. *Science* **229:** 941–945.

Mumberg D, Mueller R, Funk M. 1995. Yeast vectors for the controlled expression of heterologous proteins in different genetic backgrounds. *Gene* **156:** 119–122.

Murashige T, Skoog F. 1962. A Revised Medium for Rapid Growth and Bio Assays with Tobacco Tissue Cultures. *Physiologia Plantarum* **15:** 473–497.

Myrach T, Zhu, A Witte C-P. 2017. The assembly of the plant urease activation complex and the essential role of the urease accessory protein G (UreG) in delivery of nickel to urease. *The Journal of Biological Chemistry* **292:** 14556–14565.

Nara T, Hshimoto T, Aoki T. 2000. Evolutionary implications of the mosaic pyrimidine-biosynthetic pathway in eukaryotes. *Gene* **257:** 209–222.

Naula CM, Logan FJ, Logan FM, Wong PE, Barrett MP, Burchmore RJ. 2010. A glucose transporter can mediate ribose uptake: definition of residues that confer substrate specificity in a sugar transporter. *The Journal of Biological Chemistry* **285:** 29721–29728.

Ogbunude POJ, Lamour N, Barrett MP. 2007. Molecular Cloning, Expression and Characterization of Ribokinase of *Leishmania major. Acta Biochimica et Biophysica Sinica* **39:** 462–466.

Pao SS, Paulsen IT, Saier MH. 1998. Major facilitator superfamily. *Microbiology and Molecular Biology Reviews : MMBR* **62:** 1–34.

Park J, Gupta RS. 2008. Adenosine kinase and ribokinase-the RK family of proteins. *Cellular and Molecular Life Sciences : CMLS* **65:** 2875–2896.

Park J, van Koeverden P, Singh B, Gupta RS. 2007. Identification and characterization of human ribokinase and comparison of its properties with *E. coli* ribokinase and human adenosine kinase. *FEBS Letters* **581:** 3211–3216.

Park Y, Cho YJ, Ahn T, Park C. 1999. Molecular interactions in ribose transport: the binding protein module symmetrically associates with the homodimeric membrane transporter. *The EMBO Journal* **18:** 4149–4156.

Parry RJ, Burns MR, Skae PN, Hoyt JC, Pal B. 1996. Carbocyclic analogues of D-ribose-5-phosphate: synthesis and behavior with 5-phosphoribosyl alpha-1-pyrophosphate synthetases. *Bioorganic & Medicinal Chemistry* **4:** 1077–1088.

Paul R, Patra MD, Sen U. 2015. Crystal structure of apo and ligand bound *vibrio cholerae* ribokinase (Vc-RK): role of monovalent cation induced activation and structural flexibility in sugar phosphorylation. *Advances in Experimental Medicine and Biology* **842:** 293–307.

Poschet G, Hannich B, Raab S, Jungkunz I, Klemens PAW, Krueger S, Wic S, Neuhaus HE, Büttner M. 2011. A novel *Arabidopsis* vacuolar glucose exporter is involved in cellular sugar homeostasis and affects the composition of seed storage compounds. *Plant Physiology* **157:** 1664–1676.

Quiroga-Roger D, Babul J, Guixé V. 2015. Role of monovalent and divalent metal cations in human ribokinase catalysis and regulation. *Biometals* **28:** 401–413.

Ragauskas AJ, Williams CK, Davison BH, Britovsek G, Cairney J, Eckert CA, Frederick WJ, Hallett JP, Leak DJ, Liotta CL, Mielenz JR, Murphy R, Templer R, Tschaplinski T. 2006. The path forward for biofuels and biomaterials. *Science* **311:** 484–489.

Riegler H, Geserick C, Zrenner R. 2011. *Arabidopsis thaliana* nucleosidase mutants provide new insights into nucleoside degradation. *The New Phytologist* **191:** 349–359.

Riggs JW, Rockwell NC, Cavales PC, Callis J. 2016. Identification of the Plant Ribokinase and Discovery of a Role for *Arabidopsis* Ribokinase in Nucleoside Metabolism. *The Journal of Biological Chemistry* **291:** 22572–22582.

Santi C, Bogusz D, Franche C. 2013. Biological nitrogen fixation in non-legume plants. *Annals of botany* **111:** 743–767.

Schaefer G, Heber U. 1977. Glucose transport into spinach chloroplasts. *Plant Physiology* **60:** 286–289.

Scholz-Starke J, Büttner M, Sauer N. 2003. AtSTP6, a new pollen-specific H+-monosaccharide symporter from *Arabidopsis*. *Plant Physiology* **131:** 70–77.

Schroeder RY, Zhu A, Eubel H, Dahncke K, Witte C-P. 2018. The ribokinases of *Arabidopsis thaliana* and *Saccharomyces cerevisiae* are required for ribose recycling from nucleotide catabolism, which in plants is not essential to survive prolonged dark stress. *The New Phytologist* **217:** 233–244.

Schroeder RY. 2014. Funktionelle Charakterisierung der Ribokinase aus *Arabidopsis thaliana*. Freie Universität Berlin.

Sculley DG, Dawson PA, Emmerson BT, Gordon RB. 1992. A review of the molecular basis of hypoxanthine-guanine phosphoribosyltransferase (HPRT) deficiency. *Human genetics* **90:** 195–207.

Shelp BJ, Atkins CA. 1983. Role of Inosine Monophosphate Oxidoreductase in the Formation of Ureides in Nitrogen-Fixing Nodules of Cowpea (*Vigna unguiculata* L. Walp.). *Plant Physiology* **72:** 1029–1034.

Sheoran IS, Luthra YP, Kuhad MS, Singh R. 1982. Cluster bean-a ureide- or amide-producing legume? *Plant Physiology* **70:** 917–918.

Shi J, Wang H, Hazebroek J, Ertl DS, Harp T. 2005. The maize low-phytic acid 3 encodes a myo-inositol kinase that plays a role in phytic acid biosynthesis in developing seeds. *The Plant Journal : for Cell and Molecular Biology* **42:** 708–719.

Shimada T, Kori A, Ishihama A. 2013. Involvement of the ribose operon repressor RbsR in regulation of purine nucleotide synthesis in *Escherichia coli*. *FEMS Microbiology Letters* **344:** 159–165.

Sigrell JA, Cameron AD, Jones TA, Mowbray SL. 1997. Purification, characterization, and crystallization of *Escherichia coli* ribokinase. *Protein Science : a Publication of the Protein Society* **6:** 2474–2476.

Sigrell JA, Cameron AD, Jones TA, Mowbray SL. 1998. Structure of *Escherichia coli* ribokinase in complex with ribose and dinucleotide determined to 1.8 A resolution: insights into a new family of kinase structures. *Structure* **6:** 183–193.

Sigrell JA, Cameron AD, Mowbray SL. 1999. Induced fit on sugar binding activates ribokinase. *Journal of Molecular Biology* **290:** 1009–1018.

Smith AM, Stitt M. 2007. Coordination of carbon supply and plant growth. *Plant, Cell & Environment* **30:** 1126–1149.

Stasolla C, Katahira R, Thorpe TA, Ashihara H. 2003. Purine and pyrimidine nucleotide metabolism in higher plants. *Journal of Plant Physiology* **160:** 1271–1295.

Steensels J, Snoek T, Meersman E, Picca Nicolino M, Voordeckers K, Verstrepen KJ. 2014. Improving industrial yeast strains: exploiting natural and artificial diversity. *FEMS Microbiology Reviews* **38:** 947–995.

Stincone A, Prigione A, Cramer T, Wamelink MMC, Campbell K, Cheung E, Olin-Sandoval V, Gruening N-M, Krueger A, Tauqeer Alam M, Keller MA, Breitenbach M, Brindle KM, Rabinowitz JD, Ralser M. 2015. The return of metabolism: biochemistry and physiology of the pentose phosphate pathway. *Biological reviews of the Cambridge Philosophical Society* **90**: 927–963.

Tourneux L, Bucurenci N, Saveanu C, Kaminski PA, Bouzon M, Pistotnik E, Namane A, Marlière P, Bârzu O, La Li De Sierra I, Neuhard J, Gilles AM. 2000. Genetic and biochemical characterization of *Salmonella enterica serovar typhi* deoxyribokinase. *Journal of Bacteriology* **182**: 869–873.

Traut TW, Jones ME. 1996. Uracil metabolism–UMP synthesis from orotic acid or uridine and conversion of uracil to beta-alanine: enzymes and cDNAs. *Progress in Nucleic Acid Research and Molecular Biology* **53**: 1–78.

Udvardi M, Poole PS. 2013. Transport and metabolism in legume-rhizobia symbioses. *Annual Review of Plant Biology* **64**: 781–805.

Van der Graaff E, Hooykaas P, Lein W, Lerchl J, Kunze G, Sonnewald U, Boldt R. 2004. Molecular analysis of "de novo" purine biosynthesis in *solanaceous* species and in *Arabidopsis* thaliana. *Frontiers in Bioscience* **9**: 1803–1816.

Vervliet G, Holsters M, Teuchy H, van Montagu M, Schell J. 1975. Characterization of different plaque-forming and defective temperate phages in *Agrobacterium*. *The Journal of General Virology* **26**: 33–48.

Voet D, Voet JG. 2011. Biochemistry. Hoboken: Wiley.

Voinnet O, Rivas S, Mestre P, Baulcombe D. 2003. An enhanced transient expression system in plants based on suppression of gene silencing by the p19 protein of tomato bushy stunt virus. *The Plant Journal : for Cell and Molecular Biology* **33**: 949–956.

Wahl V, Ponnu J, Schlereth A, Arrivault S, Langenecker T, Franke A, Feil R, Lunn JE, Stitt M, Schmid M. 2013. Regulation of flowering by trehalose-6-phosphate signaling in *Arabidopsis thaliana*. *Science* **339**: 704–707.

Weber A, Servaites JC, Geiger DR, Kofler H, Hille D, Groener F, Hebbeker U, Fluegge UI. 2000. Identification, purification, and molecular cloning of a putative plastidic glucose translocator. *The Plant Cell* **12**: 787–802.

Werner AK, Witte C-P. 2011. The biochemistry of nitrogen mobilization: purine ring catabolism. *Trends in Plant Science* **16:** 381–387.

Williams LE, Lemoine R, Sauer N. 2000. Sugar transporters in higher plants-a diversity of roles and complex regulation. *Trends in Plant Science* **5:** 283–290.

Witt JJ, Roskoski R. 1975. Rapid protein kinase assay using phosphocellulose-paper absorption. *Analytical Biochemistry* **66:** 253–258.

Xiong Y, DeFraia C, Williams D, Zhang X, Mou Z. 2009. Deficiency in a cytosolic ribose-5-phosphate isomerase causes chloroplast dysfunction, late flowering and premature cell death in *Arabidopsis. Physiologia Plantarum* **137:** 249–263.

Xu Y-F, Létisse F, Absalan F, Lu W, Kuznetsova E, Brown G, Caudy AA, Yakunin AF, Broach JR, Rabinowitz JD. 2013. Nucleotide degradation and ribose salvage in yeast. *Molecular Systems Biology* **9:** 665.

Yan N. 2015. Structural Biology of the Major Facilitator Superfamily Transporters. *Annual Review of Biophysics* **44:** 257–283.

Yang Q, Liu Y, Huang F, He Z-G. 2011. Physical and functional interaction between d-ribokinase and topoisomerase I has opposite effects on their respective activity in *Mycobacterium smegmatis* and *Mycobacterium tuberculosis. Archives of Biochemistry and Biophysics* **512:** 135–142.

Yin J, Ren W, Huang X, Deng J, Li T, Yin Y. 2018. Potential Mechanisms Connecting Purine Metabolism and Cancer Therapy. *Frontiers in Immunology* **9:** 1697.

Yin Y, Katahira R, Ashihara H. 2014. Metabolism of purine nucleosides and bases in suspension-cultured *Arabidopsis thaliana* cells. *European Chemical Bulletin* **3**.

Young E, Lee S-M, Alper H. 2010. Optimizing pentose utilization in yeast: the need for novel tools and approaches. *Biotechnology for Biofuels* **3:** 24.

Zhang T, Lei J, Yang H, Xu K, Wang R, Zhang Z. 2011. An improved method for whole protein extraction from yeast Saccharomyces cerevisiae. *Yeast* **28:** 795–798.

Zhao G, Pease AJ, Bharani N, Winkler ME. 1995. Biochemical characterization of gapB-encoded erythrose 4-phosphate dehydrogenase of *Escherichia coli* K-12 and its possible role in pyridoxal 5'-phosphate biosynthesis. *Journal of Bacteriology* **177:** 2804–2812.

Zrenner R, Riegler H, Marquard CR, Lange PR, Geserick C, Bartosz CE, Chen CT, Slocum RD. 2009. A functional analysis of the pyrimidine catabolic pathway in *Arabidopsis. The New Phytologist* **183:** 117–132.

Zrenner R, Stitt M, Sonnewald U, Boldt R. 2006. Pyrimidine and purine biosynthesis and degradation in plants. *Annual Review of Plant Biology* **57:** 805–836.

Acknowledgement

First and foremost I would like to thank Prof. Dr. Claus-Peter Witte for the opportunity to be part of his group as a PhD student. I am thankful for the input and ideas when we discussed results, the support and encouragement during the publication of the ribokinase paper, and the possibility to improve my scientific work steadily. I learned a lot during our work together and I am grateful for all the opportunities to grow as a scientist and as a person.

I would like to thank Prof. Dr. Thomas Brüser for accepting my invitation to take the position as a co-referee and Prof. Dr. Hans-Peter Braun for the role of an examiner in my thesis committee.

Special thanks to Dr. Nieves Medina Escobar, for the great job as a lab manager and to Dr. Marco Herde who always had a ready ear when it came to scientific problems or a chat about shrimps, corals and fishes.
I wish to thank my colleagues at the Institute of Plant Nutrition at the Leibniz University Hanover for the enjoyable work environment and nice social time we had together. I am grateful for all the scientific or non-scientific discussions and arguments.

I would like to thank my partner Eik Jagemann for the constant moral support. The uplifting optimism and all the love you gave me, it means a lot to me. Without Eik and the enormous support of my parents Marion and Jochen Schröder and my siblings Ann-Kathrin Yi and Yessica Schröder this work would not have been possible.

Appendix of Tables

Table A1: Protein sequence of *At*RBSK (At1g17160)

MMKGISSVSQSINYNPYIEFNRPQLQISTVNPNPAQSRFSRPRSLRVLSLSADPS
ANRNPKSAVDAHAPPLVVVGSANADIYVEIERLPKEGETISAKTGQTLAGG
KGANQAACGAKLMYPTYFVGRLGEDAHGKLIAEALGDDGCGVHLDYVRSV
NNEPTGHAVVMLQSDGQNSIIIVGGANMKAWPEIMSDDDLEIVRNAGIV
LLQREIPDSINIQVAKAVKKAGVPVILDVGGMDTPIPNELLDSIDILSP
NETELSRLTGMPTETFEQISQAVAKCHKLGVKQVLVKLGSKGSALFIQG
EKPIQQSIIPAAQVVDTTGAGDTFTAAFAVAMVEGKSHEECLRFAAAAA
SLCVQVKGAIPSMPDRKSVLKLLKFSI

Table A2: Protein sequence of *Sc*RBSK (YCR36W)

MGITVIGSLNYDLDTFTDRLPNAGETFRANHFETHAGGKGLNQAAAIGKLKN
PSSRYSVRMIGNVGNDTFGKQLKDTLSDCGVDITHVGTYEGINTGTATILIE
EKAGGQNRILIVEGANSKTIYDPKQLCEIFPEGKEEEYVVFQHEIPDPLSI
IKWIHANRPNFQIVYNPSPFKAMPKKDWELVDLLVVNEIEGLQIVESVFDNE
LVEEIREKIKDDFLGEYRKICELLYEKLMNRKKRGIVVMTLGSRGVLFCSHE
SPEVQFLPAIQNVSVVDTTGAGDTFLGGLVTQLYQGETLSTAIKFSTLASSL
TIQRKGAAESMPLYKDVQKDA

Table A3: Protein sequence of pGLCT (At5g16150) from *A. thaliana*

MQSSTYAVKGNAAFAFQRRTFSSDRSTTSTGIRFAGYKSLATTGPLYCSGSEA
MGATLARADNGIQSVMSFSSVKARSVRAQASSDGDEEEAIPLRSEGKSSGTV
LPFVGVACLGAILFGYHLGVVNGALEYLAKDLGIAENTVLQGWIVSSLLAGA
TVGSFTGGALADKFGRTRTFQLDAIPLAIGAFLCATAQSVQTMIVGRLLAG
IGIGISSAIVPLYISEISPTEIRGALGSVNQLFICIGILAALIAGLPLAA
NPLWWRTMFGVAVIPSVLLAIGMAFSPESPRWLVQQGKVSEAEKAIKTLY
GKERVVELVRDLSASGQGSSEPEAGWFDLFSSRYWKVVSVGAALFLFQQL
AGINAVVYYSTSVFRSAGIQSDVAASALVGASNVFGTAVASSLMDKMGRK
SLLLTSFGGMALSMLLLSLSFTWKALAAYSGTLAVVGTVLYVLSFSLGAG
PVPALLLPEIFASRIRAKAVALSLGMHWISNFVIGLYFLSVVTKFGISSV
YLGFAGVCVLAVLYIAGNVVETKGRSLEEIELALTSGA

Table A4: Protein sequence of pGLCT-LIKE (At1g05030) *A. thaliana.*

MWVTNTVLLYRPNSMNRLTFSYPTRLAHSRKASSFSRFFRSSKRKK
RVTTLSTKKPDDDHEISPVPPEKFSADLGWLSAFPHVSVASMANFL
FGYHIGVMNGPIVSIARELGFEGNSILEGLVVSIFIAGAFIGSIVA
GPLVDKFGYRRTFQIFTIPLILGALVSAQAHSLDEILCGRFLVGLG
IGVNTVLVPIYISEVAPTKYRGSLGTLCQIGTCLGIIFSLLLGIPA
EDDPHWWRTMLYVASMPGFLLALGMQFAVESPRWLCKVGRLDDAKV
VIRNIWGGSEVEKAVEDFQSVMKNSGSNLNSRWLELLDKPHSRVAF
IGGSLFVLQQFAGINGVLYFSSLTFQNVGITSGAQASLYVGVTNFA
GALCASYLIDKQGRKKLLIGSYLGMAVSMFLIVYAVGFPLDEDLSQS
LSILGTLMYIFSFAIGAGPVTGLIIPELSSNRTRGKIMGFSFSVHWV
SNFLVGLFFLDLVEKYGVGTVYASFGSVSLLAAAFSHLFTVETKGRS
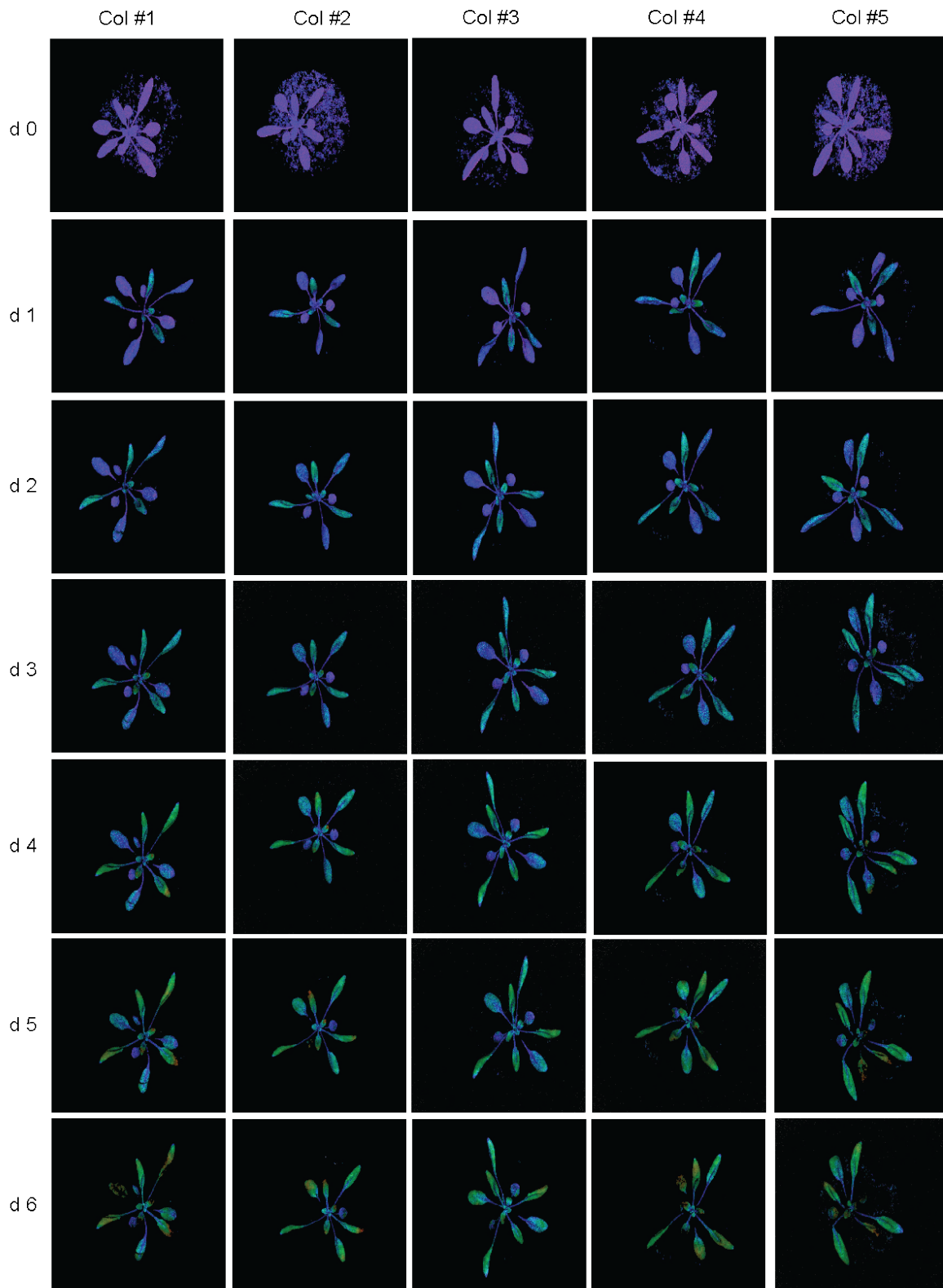LEEIELSLNSRDDLS

Appendix of Figures

Figure A1: Photosynthetic efficiency analysis of five independent *A. thaliana* Col-0 plants over the time of six consecutive days (d0 - d6). Fv/Fm values are calculated from whole plant rosettes by *ImagingWinGigE* program (Walz).
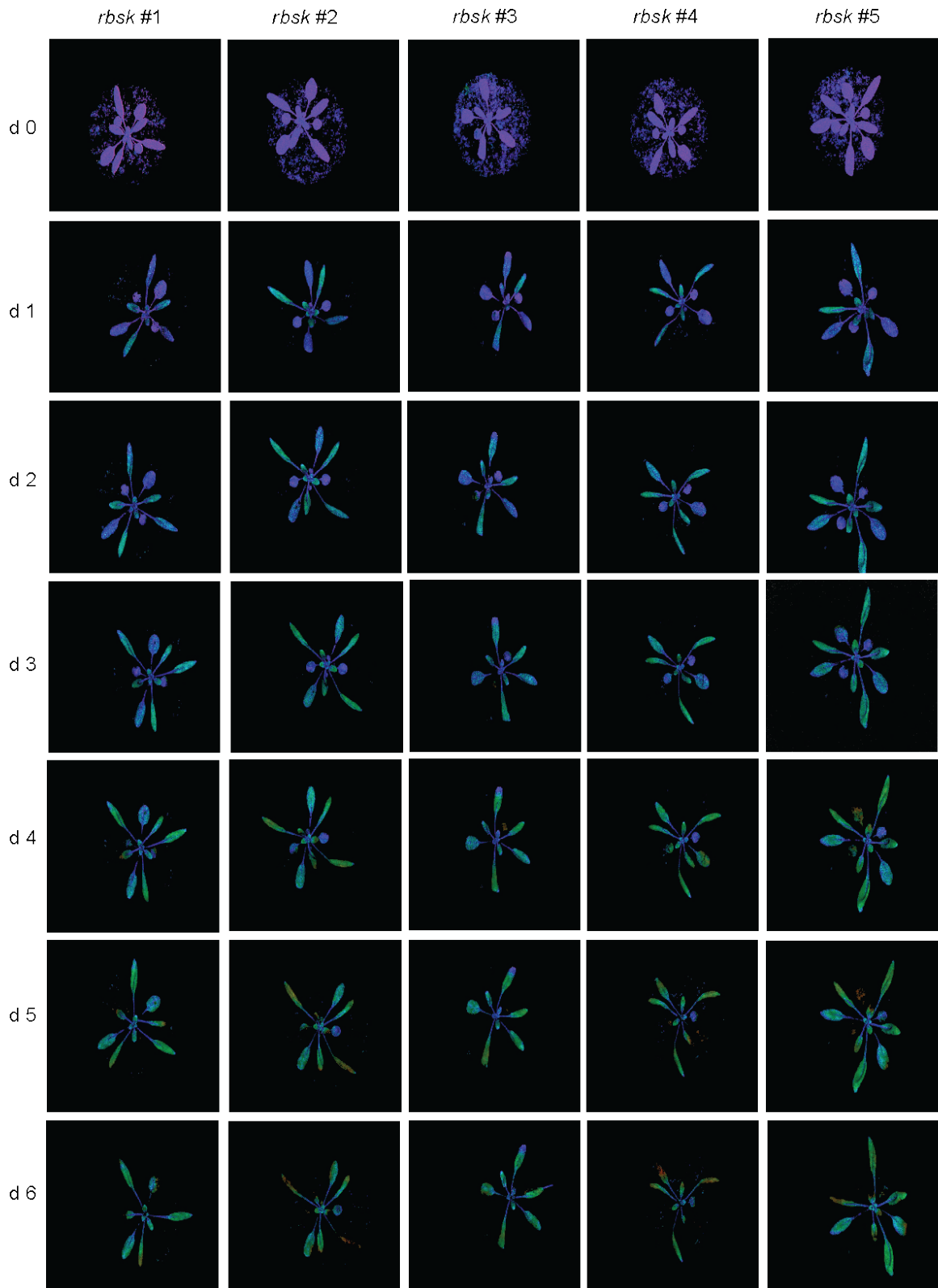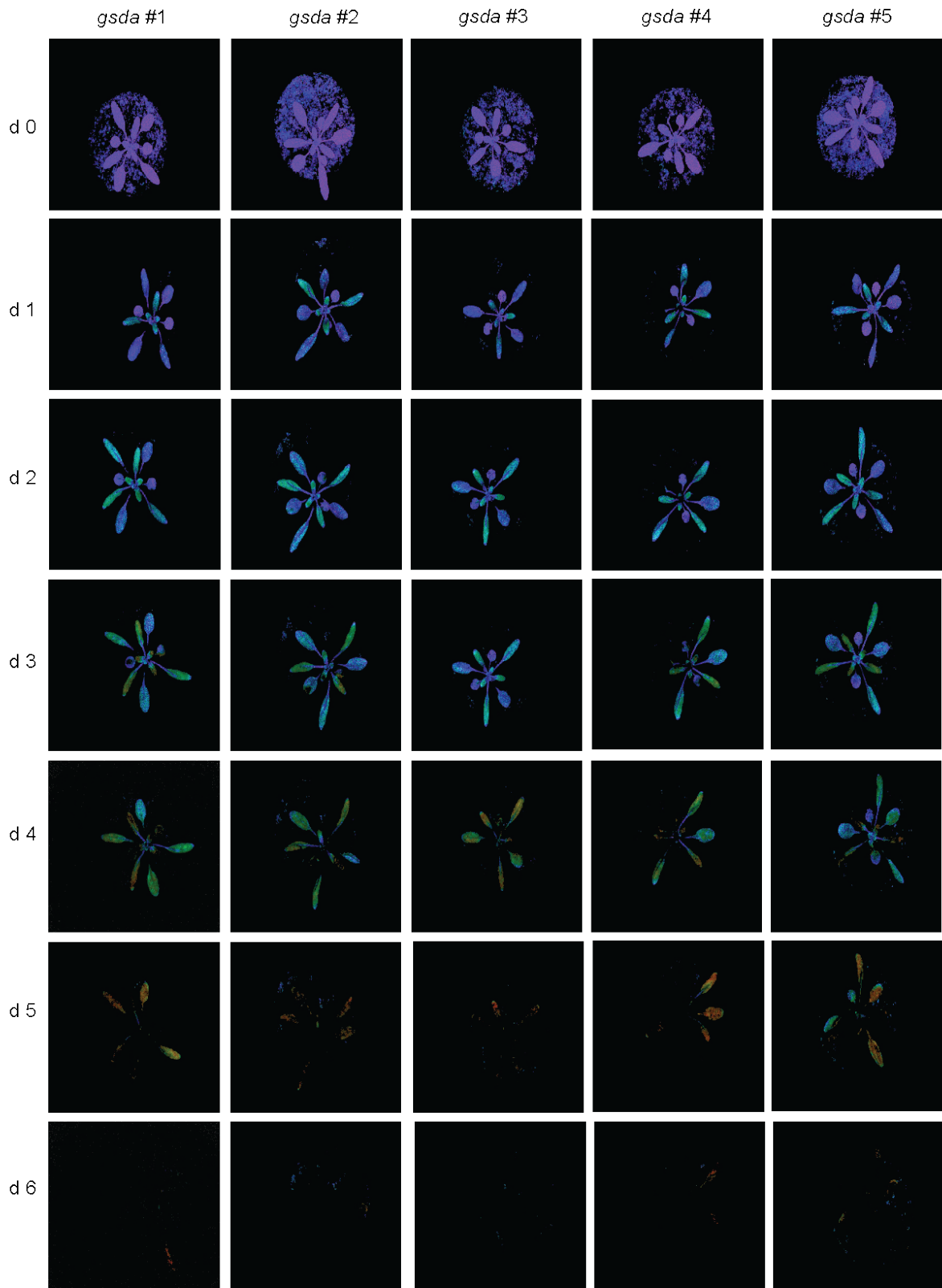
Figure A2: Photosynthetic efficiency analysis of five independent *A. thaliana rbsk* plants over the time of six consecutive days (d0 - d6). Fv/Fm values are calculated from whole plant rosettes by *ImagingWinGigE* program (Walz).

Figure A3: Photosynthetic efficiency analysis of five independent *A. thaliana gsda* plants over the time of six consecutive days. Fv/Fm values are calculated from whole plant rosettes by *ImagingWinGigE* program (Walz).
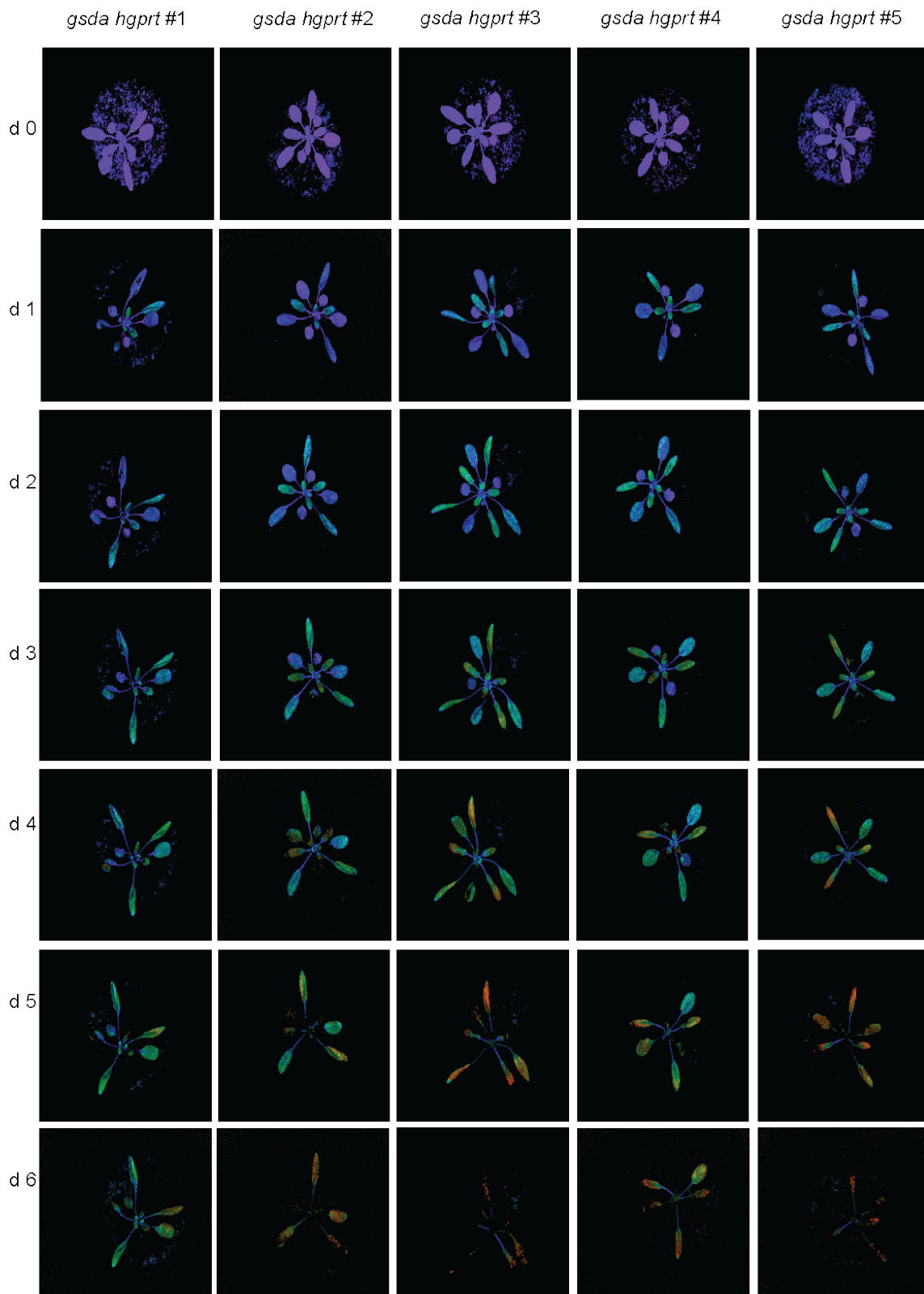
Figure A4: Photosynthetic efficiency analysis of five independent *A. thaliana gsda hgprt* plants over the time of six consecutive days (d0 - d6). Fv/Fm values are calculated from whole plant rosettes by *ImagingWinGigE* program (Walz).
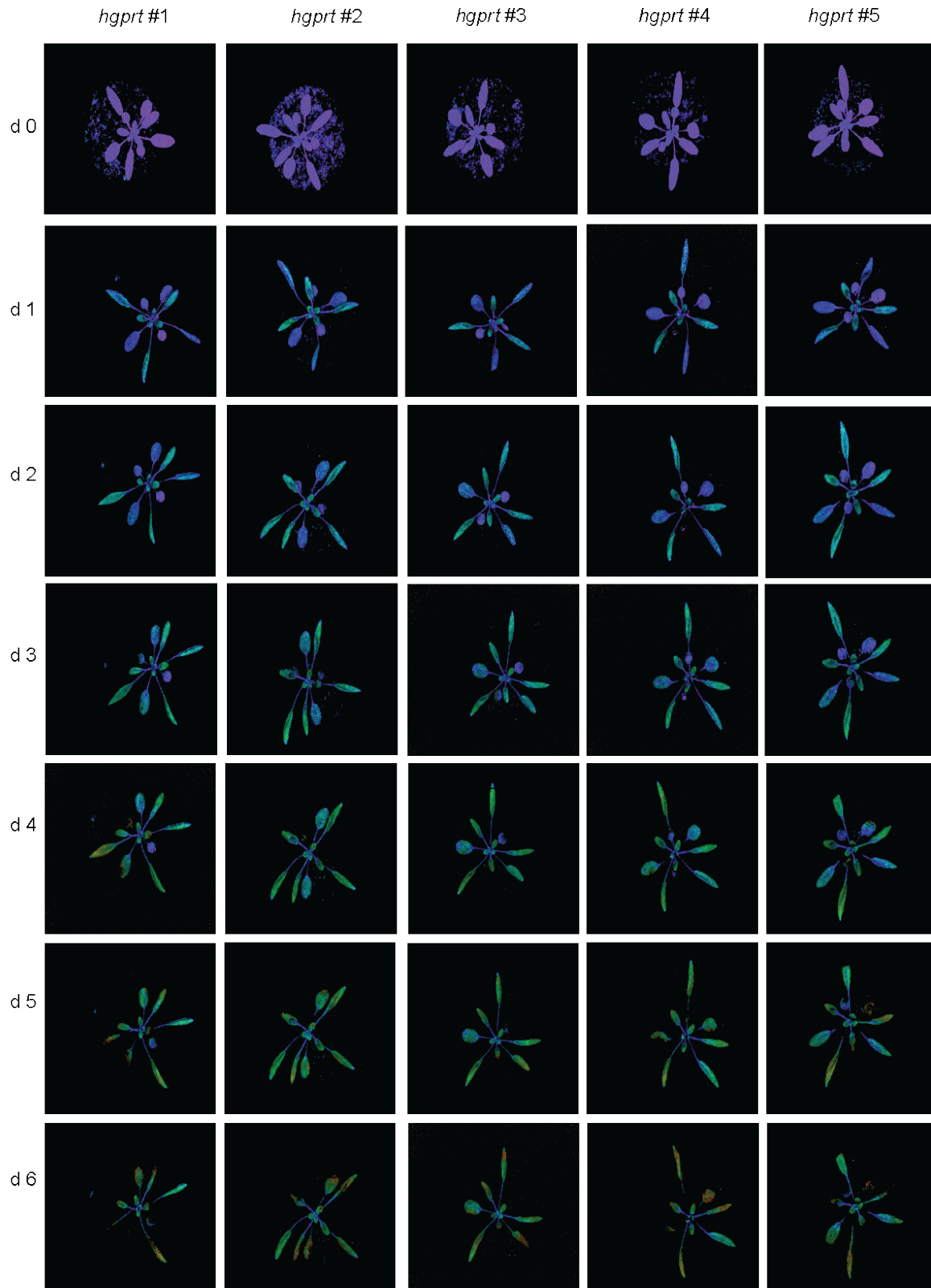
Figure A5: Photosynthetic efficiency analysis of five independent *A. thaliana hgprt* plants over the time of six consecutive days (d0 - d6). Fv/Fm values are calculated from whole plant rosettes by *ImagingWinGigE* program (Walz).
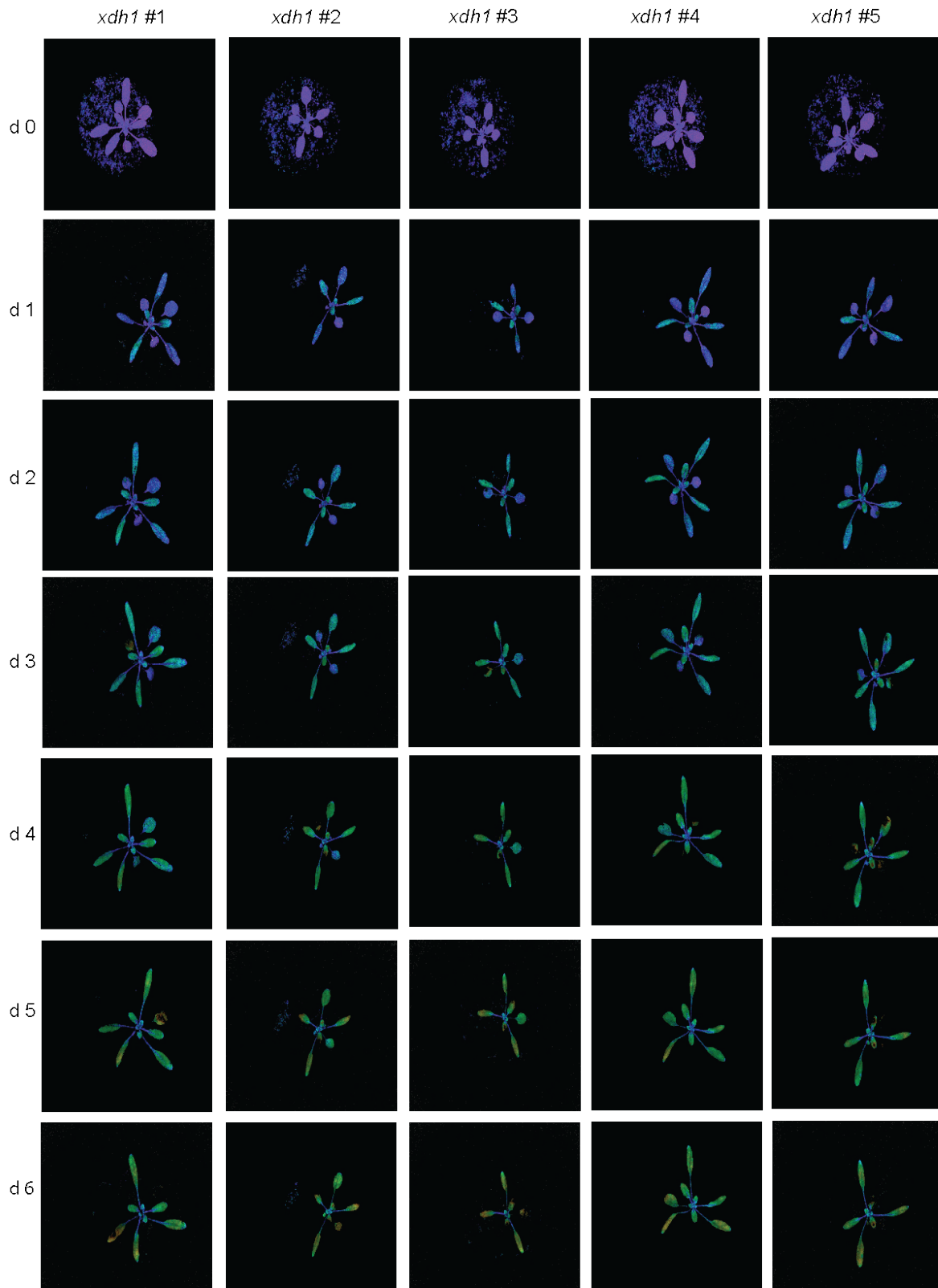
Figure A6: Photosynthetic efficiency analysis of five independent *A. thaliana xdh1* plants over the time of six consecutive days (d0 - d6). Fv/Fm values are calculated from whole plant rosettes by *ImagingWinGigE* program (Walz).
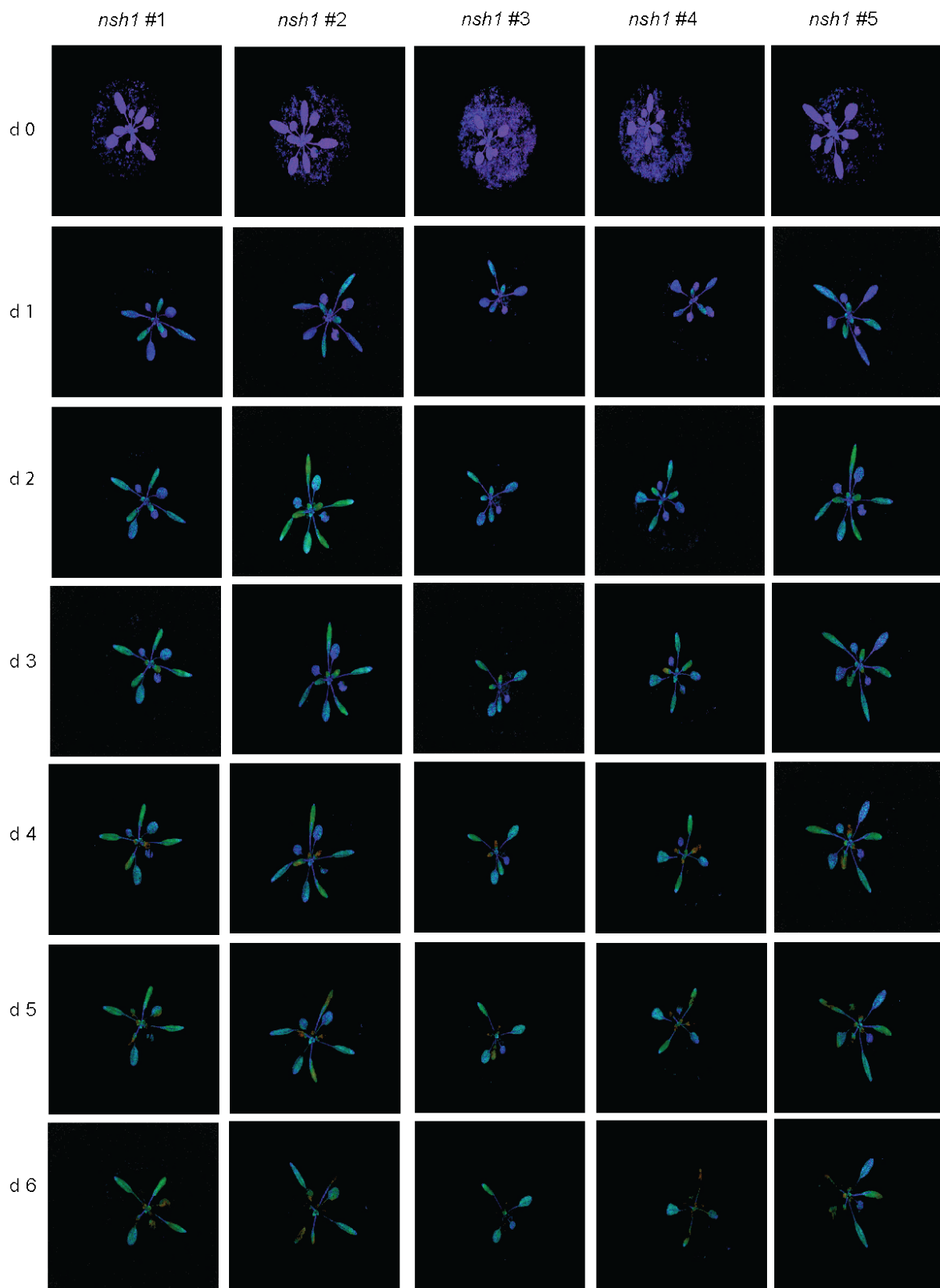
Figure A7: Photosynthetic efficiency analysis of five independent *A. thaliana nsh1* plants over the time of six consecutive days (d0 - d6). Fv/Fm values are calculated from whole plant rosettes by *ImagingWinGigE* program (Walz).

Figure A8: *pGLCT* gene map and T-DNA insertion points of *pglct-1* and *pglct-2* mutant lines, as characterised by Cho *et al.,* 2011. Exons are visualised as black boxes.

Curriculum vitae

Personal Data

Name	Rebekka Schroeder
Nationality	Germany
Date of Birth	08. January 1987
Place of Birth	Gräfelfing, Munich

Education

03.2015- present	PhD study in the Institute of Plant Nutrition at the Leibniz University Hannover, Germany
	Supervisor: Prof. Dr. Claus-Peter Witte
10.2012- 12.2014	Master studies at the Freie Universität Berlin, Germany
09.2009- 09.2012	Bachelor studies at Potsdam University, Germany
08.2003- 04.2007	Highschool education at Von-Saldern Gymnasium Brandenburg a.d.H., Germany

Conferences

2016	Molecular Biology of Plants (MBP) Dabringhausen, Germany
2017	Black Forrest Summer School, Germany

Publications

Schroeder, RY, Zhu, A, Eubel, H, Dahncke, K, Witte, C-P. 2018. The ribokinases of Arabidopsis thaliana and Saccharomyces cerevisiae are required for ribose recycling from nucleotide catabolism, which in plants is not essential to survive prolonged dark stress. *The New Phytologist* **217:** 233–244.